NASA
Technical
Paper
2867

February 1989

Conservation Equations and Physical Models for Hypersonic Air Flows in Thermal and Chemical Nonequilibrium

Peter A. Gnoffo,
Roop N. Gupta,
and Judy L. Shinn

NASA

NASA Technical Paper 2867

1989

Conservation Equations and Physical Models for Hypersonic Air Flows in Thermal and Chemical Nonequilibrium

Peter A. Gnoffo
Langley Research Center
Hampton, Virginia

Roop N. Gupta
Scientific Research & Technology, Inc.
Hampton, Virginia

Judy L. Shinn
Langley Research Center
Hampton, Virginia

National Aeronautics and Space Administration
Office of Management
Scientific and Technical Information Division

Contents

Abstract 1

Introduction 1

Symbols 2

Conservation Equations 6

- Species Conservation 8
- Mixture Momentum Conservation 8
- Vibrational Energy Conservation 8
- Electron and Electronic Excitation Energy Conservation 9
- Total Energy Conservation 10

Two-Temperature Model 10

Thermodynamic Relations 11

Chemical Kinetic Model 14

- Chemical-Vibrational Coupling 14
- Preferential Dissociation and Recombination 14
  - Treanor-Marrone model (refs. 57 and 58) 14
  - Park model (ref. 32) 15
- Reaction Sets and Reaction Rate Coefficients 15
- Vibrational Energy Reactive Source Terms 15
- Electronic Energy Reactive Source Terms 16
- Nonpreferential Dissociation and Recombination 16

Relaxation Processes 17

- Vibrational-Translational Energy Relaxation 17
- Electronic-Translational Energy Relaxation 18
- Vibrational-Electronic Energy Relaxation 18

Transport Properties 18

Upwind Formulation of the Flux Vector 20

Results and Discussion 24

- Chemical Kinetic Model Studies 24
- Grid Refinement Studies 26

Concluding Remarks 27

References 28

Abstract

The conservation equations for simulating hypersonic flows in thermal and chemical nonequilibrium and details of the associated physical models are presented. These details include the curve fits used for defining thermodynamic properties of the 11-species air model (N, O, N_2, O_2, NO, N^+, O^+, N_2^+, O_2^+, NO^+, and e^-), the curve fits for collision cross sections, the expressions for transport properties, the chemical kinetic models, and the vibrational and electronic energy relaxation models. The expressions are formulated in the context of either a two- or three-temperature model. Greater emphasis is placed on the two-temperature model, in which it is assumed that the translational and rotational energy modes are in equilibrium at the translational temperature, and the vibrational, electronic, and electron translational energy modes are in equilibrium at the vibrational temperature. The eigenvalues and eigenvectors associated with the Jacobian of the flux vector are also presented in order to accommodate the "upwind" based numerical solutions of the complete equation set.

Introduction

Future plans for space transportation and exploration call for mission trajectories with both sustained and maneuvering hypersonic flight in the Earth's atmosphere at altitudes greater than 70 km and velocities greater than 9 km/s (ref. 1). Aeroassisted orbital transfer vehicles will use this domain in returning from geosynchronous Earth orbit to low Earth orbit for rendezvous with Space Station Freedom. Lunar, planetary, and comet sample-return missions will utilize the Earth's upper atmosphere for aerobraking as well. Advanced hypersonic airbreathing cruise vehicles may ultimately be called on to fly through this domain. The trajectories for these missions include flow regimes ranging from continuum to free molecular. Substantial portions of these trajectories, in the transitional regime between free molecular and continuum, will carry the vehicle through conditions resulting in chemical and thermal nonequilibrium within the surrounding shock layer. Also, chemical nonequilibrium effects can be important well into the continuum regime.

Nonequilibrium processes occur in a flow when the time required for a process to accommodate itself to local conditions within some region is of the same order as the transit time across the region. If the accommodation time is very short compared with the transit time, the process is in equilibrium. If the accommodation time is very long compared with the transit time, the process is frozen. The length scale of the region depends on what is being studied. Useful length scales include shock standoff distance, shock-transition-zone thickness, and boundary-layer thickness. The process can be a chemical reaction or an exchange of energy among the various modes (translational, rotational, vibrational, or electronic) of the atoms and molecules in the gas flow. The accommodation is manifested through collisions among the atoms, molecules, ions, and electrons within the gas and the accommodation time is determined by the frequency with which effective collisions occur. The combination of low density in the upper atmosphere (which lowers the collision frequency) and high vehicle velocity (which lowers the transit time) creates the conditions which make nonequilibrium phenomena an important aspect of the shock-layer flow.

Nonequilibrium processes impact the flow environment over a vehicle in several important ways. They can significantly alter the shock standoff distance and shock shape. The effective isentropic exponent of the gas is changed, which in turn affects pressure distributions over expansion and compression surfaces of the vehicle. Thermal nonequilibrium, the condition wherein the distribution of energy among the translational, rotational, vibrational, and electronic modes of the gas cannot be described by a single temperature, influences the rates at which certain chemical reactions can proceed. Translational temperature behind the shock is increased, but vibrational and electronic temperatures are decreased because of the finite relaxation times for energy transfer caused by chemical and thermal relaxation processes. The onset of ionization is enhanced, relative to the thermal equilibrium state, because of the functional dependence of ionizing reactions on the translational temperature, whereas dissociation is diminished because of the functional dependence of dissociative reactions on the vibrational temperature (ref. 2). These effects compete in the determination of thermal radiation (ref. 3), which may play a significant role in the total heating load encountered by a large aeroassisted vehicle returning from geosynchronous Earth orbit (or beyond).

Most of the previous work on computational simulation of continuum, nonequilibrium, hypersonic flows has concentrated on chemical nonequilibrium. These simulations are based on inviscid equations (refs. 4 and 5), boundary-layer equations (refs. 6 to 8), viscous-shock-layer equations (refs. 9 to 11), parabolized Navier-Stokes equations (refs. 12 and 13), and Navier-Stokes equations (refs. 14 to 18). All the continuum simulations employ a chemical kinetic model for air which is used to define the production terms in the species continuity equations.

By contrast, noncontinuum simulations of hypersonic flows using a Direct-Simulation Monte Carlo algorithm intrinsically account for the effects of both chemical and thermal nonequilibrium, provided the gas components are modeled with the appropriate degrees of freedom (refs. 19 to 21). Some of the continuum work is focused particularly on determining electron number densities in the flow field in order to predict radio blackout during entry (refs. 22 to 24). The chemical kinetic models have evolved from both theoretical and experimental investigations (ref. 25). A review of both chemical and thermal nonequilibrium effects in nozzles (ref. 26) reflects the state of the art in 1967. More recently, quasi one-dimensional nozzle flow simulations have been implemented which include the effects of thermal nonequilibrium with a separate vibrational temperature for each species (ref. 27). Although no simulations are presented, equation sets and relaxation models for flows in chemical and thermal nonequilibrium were presented by Lee (ref. 2) and, earlier, by Appleton and Bray (ref. 28) for a simpler, monatomic, ionizing gas. These equation sets include a three-temperature model, in which it is assumed that there is a single temperature which describes the distribution of energy in the translational-rotational modes, a second temperature for the vibrational modes, and a third temperature for the electronic-free electron modes, and a two-temperature model, in which it is assumed that the distribution of energy in both the vibrational and electronic modes can be described by a single temperature. Much of the recent work on hypersonic flows over blunt bodies in both thermal and chemical nonequilibrium (refs. 29 to 31) employs the kinetic and thermal relaxation models summarized in the paper by Lee using one- or two-dimensional analyses.

The equations and models in the present paper are substantially derived from the work of Park (ref. 32) and Lee (ref. 2). Similar contributions appear earlier in the literature (refs. 33 and 34). Some modifications to and citations of other sources have been provided; however, this paper is not intended to justify every element of the model with first-principles statistical mechanics arguments. In fact, because of the approximate nature of the two-temperature model and because of the evolving understanding of relaxation processes through theoretical and experimental research, it is expected that some elements of the model will need to be revised. Rather, the model is presented with sufficient explanation to understand the fundamental assumptions and empiricisms involved in its present state of evolution. Also, it is presented from the perspective of a computational fluid dynamicist, and therefore consideration is given to the way the conservation equations and physical models should be formulated within a numerical algorithm. All the physical constants and requisite curve fits are included to fully define the nonequilibrium, nonradiating, two-temperature model. (The effects of radiation are carried through the equations, but the description of the radiation model itself is beyond the scope of this paper. The effects of a three-temperature model are also carried through, but no data are provided for electron-vibrational relaxation rates.)

The conservation equations are formulated within the context of the Langley Aerothermodynamic Upwind Relaxation Algorithm (LAURA, refs. 35 and 36), and sample calculations are made for a representative aeroassisted orbital transfer vehicle trajectory point. Only a two-temperature model is considered in these calculations. Various aspects of the physical model are discussed on the basis of these results. Comparisons with a Direct-Simulation Monte Carlo algorithm (ref. 37), appropriate for rarefied flows, are also presented, and some of the problems involved with the use of a continuum-based approximation scheme in the transitional region between free molecular and continuum flows are discussed. It should be mentioned that the surface slip-boundary conditions (refs. 18 and 38) should be employed for analyzing flows in the transitional region. These conditions have not been included in the results presented herein.

Symbols

$\mathbf{A}$	Jacobian matrix of $\mathbf{f}$ with respect to $\mathbf{q}$
A_k^s	curve fit constant for evaluating C_p^s
A_s	constant for determining τ_s^{MW}
a	frozen sound speed, m/s
a_e^s	curve fit constant for evaluating $C_{v,e}^s$
$\tilde{a}_s$	curve fit constant for evaluating σ_{es}
a_{sr}	nondimensional parameter for collision of species s and r used in defining thermal conductivity
a_v^s	curve fit constant for evaluating $C_{v,v}^s$
B_i^r	curve fit constant for evaluating $K_{c,r}$
b_e^s	curve fit constant for evaluating $C_{v,e}^s$

$\tilde{b}_s$	curve fit constant for evaluating σ_{es}
b_v^s	curve fit constant for evaluating $C_{v,v}^s$
$C_{b,r}$	preexponential term used in evaluating backward reaction rate coefficient
$C_{f,r}$	preexponential term used in evaluating forward reaction rate coefficient
C_p^s	specific heat at constant pressure for species s, J/kg-K
$C_{p,e}^s$	specific heat at constant pressure for species s for electronic enthalpy, J/kg-K
$C_{p,q}$	specific heat at constant pressure for mixture for energy mode q, where $q = t, r, v, e$, J/kg-K
$C_{p,r}^s$	specific heat at constant pressure for species s for rotational enthalpy, J/kg-K
$C_{p,t}^s$	specific heat at constant pressure for species s for translational enthalpy, J/kg-K
$C_{p,V}^s$	specific heat at constant pressure for species s for vibrational-electronic enthalpy, J/kg-K
$C_{p,v}^s$	specific heat at constant pressure for species s for vibrational enthalpy, J/kg-K
C_v^s	specific heat at constant volume for species s, J/kg-K
$C_{v,e}^s$	specific heat at constant volume for species s for electronic energy, J/kg-K
$C_{v,q}$	specific heat at constant volume for mixture for energy mode q, where $q = t, r, v, e$, J/kg-K
$C_{v,r}^s$	specific heat at constant volume for species s for rotational energy, J/kg-K
$C_{v,t}^s$	specific heat at constant volume for species s for translational energy, J/kg-K
$C_{v,tr}^s$	specific heat at constant volume for species s for translational-rotational energy, J/kg-K
$C_{v,V}^s$	specific heat at constant volume for species s for vibrational-electronic energy, J/kg-K
$C_{v,v}^s$	specific heat at constant volume for species s for vibrational energy, J/kg-K
c_e^s	curve fit constant for evaluating $C_{v,e}^s$
c_s	mass fraction of species s
$\tilde{c}_s$	curve fit constant for evaluating σ_{es}
$\bar{c}_s$	average molecular velocity of species s, m/s
c_v^s	curve fit constant for evaluating $C_{v,v}^s$
$\hat{c}_1, \hat{c}_2$	constants for estimating $\widehat{D}_s$
D_s	effective diffusion coefficient for species s, m^2/s
$\widehat{D}_s$	average vibrational energy per unit mass of molecule s, which is created or destroyed at rate $\dot{w}_s$, J/kg
$\widetilde{D}_s$	dissociation energy per unit mass of molecule s, J/kg or eV
D_s^a	effective ambipolar diffusion coefficient for species s, m^2/s
D_{sr}	binary diffusion coefficient for species s and r, m^2/s
E	total energy per unit mass of mixture, J/kg
$E_{b,r}$	activation energy for backward reaction r, J
$E_{f,r}$	activation energy for forward reaction r, J
e	mixture energy per unit mass, J/kg
e_e	mixture electronic energy per unit mass, J/kg
$e_{e,s}$	electronic energy per unit mass of species s, J/kg
e_s	energy per unit mass of species s, J/kg
$e_{s,o}$	energy of formation of species s, J/kg

$\tilde{e}_{tr}$	mass-weighted average of translational-rotational energy of reactant species (eq. (54a)), J/kg
e_V	mixture vibrational-electronic energy per unit mass, J/kg
$\tilde{e}_V$	mass-weighted average of vibrational-electronic energy of reactant species (eq. (54b)), J/kg
e_v	mixture vibrational energy per unit mass, J/kg
$e_{v,s}$	vibrational energy (enthalpy) per unit mass of species s, J/kg
$e^*_{v,s}$	vibrational energy (enthalpy) per unit mass of species s evaluated at temperature T, J/kg
$e^{**}_{v,s}$	vibrational energy (enthalpy) per unit mass of species s evaluated at temperature T_e, J/kg
$\mathbf{f}$	inviscid flux vector relative to computational cell wall
H	total enthalpy per unit mass of mixture, J/kg
h	mixture enthalpy per unit mass, J/kg
$h_{e,s}$	electronic enthalpy per unit mass of species s, J/kg
h_s	enthalpy per unit mass of species s, J/kg
$h_{s,o}$	enthalpy of formation of species s, J/kg
$h_{V,s}$	vibrational-electronic enthalpy per unit mass of species s, J/kg
$h_{v,s}$	vibrational enthalpy (energy) per unit mass of species s, J/kg
$\hat{I}_s$	first ionization energy of species s per kg-mole, J/kg-mole
$K_{c,r}$	equilibrium constant for reaction r
k	Boltzmann's constant, 1.380622×10^{-23} J/K
$k_{b,r}$	backward reaction rate coefficient for reaction r, units in cgs system consistent with number of products
$k_{f,r}$	forward reaction rate coefficient for reaction r, units in cgs system consistent with number of reactants
$\mathbf{L}$	matrix of column eigenvectors of $\mathbf{A}$
$\mathbf{l}$	unit vector tangent to computational cell wall
l_x, l_y, l_z	components of $\mathbf{l}$ in x, y, and z directions, respectively
M_s	molecular weight of species s, kg/kg-mole
$\mathbf{m}$	unit vector tangent to computational cell wall
m_s	mass of species s per particle, kg
m_x, m_y, m_z	components of $\mathbf{m}$ in x, y, and z directions, respectively
N_r	number of reactions in chemical kinetic model
$\mathbf{n}$	unit vector normal to computational cell wall
$n_{b,r}$	exponent of temperature in preexponential term for backward reaction r
$\dot{n}_{e,s}$	molar rate of production of species s per unit volume by electron impact ionization, kg-mole/m^3-s
$n_{f,r}$	exponent of temperature in preexponential term for forward reaction r
n_j	number density of species j, m^{-3}
n_x, n_y, n_z	components of $\mathbf{n}$ in x, y, and z directions, respectively
p	pressure, Pa
p_e	electron pressure, Pa
p_s	partial pressure due to species s, Pa
Q_{rad}	radiative energy transfer rate, J/m^3-s
$\mathbf{q}$	vector of conversed variables
$\mathbf{R}$	matrix of row eigenvectors of $\mathbf{A}$
$\overline{R}$	universal gas constant, 8314.3 J/kg-mole-K

$R_{b,r}$	backward reaction rate for reaction r, kg-mole/m^3-s
$R_{f,r}$	forward reaction rate for reaction r, kg-mole/m^3-s
T	translational-rotational temperature, K
T_d	rate-controlling temperature for dissociation reactions, K
T_e	electron-electronic excitation temperature, K
T_F	average temperature defined in equation (44c), K
T_{ref}	reference temperature for thermodynamic relations, K
T_{sh}	post-shock translational-rotational temperature, K
T_V	vibrational-electron-electronic excitation temperature, K
T_v	vibrational temperature, K
$T_{v,\text{sh}}$	post-shock vibrational temperature, K
t	time, s
U	velocity component normal to computational cell wall, m/s
$\widetilde{U}$	negative vibrational temperature of recombined molecules (eqs. (44)), K
u	velocity component in x-direction, m/s
u^j	velocity vector in three-dimensional space, $j = 1$ to 3, m/s
V	velocity component tangent to computational cell wall in l-direction, m/s
$\widetilde{V}$	vibrational coupling factor (eq. (44b))
V_∞	free-stream velocity, m/s
v	velocity component in y-direction, m/s
W	velocity component tangent to computational cell wall in m-direction, m/s
w	velocity component in z-direction, m/s
$\dot{w}_s$	mass rate of production of species s per unit volume, kg/m^3-s
x^j	positive vector in three-dimensional space, $j = 1$ to 3, m
y_s	mole fraction of species s
Z	nondimensional temperature used in evaluation of $K_{c,r}$
Z_q^s	partition function for energy mode q in species s
z	normal distance from body, m
$\alpha_{s,r}$	stoichiometric coefficient for reactants in reaction r
β	$\frac{\partial p}{\partial \rho E}$
$\beta_{s,r}$	stoichiometric coefficient for products in reaction r
$\tilde{\gamma}_r$	$\frac{\partial p}{\partial \rho r}$, J/kg
γ_s	molar concentration of species s, kg-mole/m^3
$\Delta_{sr}^{(1)}, \Delta_{sr}^{(2)}$	modified collision integrals for species s and r, m-s
δ^{ij}	Kronecker delta
η	frozen thermal conductivity for translational-rotational energy of heavy particles, J/m-s
η_e	frozen thermal conductivity for electronic energy due to collisions between electrons and all particles, J/m-s
η_r	frozen thermal conductivity for rotational energy, J/m-s
η_t	frozen thermal conductivity for translational energy, J/m-s
η_v	frozen thermal conductivity for vibrational energy due to collisions between molecules and all particles, J/m-s
$\mathbf{\Lambda}$	diagonal matrix of eigenvalues of $\mathbf{A}$
μ	mixture viscosity, N-s/m^2

μ_{sj}	reduced molecular weights of species s and j, $M_s M_j / (M_s + M_j)$
ν_{es}	effective collision frequency for electrons and heavy particles in electronic-translational (e-T) energy relaxation, 1/s
ρ	mixture density, kg/m^3
ρ_∞	free-stream mixture density, kg/m^3
ρ_s	density of species s, kg/m^3
σ_{es}	effective electron-neutral energy exchange collision cross section for species s, m^2
σ_s	effective cross section for vibrational relaxation, m^2
$< \tau_{es} >$	electronic-vibrational (e-V) energy relaxation time for molecular species s, s
$< \tau_s >$	translational-vibrational (T-V) energy relaxation time for molecular species s, s
τ_s^{MW}	translational-vibrational (T-V) energy relaxation time for species s from correlation of Millikan and White (ref. 65), s
τ_s^P	translational-vibrational (T-V) energy relaxation time for species s, limiting form at high temperatures from Park (ref. 29), s
$\bar{\tau}_v$	number-weighted average translational-vibrational (T-V) energy relaxation time for mixture, s
$\bar{\tau}_v^c$	diffusion-corrected number-weighted average translational-vibrational (T-V) energy relaxation time for mixture, s
ϕ	$\frac{\partial p}{\partial \rho e_V}$
$\overline{\Omega}_{sr}^{(1,1)}, \overline{\Omega}_{sr}^{(2,2)}$	collision integrals for species s and r, m^2

Subscripts:

The general definitions of subscripts are provided below. They are provided to augment the complete symbol list, which already includes subscript information. Subscripts may have more than one definition, in which case the meaning should be clear from the context of the expression and by reference to the symbol list above.

b	backward rate quantity
e	electronic mode; electrons
f	forward rate quantity
p	at constant pressure
q	dummy variable for translational, rotational, vibrational, or electronic states
r	rotational mode; species r; reaction r
s	species s
sh	post-shock condition
t	translational mode
V	vibrational-electronic mode in two-temperature model
v	vibrational mode only; at constant volume
x, y, z	Cartesian components
∞	free stream

Conservation Equations

The modeled system includes 11 species continuity equations, 3 momentum equations, and 3 energy equations describing the conservation of vibrational, electronic, and total energies. Species 1 to 5 are the neutral components of air consisting of N, O, N_2, O_2, and NO. Species 6 to 10 are the ions corresponding to species 1 to 5, in which one electron has been removed. Species 11 are the free electrons. The conservation equations for a reacting gas flow in which thermal nonequilibrium

is modeled with a three-temperature approximation (i.e., three-energy equations) can be expressed as follows.

Species Conservation:

$$\underbrace{\frac{\partial}{\partial t}\rho_s}_{1} + \underbrace{\frac{\partial}{\partial x^j}\rho_s u^j}_{2} = \underbrace{\frac{\partial}{\partial x^j}\left(\rho D_s \frac{\partial}{\partial x^j} y_s\right)}_{3} + \underbrace{\dot{w}_s}_{4} \tag{1}$$

Mixture Momentum Conservation:

$$\underbrace{\frac{\partial}{\partial t}\rho u^i}_{1} + \underbrace{\frac{\partial}{\partial x^j}\rho u^i u^j}_{2} = \underbrace{-\frac{\partial p}{\partial x^i}}_{3} + \underbrace{\frac{\partial}{\partial x^j}\left[\mu\left(\frac{\partial u^i}{\partial x^j} + \frac{\partial u^j}{\partial x^i}\right) - \frac{2}{3}\mu\frac{\partial u^k}{\partial x^k}\delta^{ij}\right]}_{4} \tag{2}$$

Vibrational Energy Conservation:

$$\begin{aligned}\underbrace{\frac{\partial}{\partial t}\rho e_v}_{1} + \underbrace{\frac{\partial}{\partial x^j}\rho e_v u^j}_{2} &= \underbrace{\frac{\partial}{\partial x^j}\left(\eta_v \frac{\partial T_v}{\partial x^j}\right)}_{3} + \underbrace{\frac{\partial}{\partial x^j}\left(\rho \sum_{s=1}^{11} h_{v,s} D_s \frac{\partial y_s}{\partial x^j}\right)}_{4} \\ &+ \underbrace{\sum_{s=\text{mol.}} \rho_s \frac{(e^*_{v,s} - e_{v,s})}{<\tau_s>}}_{5} + \underbrace{\sum_{s=\text{mol.}} \rho_s \frac{(e^{**}_{v,s} - e_{v,s})}{<\tau_{es}>}}_{6} + \underbrace{\sum_{s=\text{mol.}} \dot{w}_s \widehat{D}_s}_{7}\end{aligned} \tag{3}$$

Electron and Electronic Excitation Energy Conservation:

$$\begin{aligned}\underbrace{\frac{\partial}{\partial t}\rho e_e}_{1} + \underbrace{\frac{\partial}{\partial x^j}\left[u^j(\rho e_e + p_e)\right]}_{2} &= \underbrace{u^j \frac{\partial p_e}{\partial x^j}}_{3} + \underbrace{\frac{\partial}{\partial x^j}\left(\eta_e \frac{\partial T_e}{\partial x^j}\right)}_{4} + \underbrace{\frac{\partial}{\partial x^j}\left(\rho \sum_{s=1}^{11} h_{e,s} D_s \frac{\partial y_s}{\partial x_j}\right)}_{5} \\ &+ \underbrace{2\rho_e \frac{3}{2}\overline{R}(T - T_e)\sum_{s=1}^{10}\frac{\nu_{es}}{M_s}}_{6} - \underbrace{\sum_{s=6}^{10}\dot{n}_{e,s}\widehat{I}_s}_{7} - \underbrace{\sum_{s=\text{mol.}} \rho_s \frac{(e^{**}_{v,s} - e_{v,s})}{<\tau_{es}>}}_{8} - \underbrace{Q_{\text{rad}}}_{9}\end{aligned} \tag{4}$$

Total Energy Conservation:

$$\begin{aligned}\underbrace{\frac{\partial}{\partial t}\rho E}_{1} + \underbrace{\frac{\partial}{\partial x^j}\rho H u^j}_{2} &= \underbrace{\frac{\partial}{\partial x^j}\left(\eta \frac{\partial T}{\partial x^j} + \eta_v \frac{\partial T_v}{\partial x^j} + \eta_e \frac{\partial T_e}{\partial x^j}\right)}_{3} \\ &+ \underbrace{\frac{\partial}{\partial x^j}\left(\rho \sum_{s=1}^{11} h_s D_s \frac{\partial y_s}{\partial x^j}\right)}_{4} + \underbrace{\frac{\partial}{\partial x^j}\left[u^i \mu\left(\frac{\partial u^i}{\partial x^j} + \frac{\partial u^j}{\partial x^i}\right) - \frac{2}{3}u^i \mu \frac{\partial u^k}{\partial x^k}\delta^{ij}\right]}_{5} - \underbrace{Q_{\text{rad}}}_{6}\end{aligned} \tag{5}$$

Equations (1) to (5) are taken from reference 2 with some minor changes in notation, the addition of a source term in the vibrational energy equation to account for vibrational energy lost or gained with dissociation or recombination, and simplifications resulting from assumption of a zero conduction current (electron velocity equals ion velocity) and zero charge separation (electron number density equals ion number density). A review of the assumptions used in deriving these equations and a definition of terms for each equation follow.

Equations (1) to (5) have been written as partial differential equations. They are generally found in the literature in this form. The discretization of a partial differential equation can be formulated through the use of either finite differences or finite volumes. In general, one associates finite differences with the differential form of the conservation laws and finite volumes with the integral form of the conservation laws; however, the type of approximation scheme need not be tied to any particular representation of the conservation equations. In the discussion which follows, it is convenient to conceptualize physical processes as those which occur in a cell (finite volume) or which cross cell walls. The terms which describe convective and dissipative processes acting across cell walls are expressed in conservative form, in which the partial derivative of the quantity is taken with respect to x^j or x^i with no leading coefficients. All other terms are treated as cell-centered sources or sinks of mass and energy.

Species Conservation

The four terms in equation (1) represent (1) the rate of change of mass of species s per unit volume in a cell centered at point x^j, (2) the flux of mass of species s convected across cell walls with mixture velocity u^j, (3) the diffusion of species s across cell walls, and (4) the mass production rate of species s due to chemical reactions. The mixture density ρ is defined by

$$\rho = \sum_{s=1}^{11} \rho_s \tag{6}$$

The mole fraction y_s is defined by

$$y_s = \frac{(\rho_s/M_s)}{\sum_{k=1}^{11} (\rho_k/M_k)} \tag{7}$$

where the summation limit of 11 is the number of species in the mixture and M_s is the molecular weight of species s. The effective diffusion coefficient D_s is discussed in the section entitled *Transport Properties.* The production term $\dot{w}_s$ is discussed in the section entitled *Chemical Kinetic Model.* The effects of thermal and pressure diffusion have been ignored, and the binary diffusion approximation has been employed.

Mixture Momentum Conservation

The four terms in equation (2) represent (1) the rate of change of the ith component of momentum per unit volume in a cell centered at point x^j, (2) the flux of the ith component of momentum convected across cell walls with mixture velocity u^j, (3) the pressure forces acting on cell walls in the i-direction, and (4) the viscous forces acting on cell walls in the i-direction. The pressure p is defined by

$$p = \sum_{s=1}^{11} p_s \tag{8}$$

and the partial pressure of species s is defined by

$$p_s = \rho_s \overline{R} T / M_s \tag{9a}$$

where s represents an atomic, molecular, or ionic species, and

$$p_s = \rho_s \overline{R} T_e / M_s \tag{9b}$$

where s represents the free electron species. In both equations, $\overline{R}$ is the universal gas constant. The heavy-particle, translational-rotational temperature T and the electron temperature T_e are discussed in the section entitled *Thermodynamic Relations.* The viscosity μ is discussed in the section entitled *Transport Properties.* Bulk viscosity is assumed to be equal to zero in the evaluation of shear stresses. An approximation of zero charge separation removes an electric field forcing function (proportional to $\partial p_e / \partial x^i$) from the final expression.

Vibrational Energy Conservation

The seven terms in equation (3) represent (1) the rate of change of vibrational energy per unit volume in a cell centered at point x^j, (2) the flux of vibrational energy convected across cell walls with mixture velocity u^j, (3) the conduction of vibrational energy across cell walls due to vibrational temperature gradients, (4) the diffusion of vibrational energy across cell walls due to molecular concentration gradients, (5) the energy exchange (relaxation) between vibrational and translational modes due to collisions within the cell, (6) the energy exchange (relaxation) between vibrational and electronic modes, and (7) the vibrational energy lost or gained due to molecular depletion (dissociation) or production (recombination) in the cell. The vibrational energy per unit mass e_v is defined by

$$e_v = \sum_{s=1}^{11} \frac{\rho_s e_{v,s}}{\rho} \tag{10}$$

The vibrational energy per unit mass for species s, $e_{v,s}$, is defined as a function of T_v in the section entitled *Thermodynamic Relations.* The vibrational temperature T_v is related to the vibrational energy e_v in the same section. The vibrational thermal conductivity η_v is discussed in the section entitled *Transport*

Properties. The vibrational enthalpy for species s, $h_{v,s}$, is identical (ref. 39) to the vibrational energy for species s, $e_{v,s}$, and is used herein to maintain consistent notation with equation (5). The vibrational energies of species s at the translational-rotational temperature $e^{*}_{v,s}$ and at the electron temperature $e^{**}_{v,s}$ are defined as functions of their temperatures in the section entitled *Thermodynamic Relations.* The characteristic relaxation times for translational-vibrational (T-V) energy exchange $< \tau_s >$ and for electron-vibrational (e-V) energy exchange $< \tau_{es} >$ are presented in the section entitled *Relaxation Processes.* The term $\widehat{D}_s$ denotes the vibrational energy level representative of those molecules of species s which are preferentially created or destroyed (recombined or dissociated) because of their high vibrational quantum numbers. This quantity is defined in the section entitled *Chemical Kinetic Model.*

The vibrational energy conservation equation was derived under the approximation that the number density of all vibrationally excited molecules has a Boltzmann distribution characterized by a single temperature T_v. The expressions for T-V and e-V energy exchange, in which the relaxation rates are linearly proportional to the energy difference, are based on assumptions of harmonic oscillators (ref. 40). Anharmonicity has little effect on the relaxation rate near equilibrium, but the vibrational de-excitation rate is enhanced sufficiently far from equilibrium (ref. 41). This effect is not included here.

Electron and Electronic Excitation Energy Conservation

The nine terms in equation (4) represent (1) the rate of change of electronic energy per unit volume in a cell centered at point x^j, (2) the flux of electronic enthalpy convected across cell walls with mixture velocity u^j, (3) the work done on electrons by an electric field induced by the electron pressure gradient, (4) the conduction of electronic energy across cell walls due to the electron temperature gradient, (5) the diffusion of electronic energy due to concentration gradients, (6) the energy exchange due to elastic collisions between electrons and heavy particles, (7) the energy loss due to electron impact ionization, (8) the energy exchange (relaxation) due to inelastic collisions between electrons and molecules in the cell (corresponds to term 6 of eq. (3) for vibrational energy conservation), and (9) rate of energy loss due to radiation caused by electronic transitions. The electronic energy per unit mass e_e contains contributions from the electronic energy levels of all the species and is defined by

$$e_e = \sum_{s=1}^{11} \frac{\rho_s e_{e,s}}{\rho} \tag{11}$$

The electronic energy per unit mass of species s, $e_{e,s}$, is defined as a function of T_e in the section entitled *Thermodynamic Relations.* The electron temperature T_e is related to electronic energy e_e in that same section. The electronic thermal conductivity η_e is defined in the section entitled *Transport Properties.* The electronic enthalpy per unit mass of species s, $h_{e,s}$, is identical to $e_{e,s}$ for all species except free electrons. In the case of free electrons this quantity is defined by

$$h_{e,e} = e_{e,e} + \frac{\overline{R}T_e}{M_e} \tag{12}$$

The effective collision frequency of electrons with heavy particles ν_{es} is defined in the section entitled *Relaxation Processes.* The molar rate of production of species s by electron impact ionization $\dot{n}_{e,s}$ is defined in the section entitled *Chemical Kinetic Model.* The energy per unit mole lost by a free electron in producing species s through electron impact ionization $\widehat{I}_s$ is also defined in this section. The radiant energy transfer rate due to electronic transitions Q_{rad} is not considered in the present model but is important under some conditions. Consequently, its effects should be coupled in subsequent analyses in a manner similar to that presented in references 42 to 45.

The electron-electronic excitation energy conservation equation is derived under the approximation that the electronically excited states of all atoms and molecules and the translational energies of free electrons can be characterized by a Maxwell-Boltzmann distribution at temperature T_e. Furthermore, it is approximated that, in the absence of an externally applied electric or magnetic field (planetary magnetic field effects are ignored), the charge separation in a partially ionized gas is very small because of the linking of electron and ion diffusion (ambipolar diffusion). Also, there is no conduction current in the flow field under consideration, and the electron velocity is equal to the ion velocity. The inertial terms in the electron momentum equation are neglected because of the electron's small mass and viscous stress terms due to electrons are assumed to be negligible (refs. 2 and 28), both of which lead to the approximation that the electric field is proportional to the electron pressure gradient as used in equation (4). Without the assumption of negligible charge separation and conduction current, the electron momentum equation and the appropriate electrodynamic field terms

would have to be used to solve for the electron velocity vector. The present model cannot account for plasma-dynamic effects. These are not expected to be important in a continuum, forebody flow field, where the estimated magnetic pressures are orders of magnitude smaller than the fluid pressures in aero-assisted orbital transfer vehicle (AOTV) applications. The importance of these effects in the base flow region, where electrical conductivity may be higher, is not known.

Total Energy Conservation

The six terms in equation (5) represent (1) the rate of change of total energy per unit volume in a cell centered at point x^j, (2) the flux of total enthalpy convected across cell walls with mixture velocity u^j, (3) the conduction of energy across cell walls due to temperature gradients, (4) the diffusion of enthalpy across cell walls due to concentration gradients, (5) the work done by shear forces, and (6) the rate of energy loss due to radiation caused by electronic transitions. The total energy E is defined by

$$E = \frac{u^i u^i}{2} + \sum_{s=1}^{11} \frac{\rho_s e_s}{\rho} \tag{13}$$

where the energy per unit mass of species s, e_s, is defined in the section entitled *Thermodynamic Relations*. The total enthalpy H is defined by

$$H = E + \frac{p}{\rho} \tag{14}$$

The frozen thermal conductivity of heavy particles η is that part of the conductivity arising from collisions in which exchanges of translational and rotational energy occur. It is defined in the section entitled *Transport Properties*. All other terms in equation (5) have been discussed previously. An approximation of zero charge separation has been used to simplify this equation.

Two-Temperature Model

The model developed to this point assumes that the partitioning of energy among the translational, rotational, vibrational, and electronic modes in all 11 species can be described adequately by 3 temperatures. The relation between these energies and temperatures is discussed in the section entitled *Thermodynamic Relations*. What constitutes an adequate description of the energy distribution is subjective. For the purposes of simulating flow fields over hypersonic vehicles, an adequate model is one which allows accurate prediction of the aerodynamic coefficients and of both the convective and radiative heating of the vehicle surface. The adequacy of models used for the simulation of scramjet engines or gas-dynamic lasers is likely to be judged by other requirements. More detailed thermal models can be constructed in which the vibrational energy for each molecular species is modeled by its own vibrational temperature (refs. 27 and 31). This treatment requires an additional conservation law for the vibrational energy of each molecular species. Candler and MacCormack (ref. 31) show relatively small differences between vibrational temperatures of N_2 and O_2 for flow over an axisymmetric, blunted cone. Matsuzaki and Hirabayashi (ref. 27) show larger differences among vibrational temperatures for expanding flow through a nozzle and for flow behind a normal shock, though these temperature distributions are qualitatively similar to each other and are significantly different than the translational temperature. These results enhance the credibility of the simpler thermal models, in which the vibrational energies of all species are described by a single vibrational temperature. Furthermore, the accuracy of a multivibrational temperature model is limited by the accuracy of the available relaxation time data required to describe the energy exchange due to collisions among the species.

Another approach to be considered, particularly in light of uncertainties in some physical parameters and the complexities of three-dimensional flow simulation, is to reduce the thermal model to a two-temperature system. A justification for a two-temperature model presented by Park (ref. 32) is based on (1) the rapid energy transfer between the translational mode of free electrons and the vibrational mode of molecular nitrogen and (2) the rapid equilibration of the low-lying electronic states of heavy particles with the ground electronic state at the electronic temperature. This model makes the approximation that one temperature, T, describes the distribution of heavy-particle translational and rotational energies and that a second temperature, T_V, describes the distribution of vibrational, electronic, and electron translational energies. Note that subscript V denotes both the vibrational and electronic modes modeled together, whereas subscript v denotes only the vibrational modes and subscript e denotes only the electronic modes. While the approximation may be invalid in the viscous boundary layer adjacent to the wall (where the physically correct boundary conditions on the

vibrational and electronic translational energies are inconsistent with a single temperature (refs. 29 and 46)), it allows for a computationally more tractable formulation of reacting flows with thermal nonequilibrium.

The two-temperature model is obtained by combining equations (3) and (4) for vibrational energy conservation and electronic energy conservation into a single relation for vibrational-electronic energy conservation, where

$$T_v = T_e = T_V \tag{15}$$

The vibrational-electronic energy conservation equation can now be expressed.

Vibrational-Electronic Energy Conservation:

$$\underbrace{\frac{\partial}{\partial t}\rho e_V}_{1} + \underbrace{\frac{\partial}{\partial x^j}\rho e_V u^j}_{2} = \underbrace{-p_e\frac{\partial u^j}{\partial x^j}}_{3} + \underbrace{\frac{\partial}{\partial x^j}\left[(\eta_v+\eta_e)\frac{\partial T_V}{\partial x^j}\right]}_{4} + \underbrace{\frac{\partial}{\partial x^j}\left(\rho\sum_{s=1}^{11} h_{V,s}D_s\frac{\partial y_s}{\partial x^j}\right)}_{5}$$

$$+ \underbrace{\sum_{s=\text{mol.}} \rho_s\frac{(e^*_{v,s}-e_{v,s})}{<\tau_s>}}_{6} + \underbrace{2\rho_e\frac{3}{2}\overline{R}(T-T_V)\sum_{s=1}^{10}\frac{\nu_{es}}{M_s}}_{7} - \underbrace{\sum_{s=6}^{10}\dot{n}_{e,s}\widehat{I}_s}_{8} + \underbrace{\sum_{s=\text{mol.}}\dot{w}_s\widehat{D}_s}_{9} - \underbrace{Q_{\text{rad}}}_{10} \tag{16}$$

The vibrational-electronic energy per unit mass, e_V, and the vibrational-electronic enthalpy per unit mass for species s, $h_{V,s}$, can be expressed by

$$e_V = e_v + e_e \tag{17}$$

$$h_{V,s} = h_{v,s} + h_{e,s} \tag{18}$$

Note that terms 2 and 3 of equation (4), dealing with electron pressure, have been combined into a single term (term 3) in equation (16) above. The removal of the electron pressure from the convective term simplifies the expressions for eigenvalues and eigenvectors of the Jacobian of the flux vector. These quantities are important in upwind formulations of the governing equations and are presented in the section entitled *Upwind Formulation of the Flux Vector.*

Thermodynamic Relations

If a gas is in thermal equilibrium (i.e., the partitioning of energy for all modes can be described by a Maxwell-Boltzmann distribution at a single temperature T), then the energy per unit mass of species s in the gas can be expressed as

$$e_s = \int_{T_{\text{ref}}}^{T} C_v^s dT + e_{s,o} \tag{19}$$

where T_{ref} is a reference temperature, generally taken as 298.16 K, C_v^s is the specific heat at constant volume for species s, and $e_{s,o}$ is the energy of formation of species s at temperature T_{ref}. The enthalpy per unit mass of species s is similarly expressed by

$$h_s = \int_{T_{\text{ref}}}^{T} C_p^s dT + h_{s,o} \tag{20}$$

where

$$h_{s,o} = e_{s,o} + \frac{\overline{R}}{M_s}T_{\text{ref}} \tag{21}$$

$$C_p^s = C_v^s + \frac{\overline{R}}{M_s} \tag{22}$$

Values for $h_{s,o}$, M_s, and other physical constants for the 11 species considered herein are presented in table I. Tabulated values and polynomial curve fits for C_p^s and h_s, under the assumption of thermal equilibrium, are readily available (refs. 47 to 51). The curve fits employed for the 11 species considered in this report are presented at the end of this section.

In the general case of thermal nonequilibrium, e_s and h_s are functions of several temperatures, depending on the number of parameters required to adequately describe the partitioning of energy in the gas. In the three-temperature model described by equations (3) to (5), for example, it is assumed that

temperature T describes the translational and rotational energy modes of heavy particles, T_v describes the vibrational modes of all molecules, and T_e describes the electronic excitation and free electron translational modes. Consequently, it is necessary to establish how e_s and h_s are functions of these temperatures.

The partition function provides the mechanism for establishing these relationships under the assumptions that there exists a Maxwell-Boltzmann energy distribution at the temperature for each mode (i.e., translational, rotational, etc.) and that there is no coupling of energy levels between modes. Then, following the standard methods of statistical mechanics (refs. 40 and 52), one can write

$$C^s_{v,q} = \frac{\overline{R}}{M_s}\frac{\partial}{\partial T_q}\left(T_q^2\frac{\partial \ln Z^s_q}{\partial T_q}\right) \tag{23}$$

where q is a dummy index for the particular energy storage mode and Z^s_q is the partition function for species s in that mode. For the temperature range of interest ($200 \leq T \leq 50\,000$), both the translational and rotational modes are assumed to be fully excited, and the specific heat capacity for these modes reduces to

$$C^s_{v,t} = \frac{3\overline{R}}{2M_s} \tag{24}$$

for the translational modes and

$$C^s_{v,r} = \frac{\overline{R}}{M_s} \tag{25}$$

for the rotational modes.

The partition function for vibrational energy in a diatomic molecule is generally derived under the assumption of a harmonic oscillator, valid for low vibrational energies (low vibrational quantum numbers), with an anharmonic correction required at large vibrational energies. The anharmonic correction is due to the effects of interatomic forces on the potential energy curve for vibrational energy and due to the coupling of rotational and vibrational energies caused by a change in the moment of inertia of a diatomic molecule with increasing vibrational quantum numbers (ref. 52). This last effect technically violates the assumption of no coupling between modes. The entire correction is included as part of the vibrational energy partition function evaluated at temperature T_v.

The partition function for electronic energies is obtained by summing over the observed energy level data for the atoms and molecules in the gas. There is a coupling between the electronic and vibrational-rotational modes in diatomic molecules as well because the interatomic forces change when an electron leaves the ground electronic state. In this case, the partition functions for vibrational and rotational energies are taken in the ground electronic state, and the electronic energy partition function includes the correction to vibration and rotation due to electronic transitions evaluated at temperature T_e (refs. 52 to 54).

Compilations of physical constants for evaluating partition functions can be found in references 55 and 56. Balakrishnan (ref. 53) evaluated the partition functions in this manner and generated curve fits for the vibrational and electronic heat capacities in the following form:

$$C^s_{v,v} = \left(\frac{4186}{M_s}\right)\left(a^s_v + b^s_v T_v + \frac{c^s_v}{T_v^2}\right) \quad \text{(Vibrational)} \tag{26}$$

$$C^s_{v,e} = \left(\frac{4186}{M_s}\right)\left(a^s_e + b^s_e T_e + \frac{c^s_e}{T_e^2}\right) \quad \text{(Electronic)} \tag{27}$$

where the leading factor is a conversion from cal/g-mole-K to J/kg-K and the constants a, b, and c are presented in tables 3 and 4 of reference 53. For internal degrees of freedom,

$$C^s_{p,q} = C^s_{v,q} \tag{28a}$$

where $q = r, v$, or e and s represents atoms or molecules. The electron heat capacities are expressed by

$$C^e_{p,e} = \frac{5\overline{R}}{2M_e} \tag{28b}$$

$$C^e_{v,e} = \frac{3\overline{R}}{2M_e} \tag{28c}$$

The evaluations of specific heats and enthalpies are much simpler in the two-temperature model. The curve fits that are available for the enthalpies and heat capacities of species as a function of temperature are valid only under conditions of thermal equilibrium. They assume that a single temperature T (where $T = T_v = T_e$) describes the partition of energy among all the modes, and it is that temperature which must be used in the curve fits. However, in the two-temperature model, one can take advantage of the fact that the translational and rotational energy modes are assumed to be fully excited and therefore the heat capacities for these modes are independent of temperature. The vibrational-electronic heat capacity for species s can be evaluated by utilizing the curve fit for total heat capacity evaluated

at temperature T_V and subtracting out the constant contribution from the translational and rotational heat capacities. This strategy is employed in equations (29) and (30). In like manner, the contribution to enthalpy from the translational and rotational modes is linear with temperature. Consequently, the vibrational-electronic enthalpy for species s can be evaluated by utilizing the curve fit for specific enthalpy evaluated at temperature T_V and subtracting out both the contribution from the translational and rotational enthalpy evaluated at T_V and the enthalpy of formation. The correct specific enthalpy can then be recovered by adding the contribution of translational and rotational enthalpy evaluated at temperature T and the enthalpy of formation to the vibrational-electronic enthalpy. This strategy is used in the derivation of equations (35) and (36). The vibrational-electronic heat capacity can now be evaluated as follows:

$$C^s_{v,V}(T_V) = C^s_v(T_V) - C^s_{v,t} - C^s_{v,r} \tag{29}$$

where

$$C^s_v(T_V) = C^s_p(T_V) - \frac{\overline{R}}{M_s} \tag{30}$$

Curve fits and tabulated values for $C^s_p(T)$, as stated earlier, can be found in references 47 to 51. The use of curve fits significantly reduces the complexity and expense of computing the original functions. The original expressions for C^s_p were obtained from either the partition function method outlined above or a virial coefficient method. Either source is suitable for the two-temperature model.[1] The curve fits presented below should not be considered recommended data. They have been employed because of their accessibility and use in other codes or because they are the only known fits to data in a given temperature range.

The curve fits for $C^s_p(T)$ in the present model are of the form

$$C^s_p(T) = \frac{\overline{R}}{M_s} \sum_{k=1}^{5} A^s_k T^{k-1} \tag{31}$$

Values for A^s_k are presented in table II along with the original sources. The constants for the two highest temperature ranges in table II are previously unpublished data from reference 18. Values of A^s_k are linearly averaged across the curve fit boundaries (i.e., $950 < T < 1050, 5900 < T < 6100, 14\,900 < T < 15\,100$, and $24\,900 < T < 25\,100$) to ensure smooth variation of thermodynamic properties over the entire temperature range.

The evaluation of h_s with the three-temperature model is obtained by integrating the various heat capacities over the appropriate limits and adding the heat of formation. Thus,

$$h_s = \int_{T_{\text{ref}}}^{T} (C^s_{p,t} + C^s_{p,r})dT' + \int_{T_{\text{ref}}}^{T_v} C^s_{p,v}dT' + \int_{T_{\text{ref}}}^{T_e} C^s_{p,e}dT' + h_{s,o} \tag{32}$$

where T' is the dummy variable of integration and all other terms have been defined. The vibrational and electronic energies of species s can be written individually as

$$e_{v,s} = \int_{T_{\text{ref}}}^{T_v} C^s_{v,v}dT' \tag{33}$$

$$e_{e,s} = \int_{T_{\text{ref}}}^{T_e} C^s_{v,e}dT' \tag{34}$$

The integration of the curve fits for $C^s_{v,v}$ and $C^s_{v,e}$ from equations (26) and (27) is trivial and completes the definition.

In the two-temperature model, obtain $h_{V,s}$ and h_s from equations (29) to (31). Thus,

$$h_{V,s}(T_V) = h_s(T_v) - (C^s_{p,t} + C^s_{p,r})(T_V - T_{\text{ref}}) - h_{s,o} \tag{35}$$

$$h_s(T, T_V) = h_{V,s}(T_V) + (C^s_{p,t} + C^s_{p,r})(T - T_{\text{ref}}) + h_{s,o} \tag{36}$$

Curve fits for $h_s(T_V)$, which include the heat of formation, can be written with equation (31). The expression takes the form

$$h_s(T_V) = \frac{\overline{R}}{M_s}\left(\sum_{k=1}^{5} \frac{A^s_k T^k_V}{k} + A^s_6\right) \tag{37}$$

The constant A^s_6 is also provided in table II. The value of T_{ref} for these curve fits is 298.16 K.

[1] The partition function can be difficult to specify for diatomic molecules at vibrational energies near the dissociation energy, and to accurately define the anharmonic correction near these levels is not a trivial matter. For example, Balakrishnan (ref. 53) noted that his partition function evaluation of $C^{N_2}_p$ deviates from the virial coefficient approach of Browne (ref. 51) at temperatures greater than 12 000 K. Research is ongoing to improve these formulations.

Equations (19) to (37) were developed for a single species. The mixture relations are expressed as

$$C_{p,q} = \frac{1}{\rho}\sum \rho_s C^s_{p,q} \tag{38}$$

$$C_{v,q} = \frac{1}{\rho}\sum \rho_s C^s_{v,q} \tag{39}$$

$$h = \frac{1}{\rho}\sum \rho_s h_s \tag{40}$$

Equations (19) to (40) and the data in tables I and II complete all required thermodynamic relations for a two-temperature model. The addition of data available in tables 3 and 4 of reference 53 permits specification of all thermodynamic relations required for a three-temperature model.

Chemical Kinetic Model

The mass rate of production of species s per unit volume is expressed as

$$\dot{w}_s = M_s \sum_{r=1}^{N_r} (\beta_{s,r} - \alpha_{s,r})(R_{f,r} - R_{b,r}) \tag{41}$$

where N_r is the number of reactions, $\alpha_{s,r}$ and $\beta_{s,r}$ are respectively the stoichiometric coefficients for reactants and products in the r reaction, and $R_{f,r}$ and $R_{b,r}$ are respectively the forward and backward reaction rates for the r reaction. These rates are defined by

$$R_{f,r} = 1000\left[k_{f,r}\prod_{s=1}^{11}(0.001\rho_s/M_s)^{\alpha_{s,r}}\right] \tag{42}$$

$$R_{b,r} = 1000\left[k_{b,r}\prod_{s=1}^{11}(0.001\rho_s/M_s)^{\beta_{s,r}}\right] \tag{43}$$

where $k_{f,r}$ and $k_{b,r}$ are respectively the forward and backward reaction rate coefficients. Reaction rate coefficient data are generally provided in cgs units in the literature. The term in brackets is in cgs units. The factors 1000 and 0.001 are required in the conversion from cgs units to mks units. (Because most of the data in the literature for reaction rate coefficients are in cgs units, we have retained this practice in the formulation of equations (42) and (43).) A chemical kinetic model is defined when a set of N_r reactions is provided with the appropriate expressions for the forward and backward rate coefficients. Most of the sources for reaction rate coefficient data have assumed thermal equilibrium and, consequently, provide these expressions as a function of a single temperature. However, under the low-density and high-energy flow conditions of interest herein (where thermal equilibrium may not be assumed), the characteristic chemical time scale for dissociative reactions is comparable to the characteristic time for vibrational relaxation, a condition suggesting a coupling between the vibrational and chemical processes. Models for such chemical-vibrational coupling are considered below.

Chemical-Vibrational Coupling

Two types of chemical-vibrational coupling have been suggested in the literature. Under the first coupling model, known as preferential dissociation, the dissociation of molecular species is obtained more easily when the molecules are vibrationally excited. Accordingly, the molecules in the higher vibrational states are assumed to be preferentially dissociated. Molecules in the lower vibrationally excited states must "ladder climb" to the higher vibrationally excited states before dissociation can occur. However, this model may not be valid at very high velocities. Under highly energetic conditions the ladder-climbing process may not be as significant and a second model, based on nonpreferential dissociation, may be more realistic. Both models are discussed below.

Preferential Dissociation and Recombination

Treanor-Marrone model (refs. 57 and 58). In this model, the effect of vibrational relaxation on dissociation is included through the relation

$$k_{f,r} = k^*_{f,r}\widetilde{V}(T, T_V, \widetilde{U}) \tag{44a}$$

where the vibrational coupling factor $\widetilde{V}$ is obtained from

$$\widetilde{V} = \frac{Z^s_v(T)Z^s_v(T_F)}{Z^s_v(T_v)Z^s_v(-\widetilde{U})} \tag{44b}$$

The term Z^s_v is the vibrational partition function for the dissociating species and $k^*_{f,r}$ is the dissociation rate constant that would exist under conditions of thermal equilibrium. The temperature T_F is defined as

$$\frac{1}{T_F} = \frac{1}{T_v} - \frac{1}{T} - \frac{1}{\widetilde{U}} \tag{44c}$$

where the quantity $-\widetilde{U}$ may be considered as the vibrational temperature at which the molecules are formed by recombination. The negative value relates to the fact that, on the basis of an exponential distribution, more molecules are formed in upper vibrational levels than in lower levels. Marrone and

Treanor note that a value of $\widetilde{U} = E_{f,r}/3k$ gives good comparisons between experiment and computation for dissociation lag times behind a shock. (See tables III and IV for values of activation energy $E_{f,r}$.)

Park model (ref. 32). In this model Park assumes that certain classes of reactions can be described by a single rate-controlling temperature which is an appropriate average of the local translational, vibrational, and electronic temperatures. He suggests the use of a temperature (weighted heavily with the vibrational temperature due to the preferential dissociation concept) defined by

$$T_d = (TT_v)^{1/2} \tag{45}$$

to characterize dissociative reactions. This relation is empirical and has produced good comparisons with some experimental data for radiative energy flux (ref. 32), but the model cannot be justified on this basis alone. However, it does reproduce correct phenomenological trends and is simpler to apply than the corrections given by equations (44). A more recent investigation (ref. 59) found that a minor variation of equation (45) in which $T_d = T^{.7}T_v^{.3}$ gave results for reaction rate coefficients that were within a factor of 3 of those calculated on the basis of the theory of Schwartz, Slawsky, and Herzfeld (SSH theory, ref. 60). It is also assumed that the rate-controlling temperature for electron impact ionization is T_V (T_e for a three-temperature model) because the free-electron translational energy and electronic excitation energy characterize these reactions. All other reactions are characterized by the heavy-particle translational-rotational temperature T.

The forward and backward reaction rate coefficients can now be expressed by

$$k_{f,r} = C_{f,r}T_q^{n_{f,r}} \exp(-E_{f,r}/kT_q) \tag{46a}$$

$$k_{b,r} = \frac{k_{f,r}(T)}{K_{c,r}} \tag{46b}$$

where $K_{c,r}$ is the equilibrium constant for the r reaction and the preexponential parameters $C_{f,r}$ and $n_{f,r}$ and the activation energy $E_{f,r}$ divided by the Boltzmann constant k are presented in table III. The reactions, from which $\beta_{s,r}$ and $\alpha_{s,r}$ can be deduced, are also presented in table III. The term T_q is a dummy variable for the rate-controlling temperature. The equilibrium constant can be determined from the activation energy of the forward reaction and the partition functions of the reactants and products (ref. 52). Park (ref. 61) employed a curve fit for the equilibrium constant of the form

$$K_{c,r} = \exp(B_1^r + B_2^r \ln Z + B_3^r Z + B_4^r Z^2 + B_5^r Z^3) \tag{47}$$

where

$$Z = 10\,000/T \tag{48}$$

and the constants B_i^r are presented in table III.

Reaction Sets and Reaction Rate Coefficients

Two sets of chemical reactions and reaction rate coefficients have been employed within the context of a two-temperature environment. There is no overwhelming evidence at this time to prefer one over the other, so both are presented.

Park's proposed set of chemical reactions and reaction rate coefficients for his two-temperature model (ref. 32) are presented in table III as outlined in the previous section. He has provided a set of guidelines for defining the rate-controlling temperature in different types of reactions. These same guidelines have been applied to another set of chemical reactions and reaction rate coefficients proposed by Dunn and Kang (ref. 25). The list of reactions and associated parameters for Dunn and Kang's chemical kinetic model are presented in table IV. This model was originally presented in the context of a single temperature, but Park's guidelines for defining the rate-controlling temperature in dissociative and electron impact ionization reactions have been employed. Dunn and Kang defined the backward rate coefficient directly in the form

$$k_{b,r} = C_{b,r}T^{n_{b,r}} \exp(-E_{b,r}/kT) \tag{49}$$

The parameters needed to define equation (49) are included in table IV.

Vibrational Energy Reactive Source Terms

The variable $\widehat{D}_s$, which appears in equations (3) and (16), represents the vibrational energy per unit mass of the diatomic molecules, which are created or destroyed at rate $\dot{w}_s$. If one assumes preferential dissociation and recombination of molecules in the higher vibrational states (i.e., a molecule is more likely to dissociate if it is in a higher vibrational state and atoms that recombine are more likely to create molecules in a higher vibrational state), then $\widehat{D}_s$ should be larger than the average vibrational energy $e_{v,s}$ or $e_{V,s}$ of the system. The value of $\widehat{D}_s$ could be taken as some fraction of the dissociation energy of the molecule, $\widetilde{D}_s$. Thus,

$$\widehat{D}_s = \hat{c}_1 \widetilde{D}_s \tag{50a}$$

where $\hat{c}_1$ is a constant less than 1 and values for $\widetilde{D}_s$ are provided in table I. Park (ref. 62) has recently suggested a similarly motivated definition,

$$\widehat{D}_s = \widetilde{D}_s - kT \tag{50b}$$

which assumes that the vibrational energy removed by dissociation of one molecule comes from an energy level which differs from the dissociation energy by the average translational energy. A value of $\hat{c}_1 = 0.8$ has been used in equation (50a) for some test calculations. (Recent theoretical work of Sharma, Huo, and Park (ref. 59) indicates a value of $\hat{c}_1 = 0.3$ may be more appropriate.) In practice, the application of either equation (50a) (with $\hat{c}_1 = 0.8$) or equation (50b) tends to lower substantially the vibrational temperature behind the shock where dissociation occurs and to raise substantially the vibrational temperature in the boundary layer where recombination occurs when compared with a calculation using $\widehat{D}_s = e_{V,s}$. The substantial changes are caused by the large difference between $\widehat{D}_s$ and $e_{V,s}$ in the test calculation when $\widehat{D}_s$ is a factor of 10 or more greater than $e_{V,s}$ across the shock layer. In light of this result, a more moderate approximation (though still empirical) is to define

$$\widehat{D}_s = \hat{c}_2 e_{V,s} \tag{51}$$

where $\hat{c}_2$ is a constant greater than 1 for the preferential dissociation model and equal to 1 for a nonpreferential model. This approximation implies that the preferentially dissociated molecules are generally in higher vibrational states than the average molecule but need not be near the dissociation energy before a collision in order to dissociate.

Electronic Energy Reactive Source Terms

The term $\sum_{s=6}^{10} \dot{n}_{e,s} \widehat{I}_s$ in equations (4) and (16) accounts for the rate of electron energy loss when a free electron strikes a neutral particle and frees another electron (ionizes the particle), with a resulting loss in electron translational energy. The subscripts $6 \leq s \leq 10$ account for the five ionized species which potentially should be considered, $\dot{n}_{e,s}$ is the molar rate of ionization producing these species, and $\widehat{I}_s$ is the first ionization energy of the species per mole and is presented in table I. The only reactions considered in either the Park model or the Dunn and Kang model involving electron impact ionization are

$$\mathrm{O} + e^- \longleftrightarrow \mathrm{O}^+ + e^- + e^-$$

$$\mathrm{N} + e^- \longleftrightarrow \mathrm{N}^+ + e^- + e^-$$

The molar rate of ionization is simply the forward reaction rate $R_{f,r}$, where subscript r refers to the reactions listed above. Thus,

$$\dot{n}_{e,s} = R_{f,r} \tag{52}$$

where for $s = 6, r = 21$ for the Park model (table III) and $r = 22$ for the Dunn and Kang model (table IV), and for $s = 7, r = 20$ for the Park model and $r = 21$ for the Dunn and Kang model.

Note that this model assumes that all of the energy required to ionize the species comes from electron translational energy and the ionization energy is taken from the ground state. This probably overestimates the electronic energy loss rate due to electron impact ionization. In the test problems considered herein, this term is a small contributor to the overall energy balance in the two-temperature model.

Nonpreferential Dissociation and Recombination

The expressions for the reaction rate coefficients for dissociative reactions (eqs. (45) and (46)) and the definition of $\widehat{D}_s$ used in the vibrational energy reactive source term (eqs. (50) and (51)) are based on the concept, explained previously, that molecules in the higher vibrational modes are preferentially dissociated. However, Jaffe (ref. 63) used collision theory to evaluate the reaction rate coefficients for dissociative reactions in a multitemperature environment and predicted a much weaker dependence of $k_{f,r}$ on T_v than that predicted by Park's model. It may be argued that in situations when the free-stream kinetic energy per unit mass is much larger than the dissociation energies of the molecules, a vibrational ladder-climbing process is not required to dissociate the molecules. The methods of statistical mechanics give no preferential weighting to any particular energy mode in the determination of the total energy available in a collision and whether a collision will result in an elastic, inelastic, or reactive encounter. On this basis, the value of $\hat{c}_2$ in equation (51) should equal 1.0 and the value of T_q used in the Arrhenius term (exponential term) of equation (45) should be weighted by the energy available in all modes. For example,

$$T_q = \frac{\tilde{e}_t T + \tilde{e}_V T_V}{\tilde{e}_{\mathrm{tr}} + \tilde{e}_V} \tag{53}$$

where

$$\tilde{e}_{\mathrm{tr}} = \frac{\rho_{s1} e_{s1,t} + \rho_{s2} e_{s2,t}}{\rho_{s1} + \rho_{s2}} \tag{54a}$$

$$\tilde{e}_V = \frac{\rho_{s1} e_{s1,V} + \rho_{s2} e_{s2,V}}{\rho_{s1} + \rho_{s2}} \tag{54b}$$

and $s1$ and $s2$ are the indices of the reactants, $e_{s,t}$ is the translational and rotational energy per unit mass of species s, and $e_{s,V}$ is the vibrational and electronic energy per unit mass of species s. (In order to accommodate proper weighting at low temperatures (i.e., $T \approx 300$) it would be necessary to evaluate $e_{s,t}$ and $e_{s,V}$ with respect to a reference temperature of 0 K.) This specification has not yet been tested; however, sample calculations with either Park's geometric mean temperature (eq. (45)) or the translational temperature for dissociative rate constants give species energy distributions behind the shock that cause the value of T_q in equation (53) to be heavily weighted toward the translational temperature T.

The models developed from preferential and nonpreferential dissociation assumptions are empirical and are indicative of the uncertainty in the details of the kinetics. Further discussion of these points can be found in references 58, 60, and 64. Comprehensive quantum-mechanical theoretical studies and nonobtrusive laser diagnostic experimental studies are required to refine these models.

Relaxation Processes

Vibrational-Translational Energy Relaxation

Millikan and White (ref. 65) present semiempirical correlations between observed vibrational relaxation times over a temperature range of 300 to 8000 K and the relevant molecular constants. These correlations permit an estimation of τ_s^{MW}, the vibrational relaxation time for species s due to inelastic collisions. The correlation is expressed as

$$p\tau_s^{MW} = \frac{\sum_{j=1}^{10} n_j \exp\left[A_s\left(T^{-1/3} - 0/015\mu_{sj}^{1/4}\right) - 18.42\right]}{\sum_{j=1}^{10} n_j} \tag{55}$$

where μ_{sj} is the reduced molecular weight of the colliding species s and j, n_j is the number density of species j, and p is in atmospheres. Values of A_s for different molecules s are given in table I. (More recent correlations, valid over a temperature range of 300 to 9000 K, are presented in ref. 66.)

For temperatures above 8000 K, Park (ref. 29) suggests an expression for the vibrational relaxation time of the form

$$\tau_s^P = (\sigma_s \bar{c}_s n_s)^{-1} \tag{56}$$

where $\bar{c}_s$, the average molecular velocity of molecule s, is expressed by

$$\bar{c}_s = (8kT/\pi m_s)^{1/2} \tag{57}$$

n_s is the number density of molecule s, and σ_s is the effective cross section for vibrational relaxation. (Park noted that eq. (55) yields cross sections for vibrational relaxation that are far too large at temperatures above 8000 K.) The effective cross section is assumed to be an order of magnitude smaller than the elastic cross section. It is set equal to 10^{-16}cm^2 in the present model. The blending of the two relations is accomplished by defining

$$< \tau_s > = \tau_s^{MW} + \tau_s^P \tag{58}$$

Park has shown (ref. 29) that the variation of τ_s given by equation (58) agrees better with the available data for experimental O_2 vibrational relaxation time over a temperature range of 5000 to 8000 K than does the correlation of Millikan and White given by equation (55). More data are needed to better model the relaxation processes at high temperatures ($T > 8000$ K).

The vibrational energy relaxation terms in equations (3) and (16) can be further simplified by making the following approximations:

$$e_{v,s}^* - e_{v,s} \approx C_{v,v}^s (T - T_v) \tag{59}$$

$$\sum_{s=\text{mol.}} \frac{\rho_s C_{v,v}^s}{< \tau_s >} \approx \frac{\rho C_{v,v}}{\bar{\tau}_v} \tag{60}$$

where

$$\frac{1}{\bar{\tau}_v} = \frac{\sum_{s=\text{mol.}} \rho_s / M_s < \tau_s >}{\sum_{s=\text{mol.}} \rho_s / M_s} \tag{61}$$

These relations reduce the number of species-dependent parameters which must be evaluated and carried along in the calculation. They also permit the vibrational relaxation terms to be evaluated as a function of a single relaxation coefficient, given by equation (60), times the difference in the translational and vibrational temperatures. These approximations are believed to be consistent with the current model, which specifies a single vibrational temperature for all molecules. The temperature difference, which drives the relaxation process, is treated implicitly in the numerical algorithm. Test calculations show that the vibrational relaxation coefficient can be treated explicitly and time lagged, even at large Courant numbers, and still achieve stable, convergent solutions.

Note that the simple Landau-Teller equation for expressing vibrational relaxation rates used in equations (3) and (16) assumes that the relaxation rate varies linearly with the difference in the vibrational energies $e_v^* - e_v$. At high temperatures, vibrational relaxation obeys a diffusion-like equation with respect to vibrational energy levels (ref. 32), and a correction is needed for the vibrational relaxation time given by equation (61). Park (ref. 32) suggests an appropriate modification of the form

$$\frac{1}{\bar{\tau}_v^c} = \frac{1}{\bar{\tau}_v}\left|\frac{T_{\mathrm{sh}} - T_v}{T_{\mathrm{sh}} - T_{v,\mathrm{sh}}}\right|^{s-1} \tag{62}$$

where

$$s = 3.5\exp(-5000/T_{\mathrm{sh}}) \tag{63}$$

and T_{sh} and $T_{v,\mathrm{sh}}$ are respectively the translational-rotational and vibrational temperatures at the point on the shock where the relaxation process was initiated. (A recent paper (ref. 67) provides species-dependent characteristic temperatures for the argument of the exponential in eq. (63).) In one-dimensional flow, the determination of the post-shock temperatures is trivial. In two- or three-dimensional flow, a rigorous treatment of the model calls for tracing the streamline back to the point of origin at the shock. However, within the context of the total approximate nature of this model, it is more appropriate to choose some average post-shock temperature for multidimensional flows. The importance of this correction, as seen from the bridging formula of equation (62), depends on the magnitude of the average post-shock translational-rotational temperature.

Electronic-Translational Energy Relaxation

Term 6 of equation (4) and term 7 of equation (16) were derived by Appleton and Bray (ref. 28) to model the energy exchange for elastic collisions between electrons and atoms and between electrons and ions. The frictional heating of electrons by heavy particles due to differences between electron and heavy-particle velocities is ignored because of the assumption of ambipolar diffusion. Appleton and Bray's model was for plasmas which did not contain molecules with internal degrees of freedom. Their expressions for ν_{es}, the effective collision frequency of an electron with species s, are presented below for collision partners being either neutral or charged. For Coulomb collisions between electrons and ions, the expression is

$$\nu_{es} = \frac{8}{3}\left(\frac{\pi}{m_e}\right)^{1/2} n_s e^4 \frac{1}{(2kT_e)^{3/2}} \ln\left(\frac{k^3 T_e^3}{\pi n_e e^6}\right) \tag{64}$$

where n_e is the number density of electrons, n_s is the number density of species s, m_e is the electron mass, e is the magnitude of the electronic charge equal to 4.80298×10^{-10} esu, and k is Boltzmann's constant. For collisions between electrons and neutrals, the effective collision frequency is expressed as

$$\nu_{es} = n_s \sigma_{es}\left(\frac{8kT_e}{\pi m_e}\right)^{1/2} \tag{65}$$

where the effective electron-neutral energy exchange cross section is defined by a curve fit of the form

$$\sigma_{es} = \tilde{a}_s + \tilde{b}_s T_e + \tilde{c}_s T_e^2 \tag{66}$$

The constants for equation (66) are presented in table V. This curve fit was generated from effective collision cross-section data at 5000, 10 000, and 15 000 K found in reference 68.

Vibrational-Electronic Energy Relaxation

Term 6 of equation (3) and term 8 of equation (4) in the three-temperature model call for an approximation to the effective relaxation time for vibrational-electronic energy accommodation $< \tau_{es} >$. Recent data of this type are discussed by Lee (ref. 69) and Huo et al. (ref. 70). Much of these data are in tabular form, and no attempt was made to curve fit the data because of the emphasis on the two-temperature model.

Transport Properties

The derivation of the transport properties in this section closely follows the example of Lee (ref. 2). The approach is based on an extension of Yos' formula (ref. 71) to the multitemperature gas mixture. The collision integrals for heavy particles are based on the heavy-particle translational temperature T. The collision integrals for electrons with any other partner are based on the electron temperatures T_e or T_V. The collision integrals are evaluated as curve fits to the tabular data generated in reference 68. The curve fits assume a linear variation of $\log_{10}\left(\pi\overline{\Omega}_{sr}^{(1,1)}\right)$ and $\log_{10}\left(\pi\overline{\Omega}_{sr}^{(2,2)}\right)$ with $\ln(T)$, as defined by the data for these quantities at 2000 and 4000 K presented in table VI. Therefore,

$$\begin{aligned}
&\log_{10}\left(\pi\overline{\Omega}_{sr}^{(k,k)}\right) \\
&\quad = \log_{10}\left(\pi\overline{\Omega}_{sr}^{(k,k)}\right)(2000) \\
&\qquad + \frac{\log_{10}\left(\pi\overline{\Omega}_{sr}^{(k,k)}\right)(4000) - \log_{10}\left(\pi\overline{\Omega}_{sr}^{(k,k)}\right)(2000)}{\ln(4000) - \ln(2000)} \\
&\qquad \times [\ln(T) - \ln(2000)]
\end{aligned} \tag{67}$$

This temperature range is used to give the best overall agreement within the boundary layer for typical flow-field simulations. In equation (67), T_e or T_V is used for T in collisions involving electrons. The units of $\overline{\Omega}_{sr}$ are square centimeters. The data used in table VI assume an electron pressure of 0.001 atm. In general, the collision integrals should be corrected for the effects of varying electron pressure as discussed by Armaly and Sutton (refs. 72 and 73). The following formula of reference 68 may be employed to correct the collision integrals tabulated in table VI for a different electron pressure:

$$\frac{\pi\overline{\Omega}_{sr}^{(k,k)}(10^{-3})}{\pi\overline{\Omega}_{sr}^{(k,k)}(\tilde{p}_e)} = \frac{\ln[20.9(T/1000)^4 + 152(T/1000)^{8/3}]}{\ln[0.0209(T^4/10^{12}\tilde{p}_e) + 1.52(T^4/10^{12}\tilde{p}_e)^{2/3}]} \quad (68)$$

where $\tilde{p}_e$ is the electron pressure in atmospheres.

Two modified collision integrals which are used extensively in subsequent evaluations of transport properties are defined below.

$$\Delta_{sr}^{(1)}(T) = \frac{8}{3}\left[\frac{2M_sM_r}{\pi\overline{R}T(M_s+M_r)}\right]^{1/2}\pi\overline{\Omega}_{sr}^{(1,1)} \quad (69)$$

$$\Delta_{sr}^{(2)}(T) = \frac{16}{5}\left[\frac{2M_sM_r}{\pi\overline{R}T(M_s+M_r)}\right]^{1/2}\pi\overline{\Omega}_{sr}^{(2,2)} \quad (70)$$

The molar concentration of species s, γ_s, is also used extensively in subsequent calculations. It is defined as

$$\gamma_s = \frac{\rho_s}{\rho M_s} \quad (71)$$

The mixture viscosity μ can now be expressed as

$$\mu = \sum_{s=1}^{10}\frac{m_s\gamma_s}{\sum_{r=1}^{10}\gamma_r\Delta_{sr}^{(2)}(T) + \gamma_e\Delta_{se}^{(2)}(T_e)} + \frac{m_e\gamma_e}{\sum_{r=1}^{11}\gamma_r\Delta_{er}^{(2)}(T_e)} \quad (72)$$

The translational energy thermal conductivity of heavy particles η_t is expressed as

$$\eta_t = \frac{15}{4}k\sum_{s=1}^{10}\frac{\gamma_s}{\sum_{r=1}^{10}a_{sr}\gamma_r\Delta_{sr}^{(2)}(T) + 3.54\gamma_e\Delta_{se}^{(2)}(T_e)} \quad (73)$$

where a_{sr} is defined by

$$a_{sr} = 1 + \frac{[1-(m_s/m_r)][0.45 - 2.54(m_s/m_r)]}{[1+(m_s/m_r)]^2} \quad (74)$$

The rotational modes of molecules are assumed to be fully excited and the rotational energy thermal conductivity η_r is expressed as

$$\eta_r = k\sum_{s=\text{mol.}}\frac{\gamma_s}{\sum_{r=1}^{10}\gamma_r\Delta_{sr}^{(1)}(T) + \gamma_e\Delta_{se}^{(1)}(T_e)} \quad (75)$$

The frozen thermal conductivity of the mixture for translational and rotational energy of heavy particles η is now given by

$$\eta = \eta_t + \eta_r \quad (76)$$

The vibrational thermal conductivity η_v equals the rotational thermal conductivity η_r. Thus,

$$\eta_v = \eta_r \quad (77)$$

The electron thermal conductivity η_e follows the form of equation (73) and is given by

$$\eta_e = \frac{15}{4}k\frac{\gamma_e}{\sum_{r=1}^{11}1.45\gamma_r\Delta_{er}^{(2)}(T_e)} \quad (78)$$

The binary diffusion coefficient for a pair of heavy particles sr is defined as

$$D_{sr} = \frac{kT}{p\Delta_{sr}^{(1)}(T)} \quad (79)$$

The binary diffusion coefficient between electrons and heavy particles is expressed as

$$D_{er} = \frac{kT_e}{p\Delta_{er}^{(1)}(T_e)} \quad (80)$$

The effective diffusion coefficient of species s in the mixture, D_s, used in the governing equations can now be evaluated by

$$D_s = \frac{\gamma_t^2M_s(1-M_s\gamma_s)}{\sum_{\substack{r=1\\r\neq s}}^{11}(\gamma_r/D_{sr})} \quad (81)$$

where γ_t is defined by

$$\gamma_t = \sum_{s=1}^{11}\gamma_s \quad (82)$$

The diffusion of ions and electrons is linked because of the induced electric field which occurs in the presence of an electron pressure gradient. In a partially ionized gas with zero electric current, this

effect is modeled with the ambipolar diffusion coefficient D^a_{ion}, where

$$D^a_{\text{ion}} = 2D_{\text{ion}} \tag{83}$$

Each ion in a multicomponent gas mixture is assumed to diffuse as if it were the only ionic species in the mixture. Therefore, the effective diffusion coefficient of ions is set equal to the ambipolar diffusion coefficient as defined in equation (83). Within the context of the ambipolar diffusion approximation, the effective diffusion coefficient of electrons D_e is obtained by equating the diffusion velocity of electrons with the diffusion velocity of ions. This specification leads to the following relation for D_e:

$$D_e = m_e \frac{\sum_{s=6}^{10} D^a_s \gamma_s}{\sum_{s=6}^{10} m_s \gamma_s} \tag{84}$$

The relations in this section completely define all the transport properties used in the governing equations.

Upwind Formulation of the Flux Vector

Upwind, or total variation diminishing, numerical formulations of the governing conservation laws have been shown to be robust with regard to their capabilities to simulate hypersonic flows with strong shock waves and generally complex wave interactions (refs. 35, 36, 74, and 75). These formulations usually require a factorization of the Jacobian of the inviscid flux vector involving the right and left eigenvectors and the eigenvalues. In particular, if $\mathbf{f}$ is the inviscid flux vector and $\mathbf{q}$ is the vector of conserved variables, then the Jacobian of $\mathbf{f}$ with respect to $\mathbf{q}$ is given by

$$\frac{\partial \mathbf{f}}{\partial \mathbf{q}} = \mathbf{A} = \mathbf{L}\mathbf{\Lambda}\mathbf{R} \tag{85}$$

where $\mathbf{\Lambda}$ is a diagonal matrix composed of the eigenvalues of $\mathbf{A}$, $\mathbf{L}$ is a matrix of column eigenvectors, $\mathbf{R}$ is a matrix of row eigenvectors, and $\mathbf{LR}$ equals the identity matrix $\mathbf{I}$.

It is convenient to formulate the numerical solution of the governing equations within the context of a finite-volume scheme. The finite-volume schemes work with the integral forms of the conservation laws and set up approximations to flux across cell walls defined by the distribution of neighboring grid points. Once the cell wall is defined, it is a trivial procedure to define unit vectors which are normal and tangent to the cell wall. The extension to a finite-difference scheme is obtained by noting the relationship between the ratio of cell wall areas to cell volumes in the finite-volume formulations and the metric coefficients in finite-difference formulations (ref. 76).

The vector of conserved variables in the two-temperature model defined by equations (1), (2), (5), and (16) within the context of a finite-volume approximation is presented below.

$$\mathbf{q} = \begin{bmatrix} \rho_s \\ \rho u \\ \rho v \\ \rho w \\ \rho E \\ \rho e_V \end{bmatrix} \tag{86}$$

The inviscid flux vector for the two-temperature model is written as

$$\mathbf{f} = \begin{bmatrix} \rho U c_s \\ \rho U u + p n_x \\ \rho U v + p n_y \\ \rho U w + p n_z \\ \rho U H \\ \rho U e_V \end{bmatrix} \tag{87}$$

where c_s is the mass fraction of species s, defined by

$$c_s = \frac{\rho_s}{\rho} \tag{88}$$

n_x, n_y, and n_z are the x, y, and z components of a unit vector normal to a computational cell face, and U is the normal component of velocity through the cell face, defined by

$$U = un_x + vn_y + wn_z \tag{89}$$

It is useful in the evaluation of the eigenvectors to employ two unit vectors, $\mathbf{l}$ and $\mathbf{m}$, such that $\mathbf{n}$, $\mathbf{l}$, and $\mathbf{m}$ are mutually orthogonal (i.e., $n_i l_i = n_i m_i = l_i m_i = 0$). The velocity components in the $\mathbf{l}$ and $\mathbf{m}$ directions, tangent to the cell face, are then defined by

$$V = ul_x + vl_y + wl_z \tag{90}$$

$$W = um_x + vm_y + wm_z \tag{91}$$

The Jacobian of $\mathbf{f}$ with respect to $\mathbf{q}$ is expressed as

$$\mathbf{A} = \begin{bmatrix} U(\delta_{sr} - c_s) & c_s n_x & c_s n_y & c_s n_z & 0 & 0 \\ \tilde{\gamma}_r n_x - Uu & -\beta u n_x + u n_x + U & -\beta v n_x + u n_y & -\beta w n_x + u n_z & \beta n_x & \phi n_x \\ \tilde{\gamma}_r n_y - Uv & -\beta u n_y + v n_x & -\beta v n_y + v n_y + U & -\beta w n_y + v n_z & \beta n_y & \phi n_y \\ \tilde{\gamma}_r n_z - Uw & -\beta u n_z + w n_x & -\beta v n_z + w n_y & -\beta w n_z + w n_z + U & \beta n_z & \phi n_x \\ \tilde{\gamma}_r U - UH & -\beta u U + H n_x & -\beta v U + H n_y & -\beta w U + H n_z & \beta U + U & \phi U \\ -U e_V & e_V n_x & e_V n_y & e_V n_z & 0 & U \end{bmatrix} \tag{92}$$

The similarity transformation matrices $\mathbf{R}$ and $\mathbf{L}$ are defined as

$$\mathbf{R} = \begin{bmatrix} a^2\delta_{sr} - c_s\tilde{\gamma}_r & \beta u c_s & \beta v c_s & \beta w c_s & -\beta c_s & -\phi c_s \\ -V & l_x & l_y & l_z & 0 & 0 \\ -W & m_x & m_y & m_z & 0 & 0 \\ \tilde{\gamma}_r - Ua & a n_x - \beta u & a n_y - \beta v & a n_z - \beta w & \beta & \phi \\ \tilde{\gamma}_r + Ua & -a n_x - \beta u & -a n_y - \beta v & -a n_z - \beta w & \beta & \phi \\ -e_V\tilde{\gamma}_r & \beta u e_V & \beta v e_V & \beta w e_V & -\beta e_V & a^2 - \phi e_V \end{bmatrix} \tag{93}$$

$$\mathbf{L} = \begin{bmatrix} \delta_{sr}/a^2 & 0 & 0 & c_s/2a^2 & c_s/2a^2 & 0 \\ u/a^2 & l_x & m_x & (u + a n_x)/2a^2 & (u - a n_x)/2a^2 & 0 \\ v/a^2 & l_y & m_y & (v + a n_y)/2a^2 & (v - a n_y)/2a^2 & 0 \\ w/a^2 & l_z & m_z & (w + a n_z)/2a^2 & (w - a n_z)/2a^2 & 0 \\ [\beta(u^2 + v^2 + w^2) - \tilde{\gamma}_r]/\beta a^2 & V & W & (H + aU)/2a^2 & (H - aU)/2a^2 & -\phi/\beta a^2 \\ 0 & 0 & 0 & e_V/2a^2 & e_V/2a^2 & 1/a^2 \end{bmatrix} \tag{94}$$

The diagonal matrix of eigenvalues of $\mathbf{A}$ is defined by

$$\mathbf{\Lambda} = \begin{bmatrix} U & 0 & 0 & 0 & 0 & 0 \\ 0 & U & 0 & 0 & 0 & 0 \\ 0 & 0 & U & 0 & 0 & 0 \\ 0 & 0 & 0 & U+a & 0 & 0 \\ 0 & 0 & 0 & 0 & U-a & 0 \\ 0 & 0 & 0 & 0 & 0 & U \end{bmatrix} \tag{95}$$

In the matrices defined above, the first row and column correspond to the 11-species continuity equations. Subscript s refers to row s and species s and subscript r refers to column r and species r, where both s and r vary from 1 to 11 in the present model. The variables β, ϕ, and $\tilde{\gamma}_r$ are related to the partial derivatives of pressure with respect to $\mathbf{q}$, and a is the frozen speed of sound. These quantities are derived below.

The differential form of equations (8) and (9) for pressure can be written as

$$dp = \overline{R}T \sum_{s=1}^{10} \frac{d\rho_s}{M_s} + \overline{R}\, dT \sum_{s=1}^{10} \frac{\rho_s}{M_s} + \frac{\overline{R}T_V\ d\rho_e}{M_e} + \frac{\overline{R}\ dT_V\ \rho_e}{M_e} \tag{96}$$

We need to express dp as a function of $d\mathbf{q}$. This relation can be established by first expressing dT and dT_V as a function of de and de_V with the equations presented in the *Thermodynamic Relations* section. The two-temperature corollary to equation (32), written with respect to energy e as opposed to enthalpy h, is expressed as

$$e_s = \int_{T_{\text{ref}}}^{T} C_{v,tr}^s\ dT' + e_{V,s} + e_{s,o} \tag{97}$$

and

$$e_{V,s} = \int_{T_{\text{ref}}}^{T_V} C_{v,V}^s\ dT' \tag{98}$$

where

$$C_{v,tr}^s = C_{v,t}^s + C_{v,r}^s \tag{99a}$$

$$C_{v,V}^s = C_{v,v}^s + C_{v,e}^s \tag{99b}$$

It is convenient to define the specific heat capacity at constant volume for a free electron as $C_{v,V}^e$ and to set $C_{v,tr}^e = 0$ because the energy of an electron is a function only of T_V. The differential forms of equations (97) and (98) are given by

$$de_s = C_{v,tr}^s\ dT + C_{v,V}^s\ dT_V \tag{100}$$

and

$$de_{V,s} = C_{v,V}^s\ dT_V \tag{101}$$

Recall that

$$e = \sum_{s=1}^{11} c_s e_s \tag{102}$$

and

$$e_V = \sum_{s=1}^{11} c_s e_{V,s} \tag{103}$$

so the differential expressions for de and de_V can be written

$$de = \sum_{s=1}^{11} dc_s\ e_s + \sum_{s=1}^{11} c_s\ de_s = \sum_{s=1}^{11} dc_s\ e_s + \sum_{s=1}^{11} c_s(C^s_{v,tr}\ dT + C^s_{v,V}\ dT_V) \tag{104}$$

$$de_V = \sum_{s=1}^{11} dc_s\ e_{V,s} + \sum_{s=1}^{11} c_s\ de_{V,s} = \sum_{s=1}^{11} dc_s\ e_{V,s} + \sum_{s=1}^{11} c_s C^s_{v,V}\ dT_V \tag{105}$$

Solve for dT and dT_V with equations (104) and (105) to obtain

$$dT = \frac{de - de_V - \sum_{s=1}^{11} dc_s(e_s - e_{V,s})}{C_{v,tr}} \tag{106}$$

$$dT_V = \frac{de_V - \sum_{s=1}^{11} dc_s\ e_{V,s}}{C_{v,V}} \tag{107}$$

where equations (39) and (88) have been used to obtain the heat capacities of the mixture. The differential form of energy de, vibrational energy de_V, and mass fraction dc_s can be written with respect to the elements of $d\mathbf{q}$ from equations (13), (86), and (88) as follows:

$$de = \frac{d\rho E - E\ d\rho - (u\ d\rho u + v\ d\rho v + w\ d\rho w) + (u^2 + v^2 + w^2)d\rho}{\rho} \tag{108}$$

$$de_V = \frac{d\rho e_V - e_V\ d\rho}{\rho} \tag{109}$$

$$dc_s = \frac{d\rho_s - c_s\ d\rho}{\rho} \tag{110}$$

Note that $d\rho$ is easily expressed in terms of the elements of $d\mathbf{q}$ by

$$d\rho = \sum_{s=1}^{11} d\rho_s \tag{111}$$

Substitute equations (106) to (111) into equation (96) and combine terms to obtain

$$dp = \beta(d\rho E - u\ d\rho u - v\ d\rho v - w\ d\rho w) + \phi\ d\rho e_V + \tilde{\gamma}_s\ d\rho_s \tag{112}$$

where

$$\beta = \frac{\partial p}{\partial \rho E} = \frac{\overline{R}}{\rho C_{v,tr}} \sum_{r=1}^{10} \frac{\rho_r}{M_r} \tag{113}$$

$$\phi = \frac{\partial p}{\partial \rho e_V} = \frac{\overline{R}}{\rho C_{v,V}} \frac{\rho_e}{M_e} - \beta \tag{114}$$

and

$$\tilde{\gamma}_s = \frac{\partial p}{\partial \rho_s} = \frac{\overline{R} T_q}{M_s} + \beta \frac{u^2 + v^2 + w^2}{2} - \beta e_s - \phi e_{V,s} \tag{115}$$

In equation (115), $T_q = T_V$ when s is an electron; otherwise, $T_q = T$. The frozen speed of sound a can now be evaluated with equations (113) to (115):

$$a^2 = \sum_{s=1}^{11} c_s \tilde{\gamma}_s + \beta[H - (u^2 + v^2 + w^2)] + \phi e_V = (1 + \beta)\frac{p}{\rho} \tag{116}$$

This definition of a^2 comes from the evaluation of the eigenvalues of $\mathbf{A}$.

Results and Discussion

The task of validating the collection of physical models assembled here with regard to their predictive capabilities for hypersonic flows in chemical and thermal nonequilibrium is beyond the scope of this paper. Elements of the models have been validated to a limited extent in the original sources. However, validation of the ensemble in realistic conditions is currently limited because of the difficulty in obtaining the experimental data. It is expected that, as validation studies proceed using some data now available (refs. 77 and 78) and data which may be available in the near future (ref. 79), the models will evolve from the analytical forms or parametric curve fits presented herein. The present paper serves as a single source benchmark for these studies and provides guidance for implementation of the models in detailed computer codes.

Even without experimental data, it is still possible to compare results obtained from options presented herein to demonstrate the impact of uncertainties in various elements of the model. To this end, some predictions have been prepared using LAURA (refs. 35 and 36) with the strong implicit coupling (ref. 15) provided through equations (85) and (93) to (95). Comparisons with predictions made by a Direct-Simulation Monte Carlo (DSMC) algorithm (ref. 37), a kinetic-theory-based particle simulation approach to hypersonic, rarefied-flow analysis, provide additional opportunities to evaluate present capabilities. As with any continuum-based approximation scheme, the DSMC approach is also subject to physical modeling errors, particularly with regard to the description of real, reacting gases. However, the DSMC method is better at describing low-density flows and it does not require any a priori assumptions concerning the evaluation of dissipative phenomena as required in the Navier-Stokes approximation. These characteristics make DSMC a valuable benchmark for evaluating continuum-based Navier-Stokes flowfield solutions in transitional flow regimes.

Chemical Kinetic Model Studies

Profiles of mixture density, pressure, species number densities, and temperatures across the shock layer near the stagnation streamline over an axisymmetric approximation to the Aeroassist Flight Experiment (AFE) (refs. 37 and 79) are presented in figures 1(a) to 1(o). The free-stream conditions are free-stream velocity of 8917 m/s, free-stream density of 0.0000272 kg/m^3, and free-stream temperature of 197 K. These conditions correspond to an altitude of 78 km. Boundary conditions corresponding to a noncatalytic, no-slip cold wall under zero normal pressure gradient have been imposed. The grid is defined by 64 cells stretching from the body, across the captured shock, and into the free stream and 39 cells from the axis of symmetry to the circular shoulder. (Grid structure is discussed in more detail at the end of this section.) Comparisons are made between the predictions obtained with the chemical kinetic model of Dunn and Kang (D & K, ref. 25) (cases I and II) and the chemical kinetic model of Park (ref. 32) (case III). Equation (45) is used to define the rate-controlling temperatures for dissociation in both chemical kinetic models (cases I and III). In addition, a specification of $T_d = T$ is tested within the context of the Dunn and Kang chemical kinetic model (case II). The rate-controlling temperatures for recombination are set equal to the rate-controlling temperatures for dissociation. In general, the translational temperature should be used for such reactions; however, the translational temperature is very nearly equal to the vibrational temperature where recombination is significant in all test cases presented. Equation (51) is used to model the vibrational energy lost through dissociative reactions, with $\hat{c}_2 = 1$. The corrections defined by equations (62) and (63) are not applied to the calculation of the vibrational-translational relaxation time.

The mixture density and pressure are relatively insensitive to variations in the chemical kinetic models tested, as shown in figures 1(a) and 1(b). Only a slight variation in shock standoff distance is observed. Chemical nonequilibrium effects are shown in the slight overshoot of both neutral and ionized molecules behind the captured shock (figs. 1(e) to 1(g) and 1(j) to 1(l)). Specification of the geometric average temperature as the rate-controlling temperature inhibits dissociation, as expected, when compared with use of the heavy-particle translational

temperature (figs. 1(e) to 1(g)). There is significant formation of O_2 and NO occurring in the boundary layer at this condition, even with the noncatalytic wall boundary condition, as shown in figures 1(f) and 1(g). The greatest differences among the three chemical kinetic models are observed in their predictions of ionized-species profiles. Electron number density appears to arise from atomic oxygen over most of the shock layer (figs. 1(i) and 1(m)), with significant contributions from atomic nitrogen immediately behind the captured shock. Ionized molecular oxygen produced behind the shock is of the order of 0.01 percent of the total number density, but it quickly falls off as the molecule dissociates and accommodates to local conditions (fig. 1(k)). Species mole fraction profiles across the shock layer from case I for neutrals (fig. 2) and for ions (fig. 3) are presented in order to highlight the relative concentrations of the constituent species.

The chemical kinetic models of Dunn and Kang predict a significantly different profile for the deionization of N^+ and O^+ in the boundary layer than the model of Park (figs. 1(h) and 1(i)). The exact cause of these variations between the two chemical kinetic models is unknown at present, but both the reaction sets describing charge exchange and ionization and the reaction rate coefficients in these sets are very different.

Thermal nonequilibrium is evident in figures 1(n) and 1(o). The spike in translational temperature behind the captured shock is indicative of the delayed dissociation due to chemical nonequilibrium, and the corresponding low vibrational temperature shows the significant thermal nonequilibrium in this region. The specification of translational temperature as the rate-controlling temperature for dissociation yields lower peak translational temperatures, enhanced dissociation, and a more gradual accommodation of the vibrational temperature with the translational temperature.

Figure 4 presents the DSMC results, in addition to results for the other models, for species mole fraction and temperature profiles across the shock layer. Shock standoff distances for the continuum-based LAURA and the noncontinuum-based DSMC algorithm are approximately equal, as judged by the location of the peak in translational temperature. The DSMC shock thickness exceeds the LAURA prediction by about a factor of 3 as judged by the high gradient region in mole fraction of atomic nitrogen and oxygen spanning from $y = 0.001$ to post-shock levels. The DSMC methods generally predict thicker shocks than continuum-based methods and are expected to be more accurate than continuum-based predictions in this regard at low densities because of their ability to better simulate the random motions of particles across the shock front. At present, continuum-based methods compute this dissipation of mass, momentum, and energy due to random thermal motions of particles as a linear function of gradients in the flow field. They have no mechanism to recognize the significant change in mean free path across the shock front and generally utilize computational cells that are less than a mean free path in length ahead of the shock for hypersonic flows at 80 km and above.

The DSMC results show a separate rotational temperature in addition to the translational and vibrational temperatures (figs. 4(e) to 4(g)). These kinds of data arise from the modeling of diatomic molecules in the system and the monitoring of translational, rotational, and vibrational energies of such particles. The continuum prediction of peak heavy-particle temperature T, which includes both translational and rotational energies, falls between the peaks of the DSMC predictions for translational-rotational temperatures in case I and case III, as should be expected. The Park model (case III) gives the best overall agreement with temperature distribution across the shock layer as compared with DSMC predictions.

All three continuum chemical kinetic models and the DSMC predictions are in generally good agreement with the post-shock levels of species mole fraction for atomic nitrogen and oxygen (figs. 4(a) and 4(b)). Post-shock minimums in molecular nitrogen mole fraction vary from 0.04 to 0.08, with the DSMC showing the greatest concentration (lowest dissociation) of molecular nitrogen (fig. 4(c)). The most significant differences are in the predictions of electron number densities (fig. 4(d)). Only the DSMC prediction shows a well-defined peak in electron number density in this semilog plot. The sensitivity of this profile to details of the chemical kinetic and thermal relaxation models, with regard to both profile shape and peak profile values, makes electron number density measurements in flight an important contributor to help resolve unknowns in the present physical models.

All the continuum solutions are generated on identical grids with identical numerical parameters. Stagnation point heating values for these three cases are 205 kW/m^2 for the Dunn and Kang model with $T_d = (TT_v)^{1/2}$ (case I), 200 kW/m^2 for the Dunn and Kang model with $T_d = T$ (case II), and 184 kW/m^2 for the Park model with $T_d = (TT_v)^{1/2}$ (case III). Stagnation point heating for the DSMC calculation is 200 kW/m^2. In light of the many uncertainties with the physical models and the weak dependence of computed convective heat transfer rates on numerical parameters, the excellent agreement between the two

solution techniques is believed to be fortuitous. It is expected, based on results of references 18 and 80 and unpublished calculations using the present method, that larger differences between the flow fields predicted by continuum Navier-Stokes and noncontinuum DSMC algorithms will occur across the shock transition zone at approximately 90 km, but predictions of convective heating at the surface may agree up through 100 km for AOTV applications.

Grid Refinement Studies

The breakdown of the continuum-based methods in the transitional flow regime mentioned in the previous section leads to subtle contradictions with regard to evaluating solution accuracy with grid refinement studies. For example, if the goal is to obtain an accurate solution of a linear system of partial-differential equations and the approximation scheme is stable and consistent, then grid refinement studies yield computed (difference) solutions that converge to the exact solution (Lax's Equivalence Theorem, ref. 81). (This approach is used as well in the study of nonlinear systems of conservation laws, but care must be used in interpreting results because of the possibility of multiple, entropy-violating solution branches.) However, if the goal is to obtain an accurate simulation of physical phenomena under the constraint of a continuum-based Navier-Stokes approximation scheme, then excessive grid refinement may be counterproductive. The Navier-Stokes approximation fails to resolve accurately high Mach number shock structure. The failure arises from the inadequacy of linear functions of velocity and temperature gradients to describe correctly shear stresses and conduction in this high gradient region. Cell dimensions which are larger than a mean free path (cell Knudsen numbers smaller than 1) tend to give results which agree better with the DSMC calculations. Such a restriction on cell size must be viewed strictly as an empiricism which better mimics the DSMC shock structure and, perhaps, better models the dissipative phenomena across a shock, given the constraints of the Navier-Stokes approximation. These concerns become more acute as altitude increases or density decreases. For example, preliminary calculations from LAURA with shock-transition-zone Knudsen numbers greater than 1 (not presented herein) show a much greater difference in shock thickness at 90 km, where the free-stream density is a factor of 5 smaller than at 78 km. These problems of modeling dissipation with continuum-based methods in the transitional region between the free molecular and continuum flow regimes will need to be addressed more rigorously if routine application of these analysis tools to AOTV is to be achieved.

A grid refinement study was implemented which was designed to check the effects of truncation error on the computed solutions while maintaining a cell Knudsen number less than 1, as discussed above. Results of this study for test case I are presented in figures 5(a) to 5(j). Grids 1 and 2 are made up of 64 cells which are exponentially stretched from the body to the inflow boundary ahead of the shock. Grid 1 has a minimum cell size at the wall equal to 2.872×10^{-6} m and an average cell size through the shock transition zone equal to 1.5×10^{-2} m. Grid 2 has a minimum cell size at the wall equal to 105×10^{-4} m and an average cell size through the shock transition zone equal to 8.0×10^{-3} m. Grid 3 is made up of 128 exponentially stretched cells with a minimum cell size at the wall equal to 5.12×10^{-5} m and an average cell size through the shock transition zone equal to 4.0×10^{-3} m. The ratio of mean free path to cell size (cell Knudsen number) based on conditions at the beginning of the shock transition zone equals 0.193 for grid 1, 0.363 for grid 2, and 0.725 for grid 3. None of the grids violates the empirical constraint on minimum cell size discussed above, although grid 3 is very close to the limit. The cell Reynolds numbers[2] ($\rho a\ \Delta z/\mu$) at the body and in the shock transition zone are respectively 0.334 and 26.87 for grid 1, 10.8 and 12.2 for grid 2, and 5.5 and 5.27 for grid 3. Grid 1 sacrifices resolution at the shock for a very fine resolution through the boundary layer. Grids 2 and 3 utilize the same exponential stretching parameters. Grids 1 to 3 have the same lateral cell distribution around the body.[3] The actual distribution of mesh points across the shock layer is indicated by the symbol location in figures 5(a) to 5(d).

Figure 5(a) shows a sharper, higher peak in the translational temperature as the grid is refined across the captured shock. This trend is similar to one obtained in reference 82, which presents a simulation of the effects of a relatively coarse grid resolution of reacting flow crossing a normal shock through the use of artificial viscosity. The thickness of the peak

[2] The cell Reynolds number, as defined here, is proportional to the inverse of the cell Knudsen number because the viscosity μ is proportional to the product of density, sound speed, and mean free path ($\rho a \lambda$). The cell Reynolds number is often used to assess adequacy of the grid in the boundary-layer flows. The cell Knudsen number is a natural parameter to consider when dealing with low-density flows. Both are documented here for the readers' convenience.

[3] This study was completed sometime after the calculations were made for figs. 1 to 4. A different grid distribution function, which tended to an average of grids 1 and 2 in fig. 5, was used in the earlier work.

(thermal and chemical relaxation zone) for grid 3 is approximately equal to the DSMC result in figure 4(e). Further refinement would probably sharpen the peak a little more, but it is not clear that cell averages taken over a dimension less than the local mean free path would be physically meaningful. The temperature gradient approaching the wall is largest for grid 1. The vibrational-electronic temperature distribution is relatively insensitive to grid once the shock is crossed (fig. 5(b)). Differences in density (fig. 5(c)) relate mostly to the degree of dissociation of nitrogen and to the location of the shock transition zone. Post-shock-transition-zone pressure levels are independent of grid but the sharpness of the shock front is better resolved with the finest grid (fig. 5(d)). The mole fraction of atomic oxygen across the shock layer is insensitive to the grid (fig. 5(e)); however, the mole fractions of molecular and atomic nitrogen (fig. 5(f) and 5(g)) show some dependence on the shock-transition-zone processing of these species. Oxygen is fully dissociated at this condition and so is not sensitive to the details of the flow through the shock transition zone. Nitrogen is not fully dissociated and greater dependence on resolution through the shock transition zone is to be expected. Post-shock-transition-zone levels of molecular and atomic nitrogen are in good agreement for grids 2 and 3; but there is a trend in which coarse grids promote recombination in the boundary layer. There is generally good agreement across the entire shock layer for the predictions of O^+ from grids 2 and 3 (fig. 5(h)). The differences here tend to be less than the differences caused by unknowns in the physical models discussed previously for figure 4(d). Ionized molecular species appear only in the shock transition zone in any significant levels (fig. 5(i)). The rapid production and depletion of ionized, molecular species in the shock transition zone shows up as a small plateau in the free electron distribution (fig. 5(j)).

Concluding Remarks

The conservation equations for simulating hypersonic flows in thermal and chemical nonequilibrium and details of the associated physical models have been presented. These details include the curve fits used for defining thermodynamic properties of the 11-species air model (N, O, N_2, O_2, NO, N^+, O^+, N_2^+, O_2^+, NO^+, e^-), the curve fits for collision cross sections, the expressions for transport properties, the kinetic models, and the vibrational and electronic energy relaxation models. The expressions were formulated in the context of either a two- or three-temperature model. Greater emphasis is placed on the two-temperature model, in which it is assumed that the translational and rotational energy modes are in equilibrium at the translational temperature and the vibrational, electronic, and electron translational energy modes are in equilibrium at the vibrational temperature. The eigenvalues and eigenvectors associated with the Jacobian of the flux vector have also been presented in order to accommodate the "upwind" based numerical solutions of the complete equation set. Thermodynamic relations involving the partial derivatives of pressure with respect to the conserved variables were derived within the context of the two-temperature approximation.

Two chemical kinetic models and two prescriptions for the rate-controlling temperature of dissociation were studied and compared with Direct-Simulation Monte Carlo (DSMC) predictions for hypersonic flow over an axisymmetric approximation to the Aeroassist Flight Experiment vehicle. Differences among the models range from a factor of 2 for degree of dissociation to a factor of 10 for degree of ionization. Park's chemical kinetic model, which uses the most recent available kinetic data, is in closest agreement with the DSMC results for temperature distributions across the shock layer. All the predictions show that electron number density is balanced by the ionized atomic oxygen number density over most of the shock layer for the test condition. Predictions for neutral atomic species are in generally good agreement; however, the strong dependence of profile shape and magnitude of charged particles, particularly electrons, on variations in the kinetic models highlight the importance of obtaining more theoretical and experimental data at flight conditions for an aeroassisted orbital transfer vehicle (AOTV). Such data will be used to validate and improve the present chemical kinetic and thermal relaxation models so that the simulation of hypersonic flows at high altitudes (where chemical and thermal nonequilibrium effects are important) can proceed with greater confidence.

A grid refinement study was implemented to check the effects of truncation error on the computed solutions for one of the cases discussed above. Refinement of the shock transition zone sharpens and raises the peak translational temperature but has little influence on the post-shock-transition-zone translational or vibrational temperatures. Oxygen was fully dissociated in this test case, so the post-shock-transition-zone levels of atomic oxygen are insensitive to grid refinement. The two grids with the finest resolution through the shock transition zone predict equivalent levels of atomic and molecular nitrogen behind the shock. Nitrogen dissociation is inhibited by the coarsest grid through the shock transition zone. In a like manner, coarse grids tend to promote recombination in the boundary layer. Grid

refinement through the shock transition zone may be considered excessive when computational cell sizes become smaller than the local mean free path.

Limitations of the equations and models presented herein may be categorized as parametric and physical. Parametric limitations arise from uncertainties in modeling a physical process. For example, the equation sets discussed herein have the flexibility to model approximately the effects of preferential dissociation on the computed flow field. However, the magnitude of this effect is not fully understood at this time. Other parametric limitations include the thermodynamic and collision cross-section curve fits, particularly at high temperatures, and the chemical reaction sets. The constants within these models and/or the models themselves are likely to require adjustment as better data become available for comparison. Ultimately, the accuracy of the simulation is a function of the uncertainty in the values of the parameters which define the models.

Physical limitations arise from intentional simplifications and assumptions made to model the physical system. For example, the use of the Navier-Stokes equations implies a linear relation between velocity gradients and shear stresses which are not valid through strong shocks. At high altitudes and velocities, the internal shock structure becomes a significant part of the forebody merged layer flow field in which the shock and boundary layers overlap. Generally good comparisons between computed results from the continuum approach described herein and those from the kinetic approach which uses DSMC were obtained for a representative AOTV trajectory point at an altitude of 78 km (Mach 32).

Other physical limitations include the two-temperature approximation and the assumption of ambipolar diffusion. Neither of these approximations is expected to place any additional constraints on AOTV applications because of the preponderance of molecular nitrogen in the forebody flow field (compared with other molecules) and the relatively low ionization levels. At higher velocities, typical of Martian return, the two-temperature approximation may still prove valid over a significant portion of the aeropass when the flow is fully dissociated and vibrational energy contributions go to zero. Base and near-wake flow-field simulations are also of interest to AOTV designers because of payload protection. Cell Knudsen numbers will exceed 1 in this low-density region. The same concerns that limit Navier-Stokes approximations across strong shocks also apply across the low-density free shear layer. Comparisons with DSMC calculations and experimental data are required to fully understand the limitations of the continuum analysis in this region. Finally, the present model cannot account for plasma-dynamic effects. These are not expected to be important in a continuum, forebody flow field, where the estimated magnetic pressures are orders of magnitude smaller than the fluid pressures in AOTV applications. The importance of these effects in the base flow region, where electrical conductivity may be higher, is not known.

NASA Langley Research Center
Hampton, VA 23665-5225
November 8, 1988

References

1. Walberg, Gerald D.: A Survey of Aeroassisted Orbit Transfer. *J. Spacecr. & Rockets,* vol. 22, no. 1, Jan.–Feb. 1985, pp. 3–18.
2. Lee, Jong-Hun: Basic Governing Equations for the Flight Regimes of Aeroassisted Orbital Transfer Vehicles. *Thermal Design of Aeroassisted Orbital Transfer Vehicles,* H. F. Nelson, ed., Volume 96 of Progress in Astronautics and Aeronautics, American Inst. of Aeronautics and Astronautics, Inc., c.1985, pp. 3–53.
3. Park, Chul: Radiation Enhancement by Nonequilibrium in Earth's Atmosphere. AIAA-83-0410, Jan. 1983.
4. Grose, William L. (appendix A by Barbara L. Weigel): *A Thin-Shock-Layer Solution for Nonequilibrium, Inviscid Hypersonic Flows in Earth, Martian, and Venusian Atmospheres.* NASA TN D-6529, 1971.
5. Botta, Nicola; Pandolfi, Maurizio; and Germano, Massimo: Nonequilibrium Reacting Hypersonic Flow About Blunt Bodies: Numerical Prediction. AIAA-88-0514, Jan. 1988.
6. Blottner, F. G.: Nonequilibrium Laminar Boundary-Layer Flow of Ionized Air. *AIAA J.,* vol. 2, no. 11, Nov. 1964, pp. 1921–1927.
7. Nachtsheim, Philip R.: Multicomponent Diffusion in Chemically Reacting Laminar Boundary Layers. *1967 Heat Transfer and Fluid Mechanics Institute,* Stanford Univ. Press, June 1967, pp. 58–87.
8. Davy, William C.; Craig, Roger A.; and Lyle, Gilbert C.: An Evaluation of Approximations Used in the Analysis of Chemically Reacting, Stagnation-Point Boundary Layers With Wall Injection. *Proceedings of the 1970 Heat Transfer and Fluid Mechanics Institute,* Turgut Sarpkaya, ed., Stanford Univ. Press, 1970, pp. 222–237.
9. Dellinger, Thomas C.: Nonequilibrium Air Ionization in Hypersonic Fully Viscous Shock Layers. AIAA Paper No. 70-806, June–July 1970.
10. Moss, James N.: *Reacting Viscous-Shock-Layer Solutions With Multicomponent Diffusion and Mass Injection.* NASA TR R-411, 1974.
11. Adams, J. C.; Lewis, C. H.; Brahinsky, H. S.; and Marchand, E. O.: Effects of Chemical Nonequilibrium, Mass Transfer, and Viscous Interaction on Spherically Blunted Cones at Hypersonic Conditions. AIAA Paper No. 69-168, Jan. 1969.

12. Prabhu, D. K.; Tannehill, J. C.; and Marvin, J. G.: A New PNS Code for Chemical Nonequilibrium Flows. AIAA-87-0284, Jan. 1987.

13. Bhutta, Bilal A.; Lewis, Clark H.; and Kautz, Frederick A., II: A Fast Fully-Iterative Parabolized Navier-Stokes Scheme for Chemically-Reacting Reentry Flows. AIAA-85-0926, June 1985.

14. Widhopf, George F.; and Victoria, Keith J.: On the Solution of the Unsteady Navier-Stokes Equations Including Multicomponent Finite Rate Chemistry. *Comput. & Fluids,* vol. 1, no. 2, June 1973, pp. 159–184.

15. Gnoffo, Peter A.; and Greene, Francis A.: A Computational Study of the Flowfield Surrounding the Aeroassist Flight Experiment Vehicle. AIAA-87-1575, June 1987.

16. Li, C. P.: Chemistry-Split Techniques for Viscous Reactive Blunt Body Flow Computations. AIAA-87-0282, Jan. 1987.

17. Balakrishnan, A.: Application of a Flux-Split Algorithm to Chemically Relaxing, Hypervelocity Blunt-Body Flows. AIAA-87-1578, June 1987.

18. Gupta, Roop N.; and Simmonds, A. L.: Hypersonic Low-Density Solutions of the Navier-Stokes Equations With Chemical Nonequilibrium and Multicomponent Surface Slip. AIAA-86-1349, June 1986.

19. Bird, G. A.: *Molecular Gas Dynamics.* Oxford Univ. Press, 1976.

20. Bird, G. A.: Monte-Carlo Simulation in an Engineering Context. *Rarefied Gas Dynamics, Part I,* Sam S. Fisher, ed., Volume 74 of Progress in Astronautics and Aeronautics, American Inst. of Aeronautics and Astronautics, Inc., 1980, pp. 239–255.

21. Bird, G. A.: Simulation of Multi-Dimensional and Chemically Reacting Flows. *Rarefied Gas Dynamics, Volume I,* R. Campargue, ed., Commissariat a L'Energie Atomique, 1979, pp. 365–388.

22. Dunn, Michael G.: Comparison Between Predicted and Measured Blackout Boundaries for Earth Entry to Apollo. *The Entry Plasma Sheath and Its Effects on Space Vehicle Electromagnetic Systems, Volume I,* NASA SP-252, 1971, pp. 33–45.

23. Huber, P. W.; Evans, J. S.; and Schexnayder, C. J.: Comparison of Theoretical and Flight-Measured Ionization in a Blunt Body Reentry Flow Field. AIAA Paper No. 70-756, June–July 1970.

24. Kang, Sang-Wook; Jones, W. Linwood; and Dunn, Michael G.: Theoretical and Measured Electron-Density Distributions at High Altitudes. *AIAA J.,* vol. 11, no. 2, Feb. 1973, pp. 141–149.

25. Dunn, Michael G.; and Kang, Sang-Wook: *Theoretical and Experimental Studies of Reentry Plasmas.* NASA CR-2232, 1973.

26. Hall, J. Gordon; and Treanor, Charles E.: Nonequilibrium Effects in Supersonic-Nozzle Flows. AGARDograph 124, Dec. 1967.

27. Matsuzaki, Ri'ichi; and Hirabayashi, Noriaki: Prediction of Temperatures and Velocity in a Nonequilibrium Nozzle Flow of Air. AIAA-87-1477, June 1987.

28. Appleton, J. P.; and Bray, K. N. C.: The Conservation Equations for a Nonequilibrium Plasma. *J. Fluid Mech.,* vol. 20, pt. 4, Dec. 1964, pp. 659–672.

29. Park, Chul: Problems of Rate Chemistry in the Flight Regimes of Aeroassisted Orbital Transfer Vehicles. *Thermal Design of Aeroassisted Orbital Transfer Vehicles,* H. F. Nelson, ed., Volume 96 of Progress in Astronautics and Aeronautics, American Inst. of Aeronautics and Astronautics, Inc., c.1985, pp. 511–537.

30. Brown, Kevin G.: Chemical and Thermal Nonequilibrium Heat Transfer Analysis for Hypervelocity, Low Reynolds Number Flows. AIAA-85-1033, June 1985.

31. Candler, Graham V.; and MacCormack, Robert W.: The Computation of Hypersonic Ionized Flows in Chemical and Thermal Nonequilibrium. AIAA-88-0511, Jan. 1988.

32. Park, Chul: Assessment of Two-Temperature Kinetic Model for Ionizing Air. AIAA-87-1574, June 1987.

33. Camac, Morton; and Kemp, Nelson H.: *A Multitemperature Boundary Layer.* Res. Rep. 184 (Contract NASw-748), AVCO-Everett Research Lab., Div. of AVCO Corp., Aug. 1964.

34. Carlson, L. A.: *Radiative Transfer, Chemical Nonequilibrium, and Two Temperature Effects Behind a Reflected Shock Wave in Nitrogen.* Ph.D. Thesis, Ohio State Univ., 1969.

35. Gnoffo, Peter A.: Application of Program LAURA to Three-Dimensional AOTV Flowfields. AIAA-86-0565, Jan. 1986.

36. Gnoffo, Peter A.; McCandless, Ronald S.; and Yee, H. C.: Enhancements to Program LAURA for Computation of Three-Dimensional Hypersonic Flow. AIAA-87-0280, Jan. 1987.

37. Moss, James N.; Bird, Graeme A.; and Dogra, Virendra K.: Nonequilibrium Thermal Radiation for an Aeroassist Flight Experiment Vehicle. AIAA-88-0081, Jan. 1988.

38. Gupta, Roop N.; Scott, Carl D.; and Moss, James N.: *Slip-Boundary Equations for Multicomponent Nonequilibrium Airflow.* NASA TP-2452, 1985.

39. Hirschfelder, Joseph O.; Curtiss, Charles F.; and Bird, R. Byron: *Molecular Theory of Gases and Liquids.* John Wiley & Sons, Inc., c.1954.

40. Vincenti, Walter G.; and Kruger, Charles H., Jr.: *Introduction to Physical Gas Dynamics.* John Wiley & Sons, Inc., c.1965.

41. Bray, K. N. C.: Vibrational Relaxation of Anharmonic Oscillator Molecules: Relaxation Under Isothermal Conditions. *J. Phys. B (Proc. Phys. Soc.),* ser. 2, vol. 1, no. 4, July 1968, pp. 705–717.

42. Park, Chul: Calculation of Nonequilibrium Radiation in the Flight Regimes of Aeroassisted Orbital Transfer Vehicles. *Thermal Design of Aeroassisted Orbital Transfer Vehicles,* H. F. Nelson, ed., Volume 96 of Progress in Astronautics and Aeronautics, American Inst. of Aeronautics and Astronautics, Inc., c.1985, pp. 395–418.

43. Sutton, Kenneth: Air Radiation Revisited. *Thermal Design of Aeroassisted Orbital Transfer Vehicles*, H. F. Nelson, ed., Volume 96 of Progress in Astronautics and Aeronautics, American Inst. of Aeronautics and Astronautics, Inc., c.1985, pp. 419–441.
44. Balakrishnan, A.; Park, Chul; and Green, Michael J.: Radiative Viscous Shock Layer Analysis of Fire, Apollo, and PAET Flight Data. *Thermophysical Aspects of Re-Entry Flows,* James N. Moss and Carl D. Scott, eds., Volume 103 of Progress in Astronautics and Aeronautics, American Inst. of Aeronautics and Astronautics, Inc., 1985, pp. 514–540. (Available as AIAA-85-1064.)
45. Gupta, Roop N.: Navier-Stokes and Viscous Shock-Layer Solutions for Radiating Hypersonic Flows. AIAA-87-1576, June 1987.
46. Okuno, Arthur F.; and Park, Chul: Stagnation-Point Heat Transfer Rate in Nitrogen Plasma Flows: Theory and Experiment. *Trans. ASME, Ser. C: J. Heat Transf.*, vol. 92, no. 3, Aug. 1970, pp. 372–384.
47. Esch, D. D.; Siripong, A.; and Pike, R. W.: *Thermodynamic Properties of Polynomial Form for Carbon, Hydrogen, Nitrogen, and Oxygen Systems From 300 to 15 000° K.* NASA CR-111989, 1970.
48. Gordon, Sanford; and McBride, Bonnie J.: *Computer Program for Calculation of Complex Chemical Equilibrium Compositions, Rocket Performance, Incident and Reflected Shocks, and Chapman-Jouguet Detonations.* NASA SP-273, 1971.
49. McBride, Bonnie J.; Heimel, Sheldon; Ehlers, Janet G.; and Gordon, Sanford: *Thermodynamic Properties to 6000° K for 210 Substances Involving the First 18 Elements.* NASA SP-3001, 1963.
50. Browne, William G.: *Thermodynamic Properties of Some Atoms and Atomic Ions.* Eng. Phys. Tech. Memo #2, Missile & Space Vehicle Dep., General Electric Co., May 14, 1962.
51. Browne, William G.: *Thermodynamic Properties of Some Diatoms and Diatomic Ions at High Temperatures.* Advanced Aerospace Phys. Tech. Memo. No. 8, Missile & Space Vehicle Dep., General Electric Co., May 14, 1962.
52. Davidson, Norman: *Statistical Mechanics.* McGraw-Hill Book Co., Inc., 1962.
53. Balakrishnan, A.: Correlations of Specific Heats of Air Species to 50,000 K. AIAA-86-1277, June 1986.
54. Sinanoglu, O.; and Pitzer, K. S.: Equation of State and Thermodynamic Properties of Gases at High Temperatures. I. Diatomic Molecules. *J. Chem. Phys.*, vol. 31, no. 4, Oct. 1959, pp. 960–967.
55. Moore, Charlotte E.: *Atomic Energy Levels as Derived From the Analyses of Optical Spectra. Volume I—^{1}H to ^{23}V.* NSRDS-NBS 35, U.S. Dep. of Commerce, Reissued Dec. 1971.
56. Rosen, B., ed.: *Spectroscopic Data Relative to Diatomic Molecules.* Volume 17 of International Tables of Selected Constants, Pergamon Press, Inc., 1970.
57. Treanor, Charles E.; and Marrone, Paul V.: Effect of Dissociation on the Rate of Vibrational Relaxation. *Phys. Fluids,* vol. 5, no. 9, Sept. 1962, pp. 1022–1026.
58. Marrone, Paul V.; and Treanor, Charles E.: Chemical Relaxation With Preferential Dissociation From Excited Vibrational Levels. *Phys. Fluids,* vol. 6, no. 9, Sept. 1963, pp. 1215–1221.
59. Sharma, Surendra P.; Huo, Winifred M.; and Park, Chul: The Rate Parameters for Coupled Vibration-Dissociation in a Generalized SSH Approximation—Schwartz, Slawsky, and Herzfeld. AIAA-88-2714, June 1988.
60. Schwartz, R. N.; Slawsky, Z. I.; and Herzfeld, K. F.: Calculation of Vibrational Relaxation Times in Gases. *J. Chem. Phys.*, vol. 20, no. 10, Oct. 1952, pp. 1591–1599.
61. Park, Chul: Convergence of Computation of Chemical Reacting Flows. *Thermophysical Aspects of Re-Entry Flows,* James N. Moss and Carl D. Scott, eds., Volume 103 of Progress in Astronautics and Aeronautics, American Inst. of Aeronautics and Astronautics, Inc., 1985, pp. 478–513. (Available as AIAA-85-0247.)
62. Park, Chul: Two-Temperature Interpretation of Dissociation Rate Data for N_2 and O_2. AIAA-88-0458, Jan. 1988.
63. Jaffe, Richard L.: Rate Constants for Chemical Reactions in High-Temperature Nonequilibrium Air. *Thermophysical Aspects of Re-Entry Flows,* James N. Moss and Carl D. Scott, eds., Volume 103 of Progress in Astronautics and Aeronautics, American Inst. of Aeronautics and Astronautics, Inc., 1985, pp. 123–151. (Available as AIAA-85-1038.)
64. Ford, D. I.; and Johnson, R. E.: Dependence of Rate Constants on Vibrational Temperatures: An Arrhenius Description. AIAA-88-0461, Jan. 1988.
65. Millikan, Roger C.; and White, Donald R.: Systematics of Vibrational Relaxation. *J. Chem. Phys.*, vol. 39, no. 12, Dec. 15, 1963, pp. 3209–3213.
66. Ali, A. W.: *The Harmonic and Anharmonic Models for Vibrational Relaxation and Dissociation of the Nitrogen Molecule.* NRL Memo. Rep. 5924, U.S. Navy, Dec. 31, 1986.
67. Candler, Graham; and Park, Chul: The Computation of Radiation From Nonequilibrium Hypersonic Flows. AIAA-88-2678, June 1988.
68. Gupta, Roop N.; Yos, Jerrold M.; and Thompson, Richard A.: *A Review of Reaction Rates and Thermodynamic and Transport Properties for the 11-Species Air Model for Chemical and Thermal Nonequilibrium Calculations to 30000 K.* NASA TM-101528, 1989.
69. Lee, Jong-Hun: Electron-Impact Vibrational Excitation Rates in the Flowfield of Aeroassisted Orbital Transfer Vehicles. *Thermophysical Aspects of Re-Entry Flows,* James N. Moss and Carl D. Scott, eds., Volume 103 of Progress in Astronautics and Aeronautics, American Inst. of Aeronautics and Astronautics, Inc., 1985, pp. 197–224. (Available as AIAA-85-1035.)
70. Huo, W. M.; McKoy, V.; Lima, M. A. P.; and Gibson, T. L.: Electron-Nitrogen Molecule Collisions in High-Temperature Nonequilibrium Air. *Thermophysical*

Aspects of Re-Entry Flows, James N. Moss and Carl D. Scott, eds., Volume 103 of Progress in Astronautics and Aeronautics, American Inst. of Aeronautics and Astronautics, Inc., 1985, pp. 152–196. (Available as AIAA-85-0134.)

71. Yos, Jerrold M.: *Transport Properties of Nitrogen, Hydrogen, Oxygen, and Air to 30,000° K.* Tech. Memo. RAD-TM-63-7 (Contract AF33(616)-7578), AVCO Corp., Mar. 22, 1963.
72. Armaly, Bassem F.; and Sutton, Kenneth: Viscosity of Multicomponent Partially Ionized Gas Mixtures. AIAA-80-1495, July 1980.
73. Armaly, Bassem F.; and Sutton, Kenneth: Thermal Conductivity of Partially Ionized Gas Mixtures. AIAA-81-1174, June 1981.
74. Yee, H. C.; and Shinn, Judy L.: Semi-Implicit and Fully Implicit Shock-Capturing Methods for Hyperbolic Conservation Laws With Stiff Source Terms. *AIAA 8th Computational Fluid Dynamics Conference—A Collection of Technical Papers,* June 1987, pp. 159–176. (Available as AIAA-87-1116.)
75. Montagné, J. L.; Yee, H. C.; and Vinokur, M.: *Comparative Study of High-Resolution Shock-Capturing Schemes for a Real Gas.* NASA TM-100004, 1987.
76. Gnoffo, Peter Anthony: *A Solution-Adaptive Finite-Volume Algorithm With Application to Problems in Planetary Entry.* Ph.D. Diss., Princeton Univ., 1983.
77. Miller, Charles G., III; Micol, John R.; and Gnoffo, Peter A.: *Laminar Heat-Transfer Distributions on Biconics at Incidence in Hypersonic-Hypervelocity Flows.* NASA TP-2213, 1985.
78. Evans, John S.; Schexnayder, Charles J., Jr.; and Huber, Paul W.: *Boundary-Layer Electron Profiles for Entry of a Blunt Slender Body at High Altitude.* NASA TN D-7332, 1973.
79. Jones, Jim J.: The Rationale for an Aeroassist Flight Experiment. AIAA-87-1508, June 1987.
80. Gupta, Roop N.; and Simmonds, Ann L.: Stagnation Flowfield Analysis for an Aeroassist Flight Experiment Vehicle. AIAA-88-2613, June 1988.
81. Richtmyer, Robert D.; and Morton, K. W.: *Difference Methods for Initial-Value Problems, Second ed.* Interscience Publ., c.1967.
82. Macaraeg, Michéle G.; and Streett, Craig L.: An Analysis of Artificial Viscosity Effects on Reacting Flows Using a Spectral Multi-Domain Technique. *Computational Fluid Dynamics,* G. de Vahl Davis and C. Fletcher, eds., Elsevier Science Publ., 1988, pp. 503–514.

Table I. Species Data

s	M_s	$h_{s,o}$, kcal/g-mole	$\widetilde{D}_s$, eV (a)	$\widehat{I}_s$, eV (a)	A_s
N	14	112.951		14.53	
O	16	59.544		13.614	
N_2	28	0	9.759	15.51	220
O_2	32	0	5.115	12.5	129
NO	30	21.6009	6.496	9.5	168
N^+	14	449.709			
O^+	16	374.867			
N_2^+	28	364.9392	8.712		220
O_2^+	32	280.2099	6.663		129
NO^+	30	237.3239	10.85		168
e^-	.00054860	0			

$^a 1$ eV $= 9.65 \times 10^7$ J/kg-mole $= \frac{9.65 \times 10^7}{M_s}$ J/kg.

Table II. Constants for Curve Fits of Thermodynamic Properties

(a) Neutrals

Species	Range (a)	A_1	A_2	A_3	A_4	A_5	A_6	Source
N	1	0.2503071E+01	−0.2180018E−04	0.5420528E−07	−0.5647560E−10	0.2099904E−13	0.5609890E+05	Ref. 48
N	2	.2450268E+01	.1066145E−03	−.7465337E−07	.1879652E−10	−.1025983E−14	.5611600E+05	Ref. 48
N	3	.2748E+01	−.3909E−03	.1338E−06	−.1191E−10	.3369E−15	.5609E+05	Ref. 47
N	4	−.1227990E+01	.1926850E−02	−.2437050E−06	.1219300E−10	−.1991840E−15	.5609000E+05	*b*
N	5	.1552020E+02	−.3885790E−02	.3228840E−06	−.9605270E−11	.9547220E−16	.5609000E+05	*b*
O	1	.2946428E+01	−.1638166E−02	.2421031E−05	−.1602843E−08	.3890696E−12	.2914760E+05	Ref. 48
O	2	.2542059E+01	−.2755061E−04	−.3102803E−08	.4551067E−11	−.4368051E−15	.2923080E+05	Ref. 48
O	3	.2546E+01	−.5952E−04	.2701E−07	−.2798E−11	.9380E−16	.29150E+05	Ref. 47
O	4	−.9787120E−02	.1244970E−02	−.1615440E−06	.8037990E−11	−.1262400E−15	.2915000E+05	*b*
O	5	.1642810E+02	−.3931300E−02	.2983990E−06	−.8161280E−11	.7500430E−16	.2915000E+05	*b*
N_2	1	.3674826E+01	−.1208150E−02	.2324010E−05	−.6321755E−09	−.2257725E−12	−.1061160E+04	Ref. 48
N_2	2	.2896319E+01	.1515486E−02	−.5723527E−06	.9980739E−10	−.6522355E−14	−.9058620E+03	Ref. 48
N_2	3	.3727E+01	.4684E−03	−.1140E−06	.1154E−10	−.3293E−15	−.1043E+04	Ref. 47
N_2	4	.9637690E+01	−.2572840E−02	.3301980E−06	−.1431490E−10	.2033260E−15	−.1043000E+04	*b*
N_2	5	−.5168080E+01	.2333690E−02	−.1295340E−06	.2787210E−11	−.2135960E−16	−.1043000E+04	*b*
O_2	1	.3625598E+01	−.1878218E−02	.7055454E−05	−.6763513E−08	.2155599E−11	−.1047520E+04	Ref. 48
O_2	2	.3621953E+01	.7361826E−03	−.1965222E−06	.3620155E−10	−.2894562E−14	−.1201980E+04	Ref. 48
O_2	3	.3721E+01	.4254E−03	−.2835E−07	.6050E−12	−.5186E−17	−.1044E+04	Ref. 47
O_2	4	.3486660E+01	.5238420E−03	−.3912340E−07	.1009350E−11	−.8871830E−17	−.1044000E+04	*b*
O_2	5	.3961980E+01	.3944550E−03	−.2950580E−07	.7397450E−12	−.6420930E−17	−.1044000E+04	*b*
NO	1	.4045952E+01	−.3418178E−02	.7981919E−05	−.6113931E−08	.1591907E−11	.9745390E+04	Ref. 48
NO	2	.3189000E+01	.1338228E−02	−.5289932E−06	.9591933E−10	−.6484793E−14	.9828330E+04	Ref. 48
NO	3	.3845E+01	.2521E−03	−.2658E−07	.2162E−11	−.6381E−16	.9764000E+04	Ref. 47
NO	4	.4330870E+01	−.5808630E−04	.2805950E−07	−.1569410E−11	.2410390E−16	.9764000E+04	*b*
NO	5	.2350750E+01	.5864300E−03	−.3131650E−07	.6049510E−12	−.4055670E−17	.9764000E+04	*b*

[a]Ranges as follows: 1—300 ≤ T ≤ 1000; 2—1000 ≤ T ≤ 6000; 3—6000 ≤ T ≤ 15 000; 4—15 000 ≤ T ≤ 25 000; 5—25 000 ≤ T ≤ 35 000.

[b]Previously unpublished data from ref. 18.

Table II. Concluded

(b) Ions and electrons

Species	Range (a)	A_1	A_2	A_3	A_4	A_5	A_6	Source
N^+	1	0.2727E+01	−0.2820E−03	0.1105E−06	−0.1551E−10	0.7847E−15	0.2254E+06	Ref. 47
N^+	2	.2727E+01	−.2820E−03	.1105E−06	−.1551E−10	.7847E−15	.2254E+06	Ref. 47
N^+	3	.2499E+01	−.3725E−05	.1147E−07	−.1102E−11	.3078E−16	.2254E+06	Ref. 47
N^+	4	.2385610E+01	.8349470E−04	−.5881510E−08	.1884970E−12	−.1611950E−17	.2254E+06	*b*
N^+	5	.2228570E+01	.1245820E−03	−.8763570E−08	.2620400E−12	−.2167420E−17	.2254E+06	*b*
O^+	1	.2498479E+01	.1141097E−04	−.2976139E−07	.3224653E−10	−.1237551E−13	.1879490E+06	Ref. 48
O^+	2	.2506048E+01	−.1446424E−04	.1244604E−07	−.4685847E−11	.6554887E−15	.1879470E+06	Ref. 48
O^+	3	.2944E+01	−.4108E−03	.9156E−07	−.5848E−11	.1190E−15	.1879000E+06	Ref. 47
O^+	4	.1278400E+01	.4086590E−03	−.2173100E−07	.3325180E−12	.6316040E−18	.1879000E+06	*b*
O^+	5	.1288860E+01	.4334250E−03	−.2675820E−07	.6215900E−12	−.4513150E−17	.1879000E+06	*b*
N_2^+	1	.3397000E+01	.4525000E−03	.1272000E−06	−.3879000E−10	.2459000E−14	.1826000E+06	*b*
N_2^+	2	.3397390E+01	.4524870E−03	.1272300E−06	−.3879340E−10	.2458950E−14	.1826000E+06	Ref. 47
N_2^+	3	.3369950E+01	.8628820E−03	−.1275510E−06	.8087120E−11	−.1879660E−15	.1826000E+06	Ref. 47
N_2^+	4	.4394250E+01	.1886760E−03	−.7127180E−08	−.1751090E−12	.6717580E−17	.1826000E+06	*b*
N_2^+	5	.3949290E+01	.3679480E−03	−.2691020E−07	.6711050E−12	−.5824370E−17	.1826000E+06	*b*
O_2^+	1	.3243000E+01	.1174000E−02	−.3900000E−06	.5437000E−10	−.2392000E−14	.1400000E+06	*b*
O_2^+	2	.3242980E+01	.1173910E−02	−.3900420E−06	.5437260E−10	−.2392320E−14	.1400000E+06	Ref. 47
O_2^+	3	.5168650E+01	−.8619690E−03	.2041410E−06	−.1300410E−10	.2494210E−15	.1400000E+06	Ref. 47
O_2^+	4	−.2801710E+00	.1667410E−02	−.1210740E−06	.3211290E−11	−.2834890E−16	.1400000E+06	*b*
O_2^+	5	.2044550E+01	.1031320E−02	−.7404630E−07	.1925750E−11	−.1746100E−16	.1400000E+06	*b*
NO^+	1	.3668506E+01	−.1154458E−02	.2175561E−05	−.4822747E−09	−.2784791E−12	.1180340E+06	Ref. 48
NO^+	2	.2888549E+01	.1521712E−02	−.5753124E−06	.1005108E−09	−.6604429E−14	.1181920E+06	Ref. 48
NO^+	3	.2214170E+01	.1776060E−02	−.4303860E−06	.4173770E−10	−.1282890E−14	.1181920E+06	Ref. 48
NO^+	4	−.3324050E+01	.2441960E−02	−.1905720E−06	.6858000E−11	−.9911240E−16	.1181920E+06	*b*
NO^+	5	−.4348760E+01	.2401210E−02	−.1445990E−06	.3381320E−11	−.2825510E−16	.1181920E+06	*b*
e^-	1	.2500000E+01	0	0	0	0	−.7453750E+03	Ref. 48
e^-	2	.2500000E+01	0	0	0	0	−.7453750E+03	Ref. 48
e^-	3	.2508E+01	−.6332E−05	.1364E−08	−.1094000E−12	.2934E−17	−.7450000E+03	Ref. 47
e^-	4	.250010E+01	−.311281E−09	.357207E−13	−.16036700E−17	.250707E−22	−.7450000E+03	*b*
e^-	5	.250010E+01	.301577E−09	−.226204E−13	.667344E−18	−.689169E−23	−.7450000E+03	*b*

[a]Ranges as follows: 1—$300 \le T \le 1000$; 2—$1000 \le T \le 6000$; 3—$6000 \le T \le 15\,000$; 4—$15\,000 \le T \le 25\,000$; 5—$25\,000 \le T \le 35\,000$.

[b]Previously unpublished data from ref. 18.

Table III. Kinetic Model of Park

r	Reaction	$C_{f,r}$	$n_{f,r}$	$E_{f,r}/k$	B_1^r	B_2^r	B_3^r	B_4^r	B_5^r
1	$O_2 + M \leftrightarrow 2O + M$ (M = N,O)	2.900E+23	−2.00	5.975E+04	2.855	0.988	−6.181	−0.023	−0.001
2	$O_2 + M \leftrightarrow 2O + M$ (M = N_2, O_2, NO, ions)	9.680E+22	−2.00	5.975E+04	2.855	.988	−6.181	−.023	−.001
3	$N_2 + N \leftrightarrow 2N + N$	1.600E+22	−1.60	1.132E+05	1.858	−1.325	−9.856	−.174	.008
4	$N_2 + O \leftrightarrow 2N + O$	4.980E+22	−1.60	1.132E+05	1.858	−1.325	−9.856	−.174	.008
5	$N_2 + M \leftrightarrow 2N + M$ (M = N_2, O_2)	3.700E+21	−1.60	1.132E+05	1.858	−1.325	−9.856	−.174	.008
6	$N_2 + NO \leftrightarrow 2N + NO$	4.980E+21	−1.60	1.132E+05	1.858	−1.325	−9.856	−.174	.008
7	$N_2 +$ ions $\leftrightarrow 2N +$ ions	8.300E+24	−1.60	1.132E+05	1.858	−1.325	−9.856	−.174	.008
8	$NO + M \leftrightarrow N + O + M$ (M = N, O, N_2, O_2, NO, ions)	7.950E+23	−2.00	7.550E+04	.792	−.492	−6.761	−.091	.004
9	$NO + O \leftrightarrow O_2 + N$	8.370E+12	0	1.945E+04	−2.063	−1.480	−.580	−.114	.005
10	$N_2 + O \leftrightarrow NO + N$	6.440E+17	−1.00	3.837E+04	1.066	−.833	−3.095	−.084	.004
11	$O_2^+ + O \leftrightarrow O_2 + O^+$	6.850E+13	−.52	1.860E+04	−.276	.888	−2.180	.055	−.003
12	$N_2 + N^+ \leftrightarrow N_2^+ + N$	9.850E+12	−.18	1.210E+04	.307	−1.076	−.878	−.004	−.001
13	$NO^+ + O \leftrightarrow NO + O^+$	2.750E+13	.01	5.100E+04	.148	−1.011	−4.121	−.132	.006
14	$N_2 + O^+ \leftrightarrow N_2^+ + O$	6.330E+13	−.21	2.220E+04	2.979	.382	−3.237	.168	−.009
15	$NO^+ + O_2 \leftrightarrow NO + O_2^+$	1.030E+16	−.17	3.240E+04	.424	−1.098	−1.941	−.187	.009
16	$NO^+ + N \leftrightarrow N_2^+ + O$	1.700E+13	.40	3.550E+04	2.061	.204	−4.263	.119	−.006
17	$N + O \leftrightarrow NO^+ + e^-$	1.530E+09	.37	3.200E+04	−7.053	−.532	−4.429	.150	−.007
18	$O + O \leftrightarrow O_2^+ + e^-$	3.850E+09	.49	8.060E+04	−8.692	−3.110	−6.950	−.151	.007
19	$N + N \leftrightarrow N_2^+ + e^-$	1.790E+09	.77	6.750E+04	−4.992	−.328	−8.693	.269	−.013
20	$O + e^- \leftrightarrow O^+ + e^- + e^-$	3.900E+33	−3.78	1.585E+05	−6.113	−2.035	−15.311	−.073	.004
21	$N + e^- \leftrightarrow N^+ + e^- + e^-$	2.500E+33	−3.82	1.686E+05	−3.441	−.577	−17.671	.099	−.005

Table IV. Kinetic Model of Dunn and Kang

r	Reaction	$C_{f,r}$	$n_{f,r}$	$E_{f,r}/k$	$C_{b,r}$	$n_{b,r}$	$E_{b,r}/k$
1	$O_2 + M \leftrightarrow 2O + M$ (M = N, NO)	3.600E+18	−1.00	5.950E+04	3.000E+15	−0.50	0.000E+00
2	$O_2 + O \leftrightarrow 2O + O$	9.000E+19	−1.00	5.950E+04	7.500E+16	−.50	.000E+00
3	$O_2 + O_2 \leftrightarrow 2O + O_2$	3.240E+19	−1.00	5.950E+04	2.700E+16	−.50	.000E+00
4	$O_2 + N_2 \leftrightarrow 2O + N_2$	7.200E+18	−1.00	5.950E+04	6.000E+15	−.50	.000E+00
5	$N_2 + M \leftrightarrow 2N + M$ (M = O, NO, O_2)	1.900E+17	−.50	1.130E+05	1.100E+16	−.50	.000E+00
6	$N_2 + N \leftrightarrow 2N + N$	4.085E+22	−1.50	1.130E+05	2.270E+21	−1.50	.000E+00
7	$N_2 + N_2 \leftrightarrow 2N + N_2$	4.700E+17	−.50	1.130E+05	2.720E+16	−.50	.000E+00
8	$NO + M \leftrightarrow N + O + M$ (M = O_2, N_2)	3.900E+20	−1.50	7.550E+04	1.000E+20	−1.50	.000E+00
9	$NO + M \leftrightarrow N + O + M$ (M = O, N, NO)	7.800E+21	−1.50	7.550E+04	2.000E+21	−1.50	.000E+00
10	$NO + O \leftrightarrow O_2 + N$	3.200E+09	1.00	1.970E+04	1.300E+10	1.00	3.580E+03
11	$N_2 + O \leftrightarrow NO + N$	7.000E+13	0	3.800E+04	1.560E+13	0	.000E+00
12	$O_2^+ + O \leftrightarrow O_2 + O^+$	2.920E+18	−1.11	2.800E+04	7.800E+11	.50	.000E+00
13	$N_2 + N^+ \leftrightarrow N_2^+ + N$	2.020E+11	.81	1.300E+04	7.800E+11	.50	.000E+00
14	$NO^+ + O \leftrightarrow NO + O^+$	3.630E+15	−.60	5.080E+04	1.500E+13	0	.000E+00
15	$N_2 + O^+ \leftrightarrow N_2^+ + O$	3.400E+19	−2.00	2.300E+04	2.480E+19	−2.20	.000E+00
16	$NO^+ + O_2 \leftrightarrow NO + O_2^+$	1.800E+15	.17	3.300E+04	1.800E+13	.50	.000E+00
17	$NO^+ + N \leftrightarrow NO + N^+$	1.000E+19	−.93	6.100E+04	4.800E+14	0	.000E+00
18	$N + O \leftrightarrow NO^+ + e^-$	1.400E+06	1.50	3.190E+04	6.700E+21	−1.50	.000E+00
19	$O + O \leftrightarrow O_2^+ + e^-$	1.600E+17	−.98	8.080E+04	8.000E+21	−1.50	.000E+00
20	$N + N \leftrightarrow N_2^+ + e^-$	1.400E+13	0	6.780E+04	1.500E+22	−1.50	.000E+00
21	$O + e \leftrightarrow O^+ + e^- + e^-$	3.600E+31	−2.91	1.580E+05	2.200E+40	−4.50	.000E+00
22	$N + e^- \leftrightarrow N^+ + e^- + e^-$	1.100E+32	−3.14	1.690E+05	2.200E+40	−4.50	.000E+00
23	$O_2 + N_2 \leftrightarrow NO + NO^+ + e^-$	1.380E+20	−1.84	1.410E+05	1.000E+24	−2.50	.000E+00
24	$N_2 + NO \leftrightarrow N_2 + NO^+ + e^-$	2.200E+15	−.35	1.080E+05	2.200E+26	−2.50	.000E+00
25	$NO^+ + O \leftrightarrow O_2 + N^+$	1.340E+13	.31	7.727E+04	1.000E+14	0	.000E+00
26	$O_2 + NO \leftrightarrow NO^+ + O_2 + e^-$	8.800E+16	−.35	1.080E+05	8.800E+26	−2.50	.000E+00

Table V. Constants for Curve Fits of Electron-Neutral Energy Exchange Cross Section, σ_{es}

s	$\bar{a}_s$	$\bar{b}_s$	$\bar{c}_s$
N	5E−20	0	0
O	1.2E−20	1.7E−24	−2E−29
N_2	7.5E−20	5.5E−24	−1E−28
O_2	2E−20	6E−24	0
NO	1E−19	0	0

Table VI. Collision Integrals for 11-Species Air Model at $p_e = 0.001$ atm

Pairs		$\log_{10}\left(\pi\overline{\Omega}_{sr}^{(1,1)}\right)$ at—		$\log_{10}\left(\pi\overline{\Omega}_{sr}^{(2,2)}\right)$ at—	
s	r	$T = 2000$ K	$T = 4000$ K	$T = 2000$ K	$T = 4000$ K
N	N	−14.08	−14.11	−14.74	−14.82
N	O	−14.76	−14.86	−14.69	−14.80
N	N_2	−14.67	−14.75	−14.59	−14.66
N	O_2	−14.66	−14.74	−14.59	−14.66
N	NO	−14.66	−14.75	−14.67	−14.66
N	N^+	−14.08	−14.11	−14.37	−14.49
N	O^+	−14.34	−14.46	−14.38	−14.50
N	N_2^+	−14.34	−12.19	−14.38	−14.50
N	O_2^+	−14.34	−12.19	−14.38	−14.50
N	NO^+	−14.34	−14.46	−14.38	−14.50
N	e^-	−15.30	−15.30	−15.30	−15.30
O	O	−14.11	−14.14	−14.71	−14.79
O	N_2	−14.63	−14.72	−14.55	−14.64
O	O_2	−14.69	−14.76	−14.62	−14.69
O	NO	−14.66	−14.74	−14.59	−14.66
O	N^+	−14.34	−14.46	−14.38	−14.50
O	O^+	−14.11	−14.14	−14.45	−14.58
O	N_2^+	−14.34	−14.46	−14.38	−14.50
O	O_2^+	−14.34	−14.46	−14.38	−14.50
O	NO^+	−14.34	−14.46	−14.38	−14.50
O	e^-	−15.94	−15.82	−15.94	−15.82
N_2	N_2	−14.56	−14.65	−14.50	−14.58
N_2	O_2	−14.58	−14.63	−14.51	−14.54
N_2	NO	−14.57	−14.64	−14.51	−14.56
N_2	N^2	−14.34	−14.46	−14.38	−14.50
N_2	O^+	−14.34	−14.46	−14.38	−14.50
N_2	N_2	−14.34	−14.46	−14.38	−14.50
N_2	O_2^+	−14.34	−14.46	−14.38	−14.50
N_2	NO^+	−14.34	−14.46	−14.38	−14.50
N_2	e^-	−15.11	−15.02	−15.11	−15.02

Table VI. Continued

Pairs		$\log_{10}\left(\pi\overline{\Omega}_{sr}^{(1,1)}\right)$ at—		$\log_{10}\left(\pi\overline{\Omega}_{sr}^{(2,2)}\right)$ at—	
s	r	$T = 2000$ K	$T = 4000$ K	$T = 2000$ K	$T = 4000$ K
O_2	O_2	−14.60	−14.64	−14.54	−14.57
O_2	NO	−14.59	−14.63	−14.52	−14.56
O_2	N^+	−14.34	−14.46	−14.38	−14.50
O_2	O^+	−14.34	−14.46	−14.38	−14.50
O_2	N_2^+	−14.34	−14.46	−14.38	−14.50
O_2	O_2^+	−14.34	−14.46	−14.38	−14.50
O_2	NO^+	−14.34	−14.46	−14.38	−14.50
O_2	e^-	−15.52	−15.39	−15.52	−15.39
NO	NO	−14.58	−14.64	−14.52	−14.56
NO	N^+	−14.34	−14.46	−14.38	−14.50
NO	O^+	−14.34	−14.46	−14.38	−14.50
NO	N_2^+	−14.34	−14.46	−14.38	−14.50
NO	O_2^+	−14.34	−14.46	−14.38	−14.50
NO	NO^+	−14.18	−14.22	−14.38	−14.50
NO	e^-	−15.30	−15.08	−15.30	−15.08
N^+	N^+	−11.70	−12.19	−11.49	−11.98
N^+	O^+	−11.70	−12.19	−11.49	−11.98
N^+	N_2^+	−11.70	−12.19	−11.49	−11.98
N^+	O_2^+	−11.70	−12.19	−11.49	−11.98
N^+	NO^+	−11.70	−12.19	−11.49	−11.98
N^+	e^-	−11.70	−12.19	−11.49	−11.98
O^+	O^+	−11.70	−12.19	−11.49	−11.98
O^+	N_2^+	−11.70	−12.19	−11.49	−11.98
O^+	O_2^+	−11.70	−12.19	−11.49	−11.98
O^+	NO^+	−11.70	−12.19	−11.49	−11.98
O^+	e^-	−11.70	−12.19	−11.49	−11.98
N_2^+	N_2^+	−11.70	−12.19	−11.49	−11.98
N_2^+	O_2^+	−11.70	−12.19	−11.49	−11.98
N_2^+	NO^+	−11.70	−12.19	−11.49	−11.98

Table VI. Concluded

Pairs		$\log_{10}\left(\pi\overline{\Omega}_{sr}^{(1,1)}\right)$ at—		$\log_{10}\left(\pi\overline{\Omega}_{sr}^{(2,2)}\right)$ at—	
s	r	$T = 2000$ K	$T = 4000$ K	$T = 2000$ K	$T = 4000$ K
N_2^+	e^-	−11.70	−12.19	−11.49	−11.98
O_2^+	O_2^+	−11.70	−12.19	−11.49	−11.98
O_2^+	NO^+	−11.70	−12.19	−11.49	−11.98
O_2^+	e^-	−11.70	−12.19	−11.49	−11.98
NO^+	NO^+	−11.70	−12.19	−11.49	−11.98
NO^+	e^-	−11.70	−12.19	−11.49	−11.98
e^-	e^-	−11.70	−12.19	−11.49	−11.98

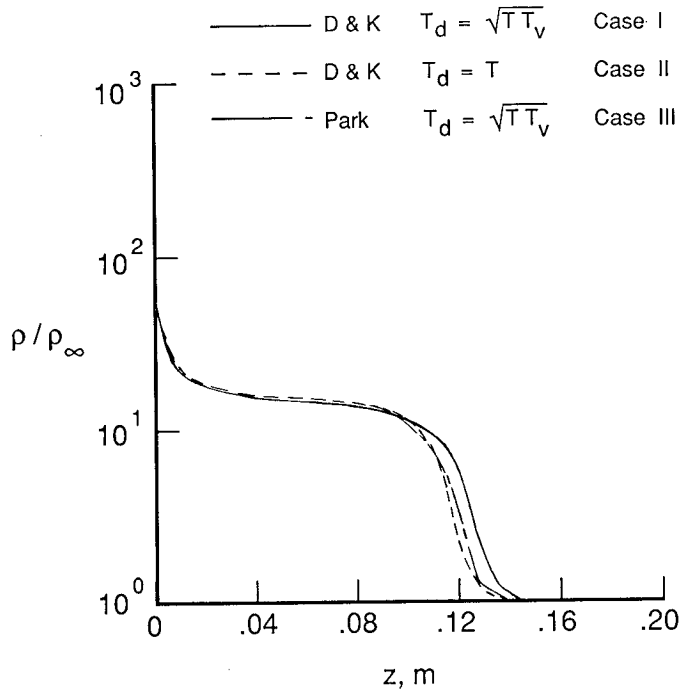

(a) Density, ρ/ρ_∞.

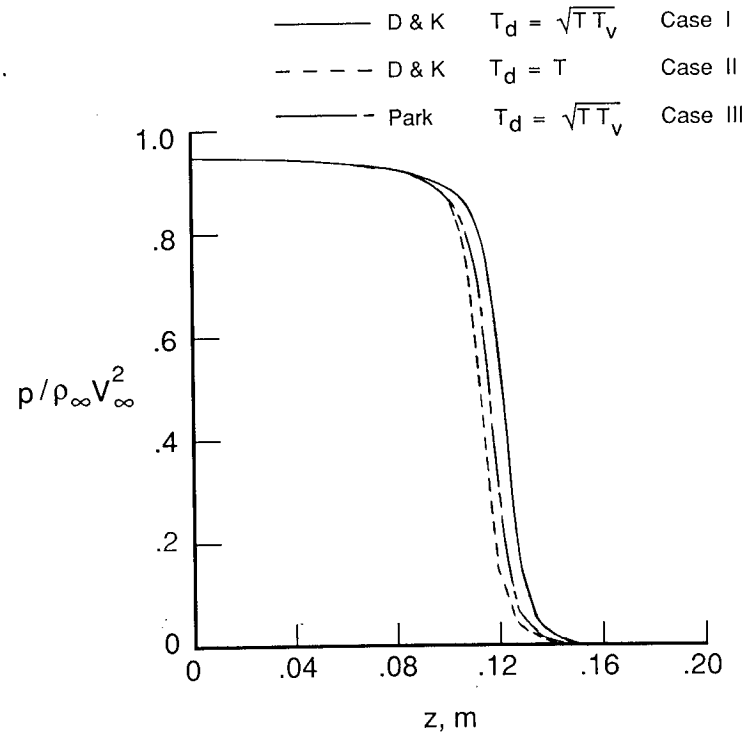

(b) Pressure, $p/\rho_\infty V_\infty^2$.

Figure 1. Stagnation streamline distributions across shock layer of axisymmetric approximation to Aeroassist Flight Experiment vehicle from three different chemical kinetic models.

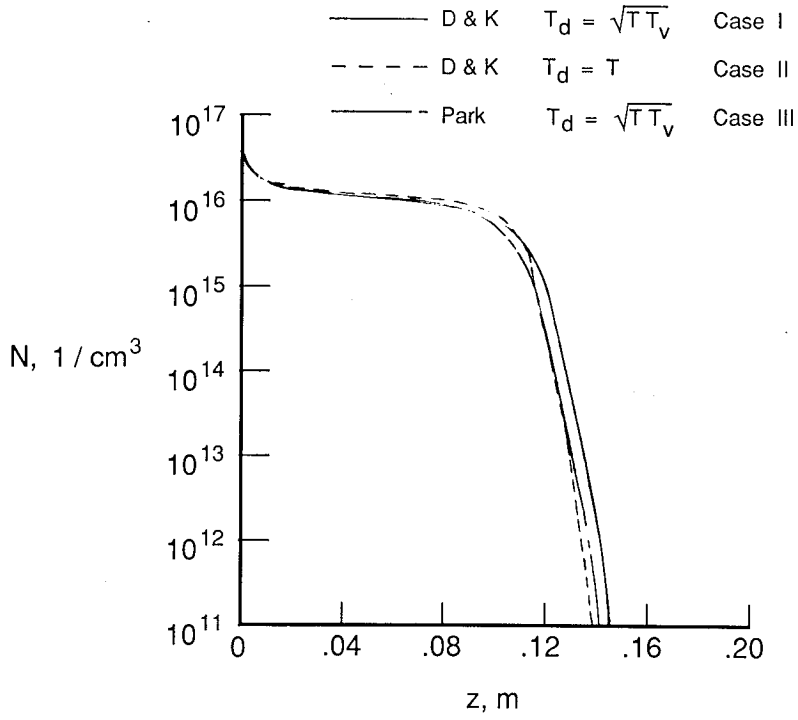

(c) N number density.

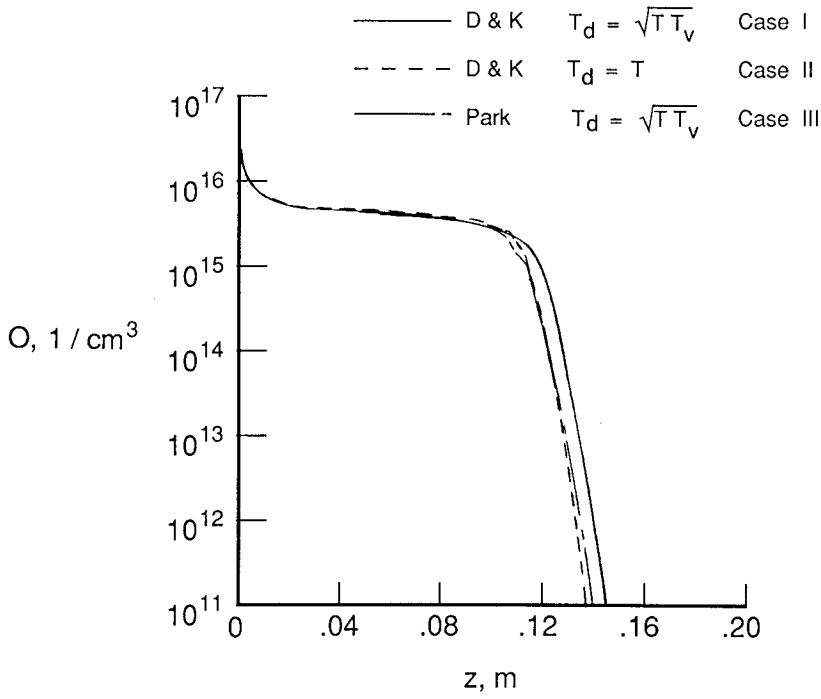

(d) O number density.

Figure 1. Continued.

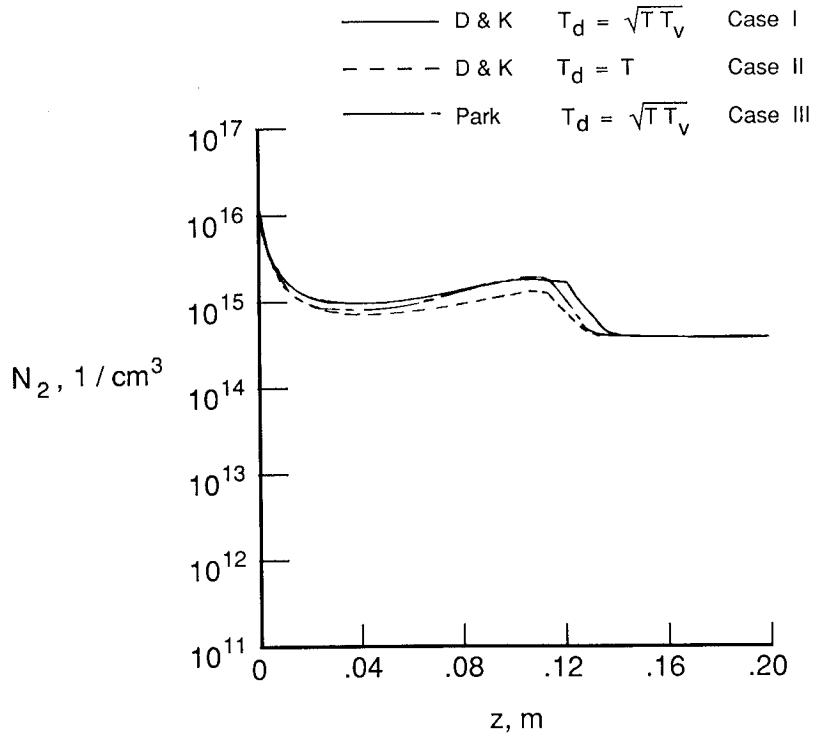

(e) N_2 number density.

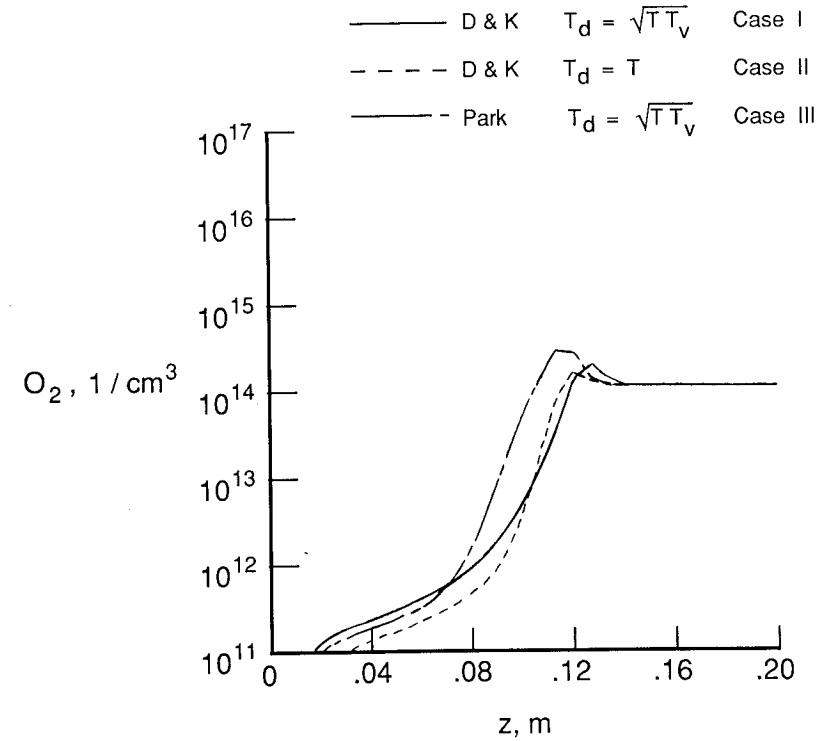

(f) O_2 number density.

Figure 1. Continued.

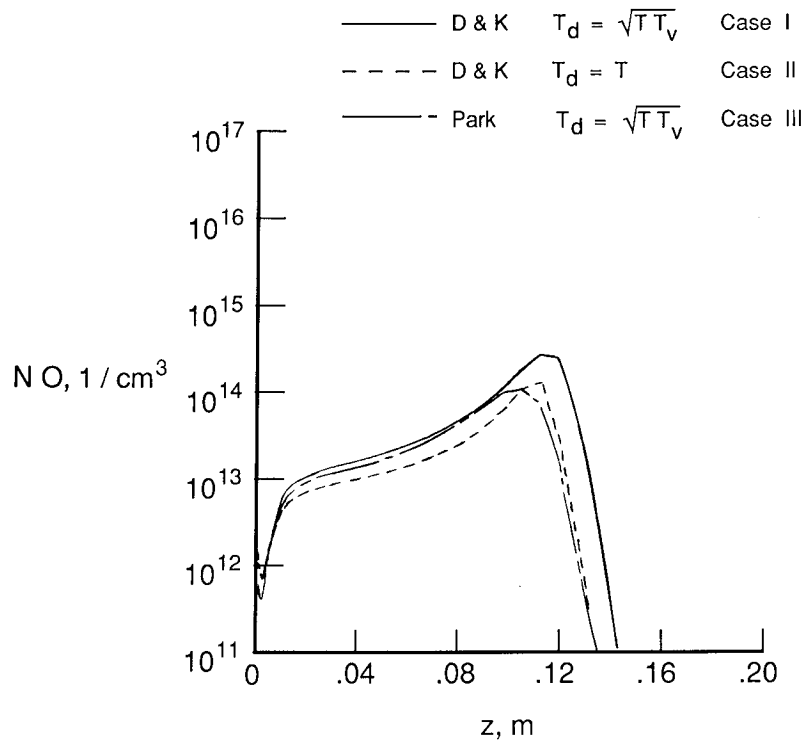

(g) NO number density.

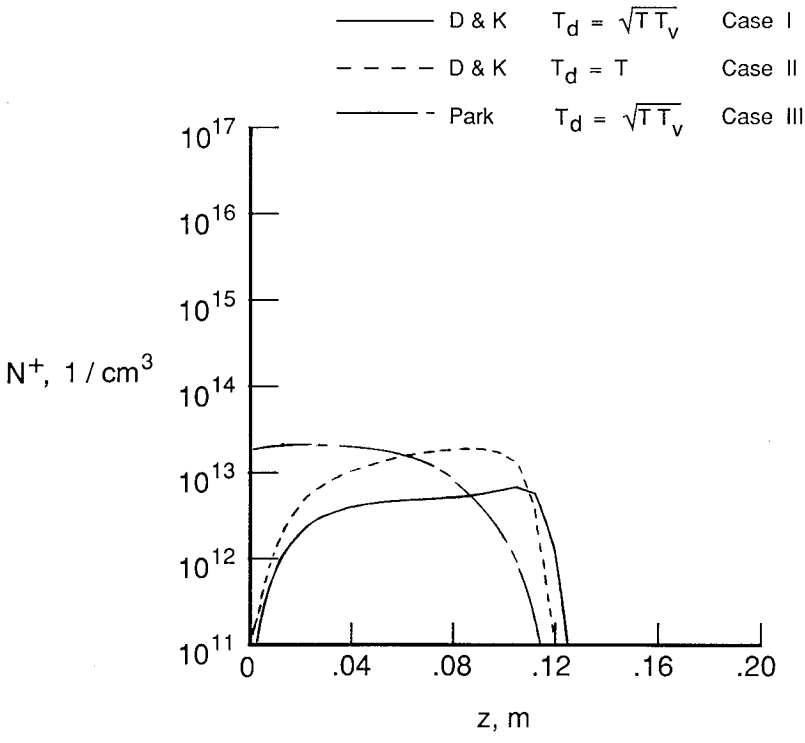

(h) N^+ number density.

Figure 1. Continued.

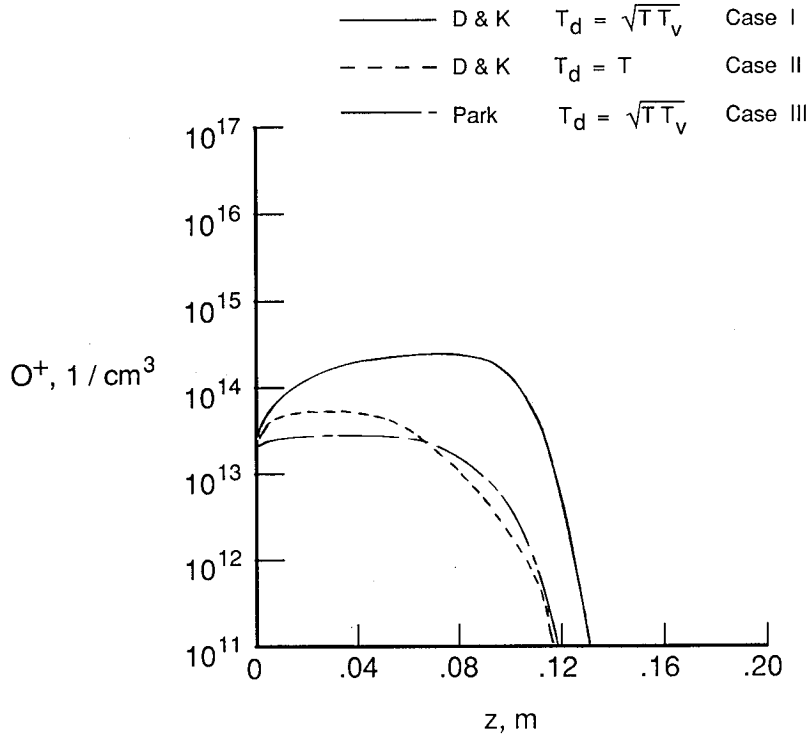

(i) O^+ number density.

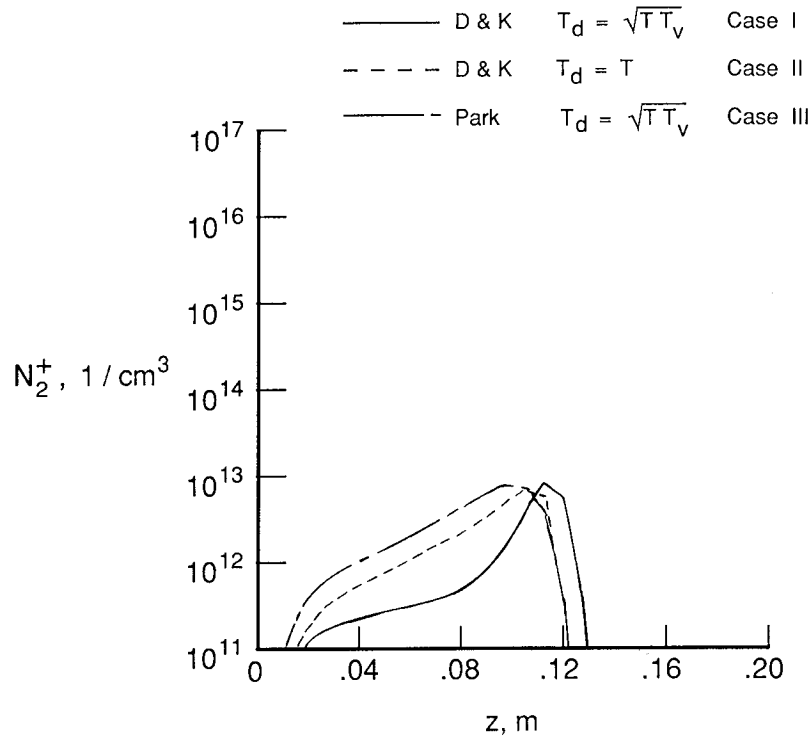

(j) N_2^+ number density.

Figure 1. Continued.

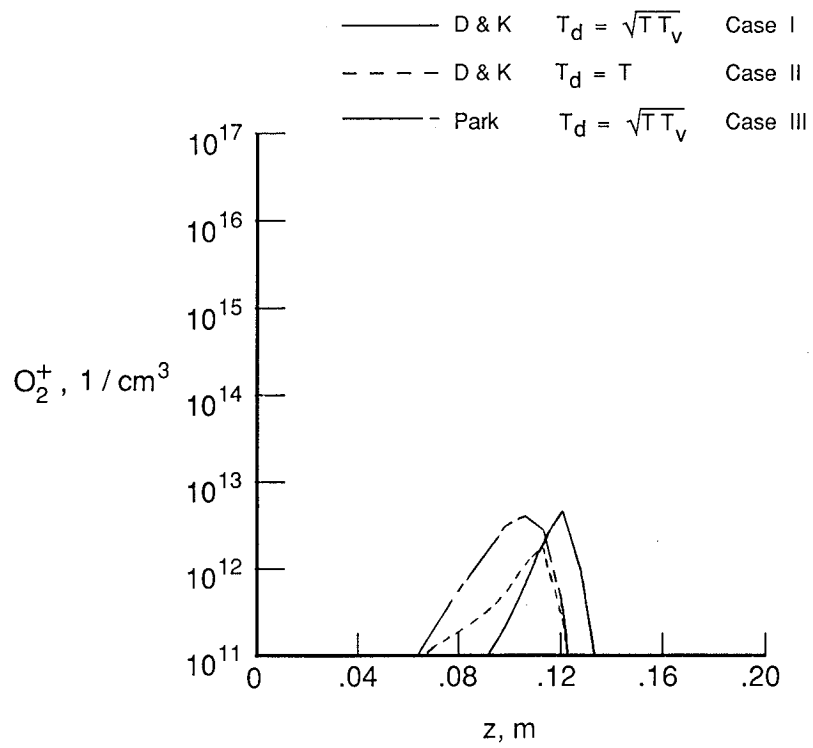

(k) O_2^+ number density.

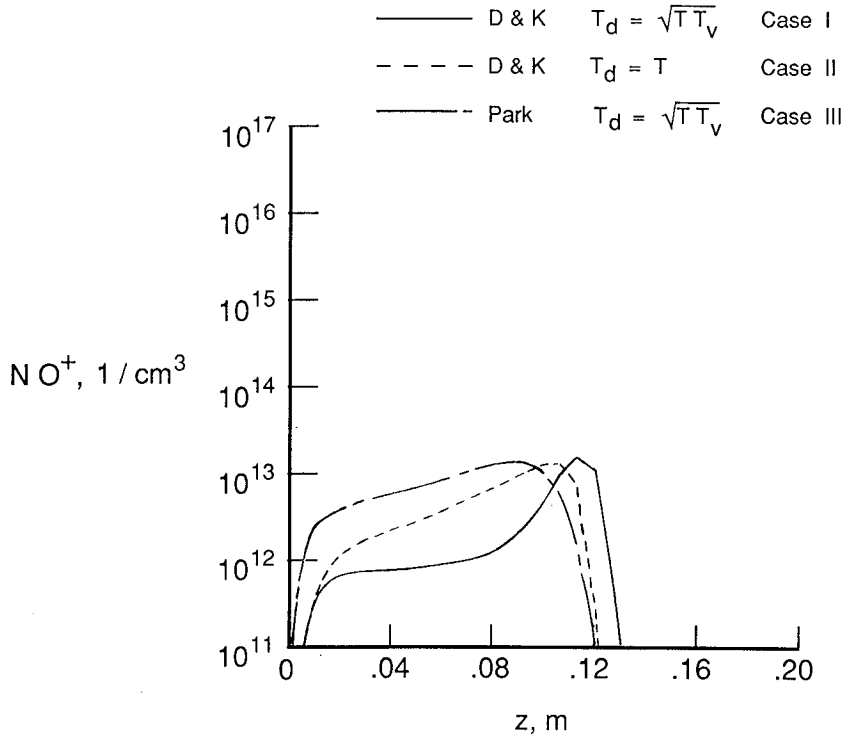

(l) NO^+ number density.

Figure 1. Continued.

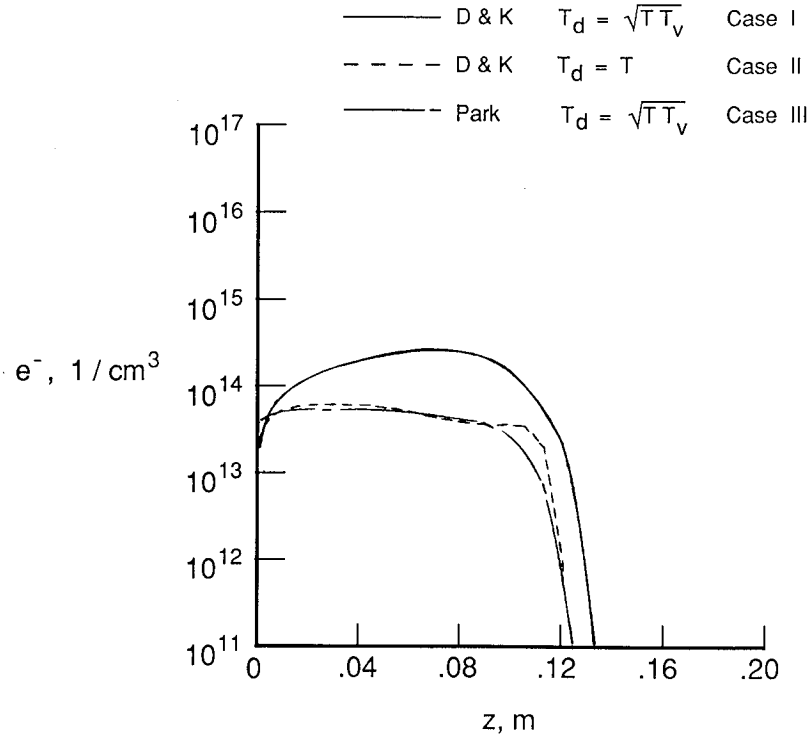

(m) e^- number density.

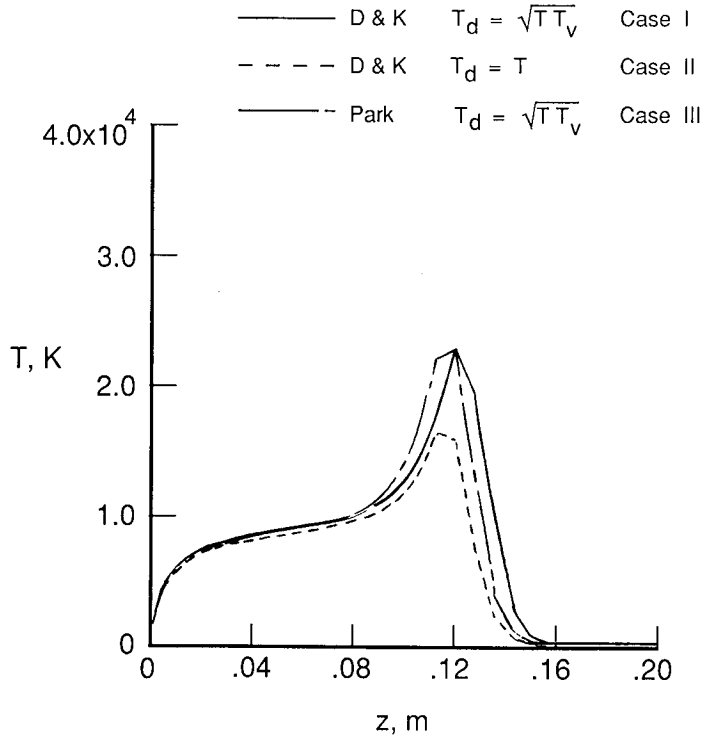

(n) Translational-rotational temperature, T.

Figure 1. Continued.

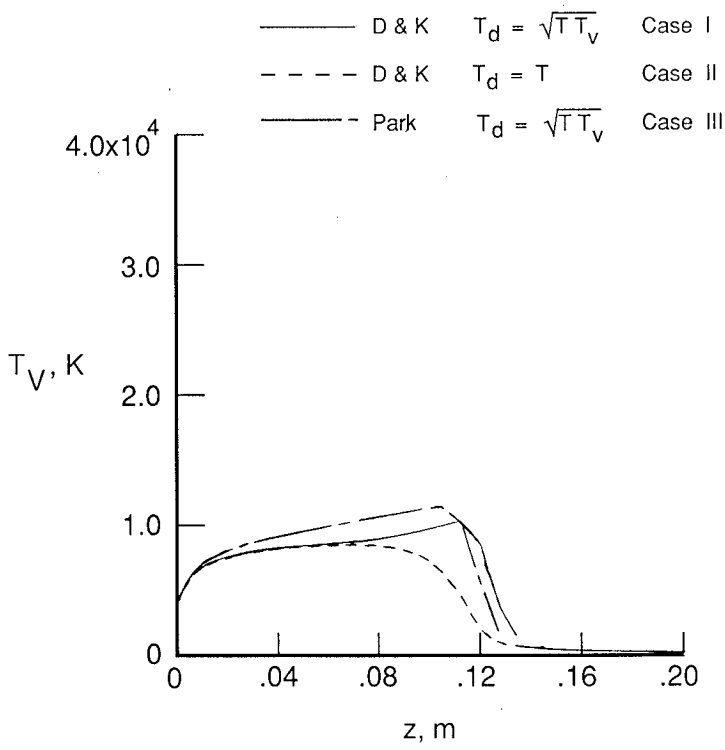

(o) Vibrational-electronic temperature, T_V.

Figure 1. Concluded.

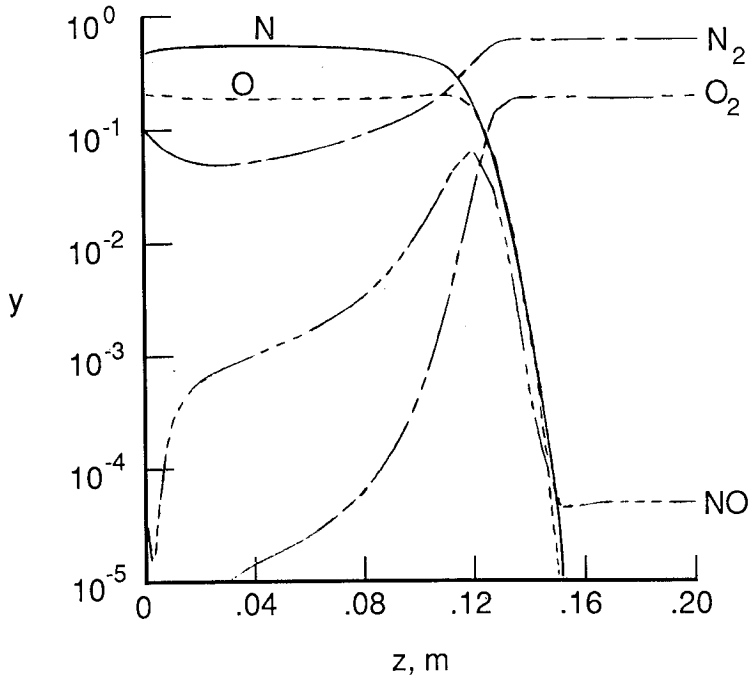

Figure 2. Mole fraction of neutral species across stagnation streamline of shock layer for case I.

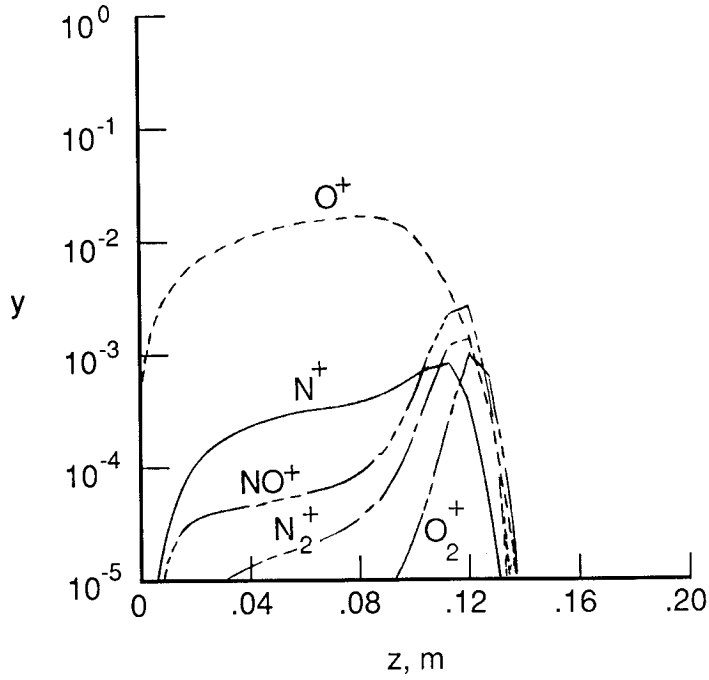

Figure 3. Mole fraction of ionized species across stagnation streamline of shock layer for case I.

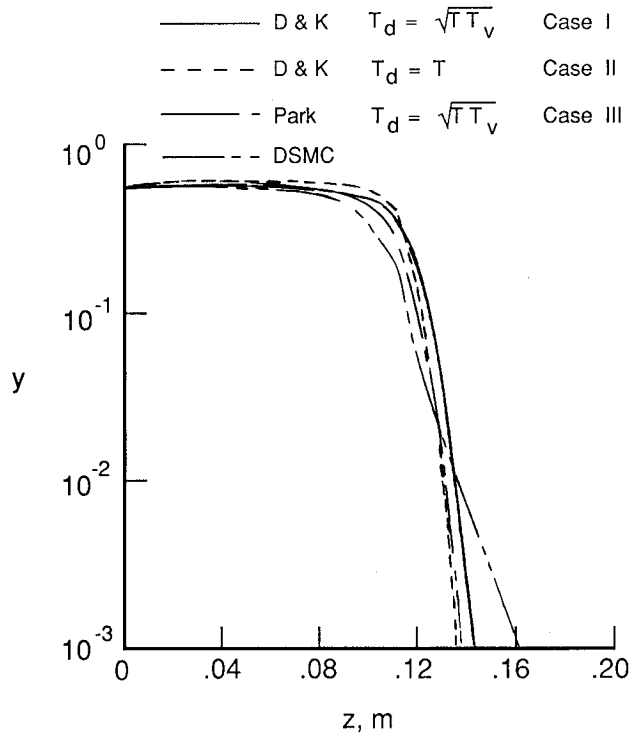

(a) N mole fraction.

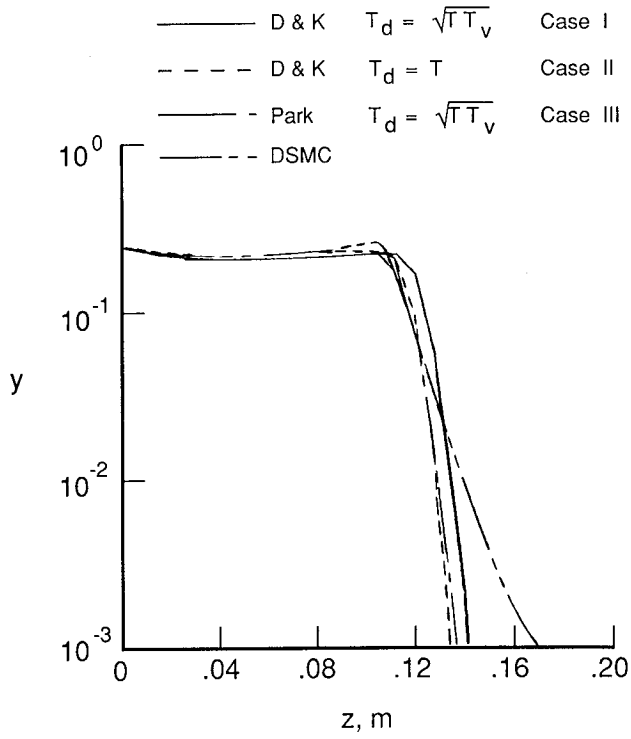

(b) O mole fraction.

Figure 4. Profile predictions across stagnation streamline for noncontinuum, Direct-Simulation Monte Carlo algorithm and continuum LAURA algorithm.

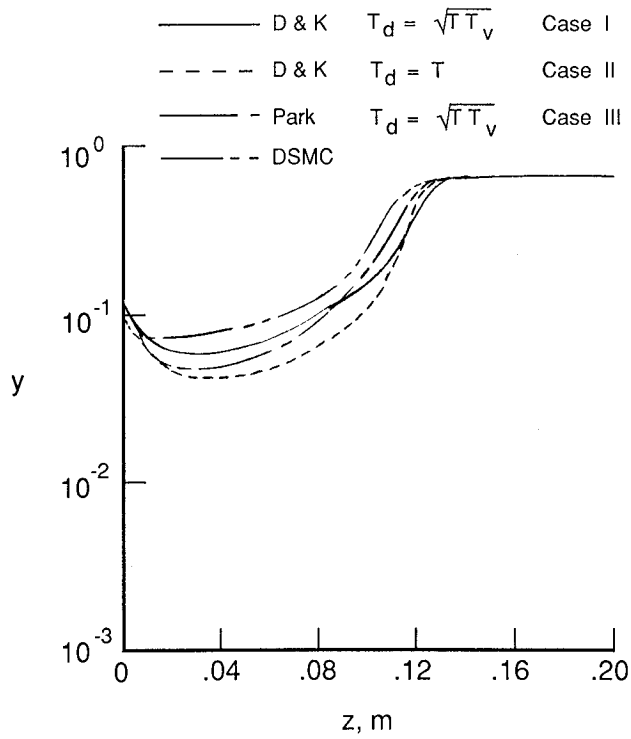

(c) N_2 mole fraction.

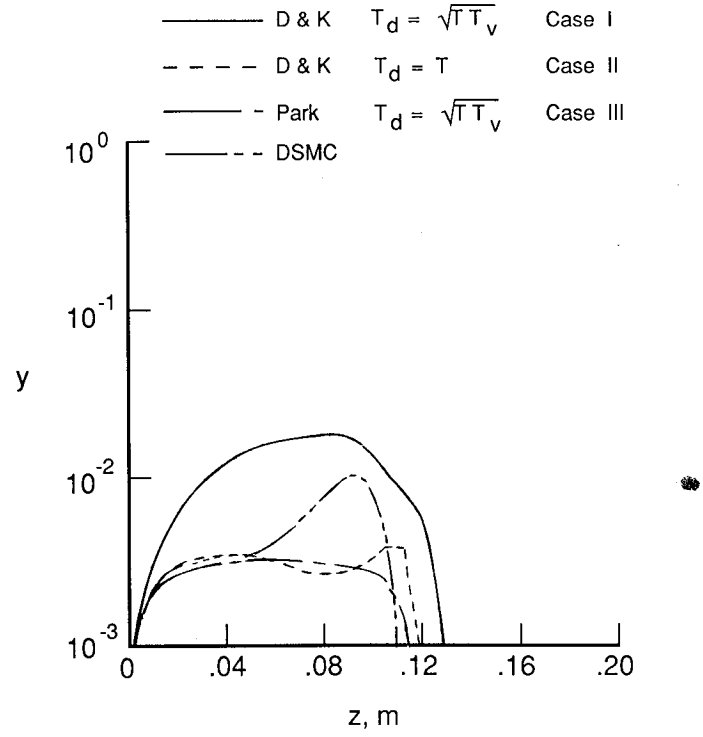

(d) e^- mole fraction.

Figure 4. Continued.

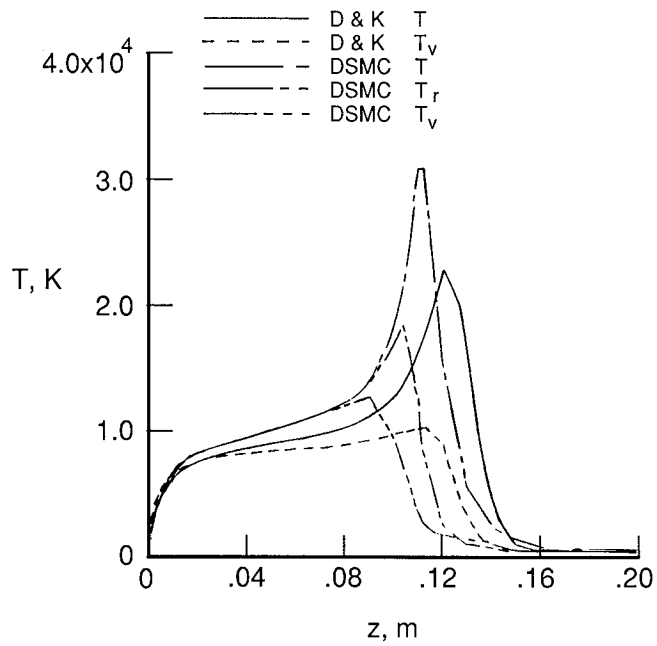

(e) T and T_v (case I).

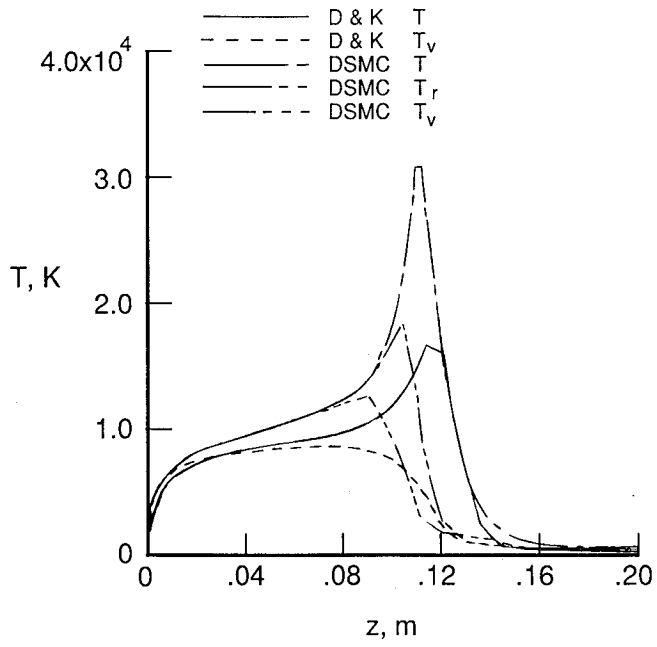

(f) T and T_v (case II).

Figure 4. Continued.

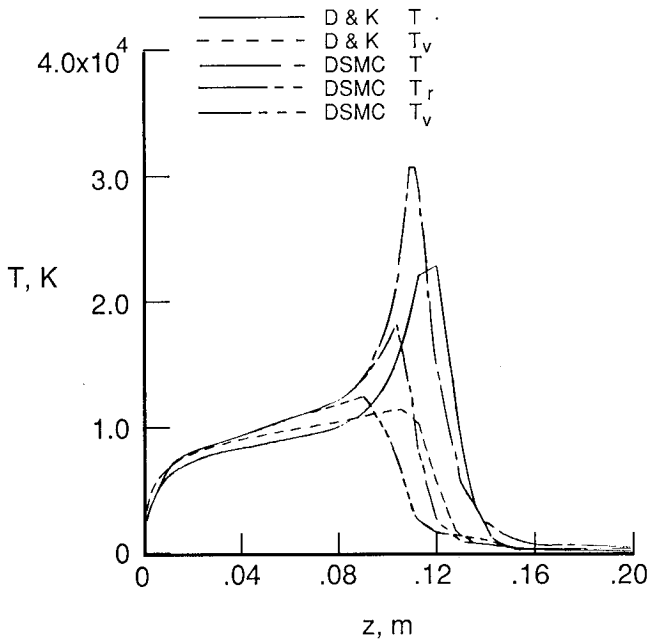

(g) T and T_v (case III).

Figure 4. Concluded.

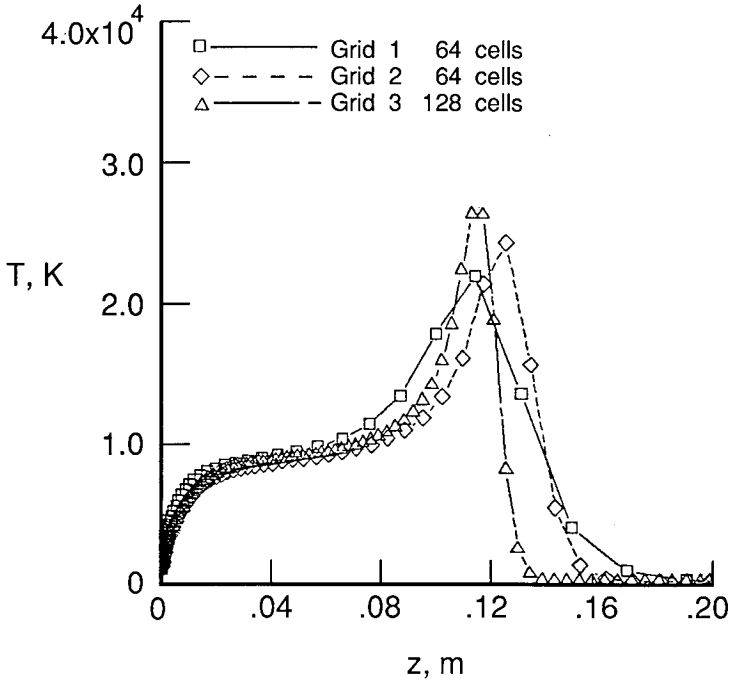

(a) Translational-rotational temperature.

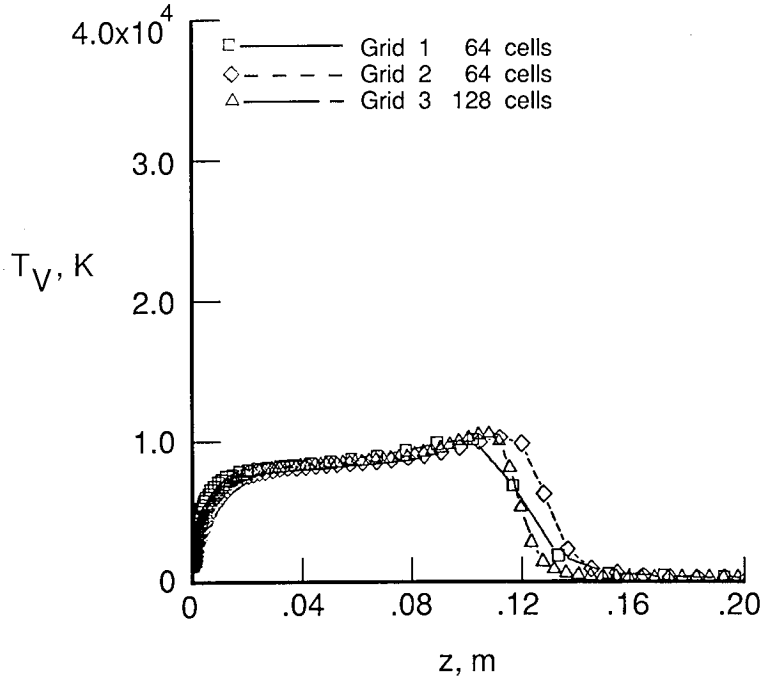

(b) Vibrational-electronic temperature.

Figure 5. Profile predictions across stagnation streamline with three different grids for case I.

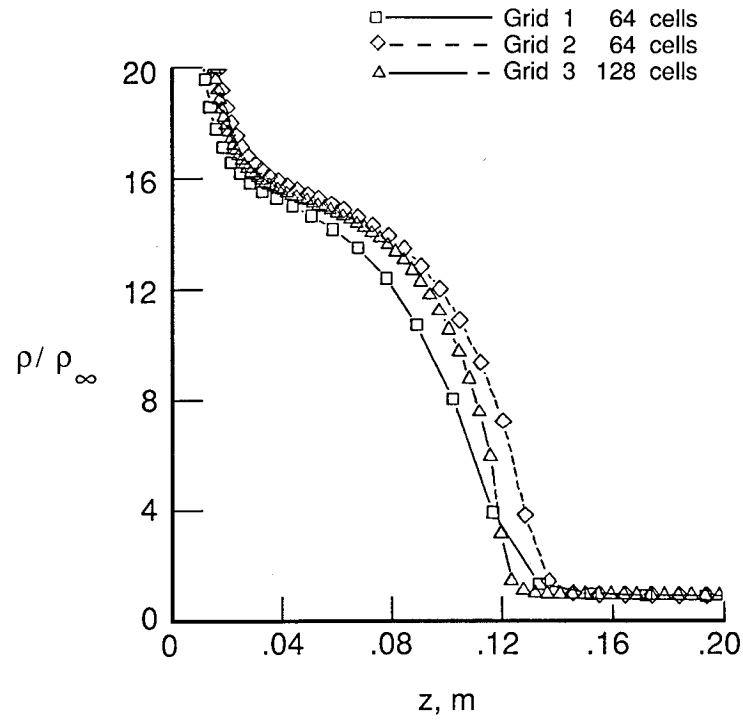

(c) Density, ρ/ρ_∞.

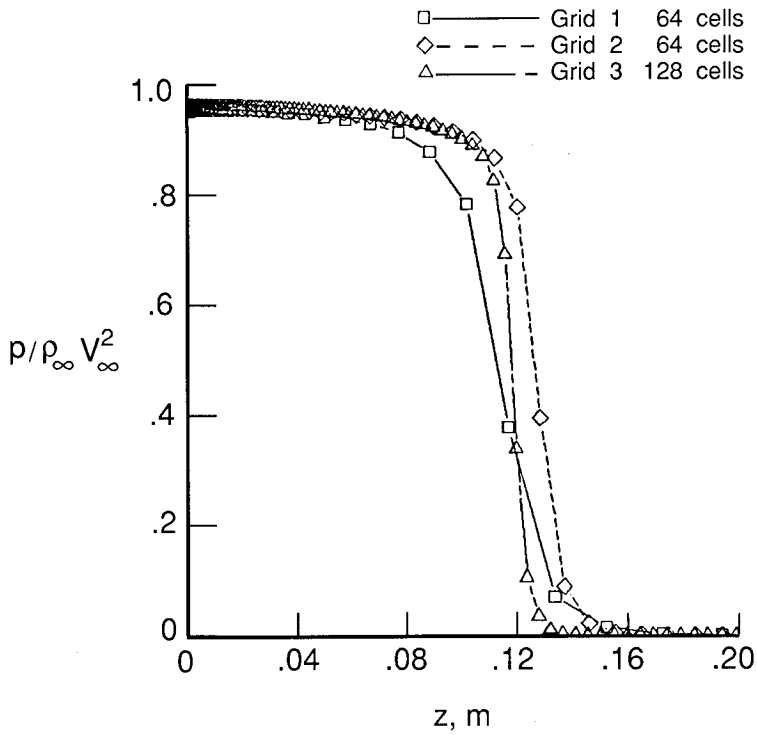

(d) Pressure, $p/\rho_\infty V_\infty^2$.

Figure 5. Continued.

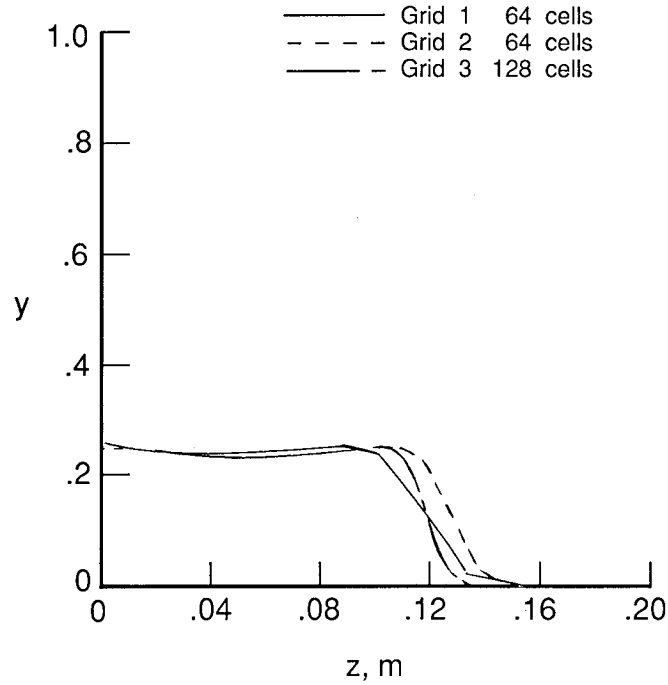

(e) O mole fraction.

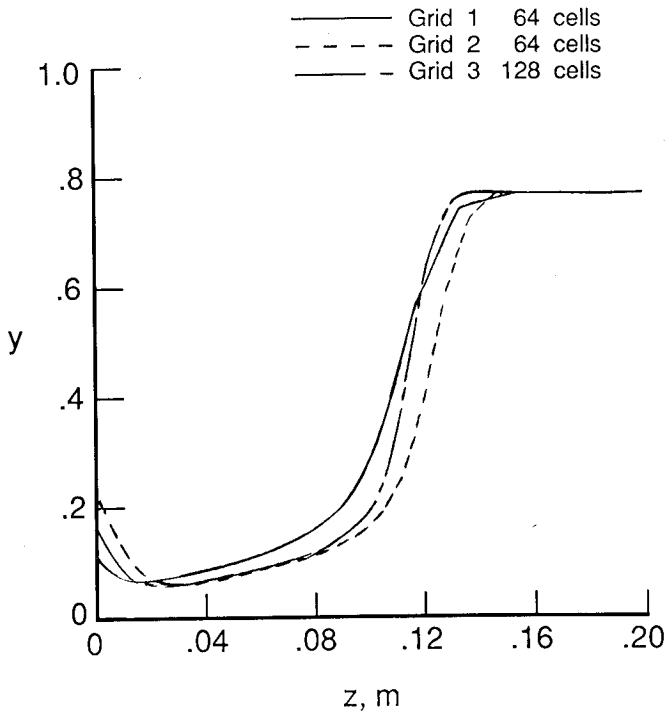

(f) N_2 mole fraction.

Figure 5. Continued.

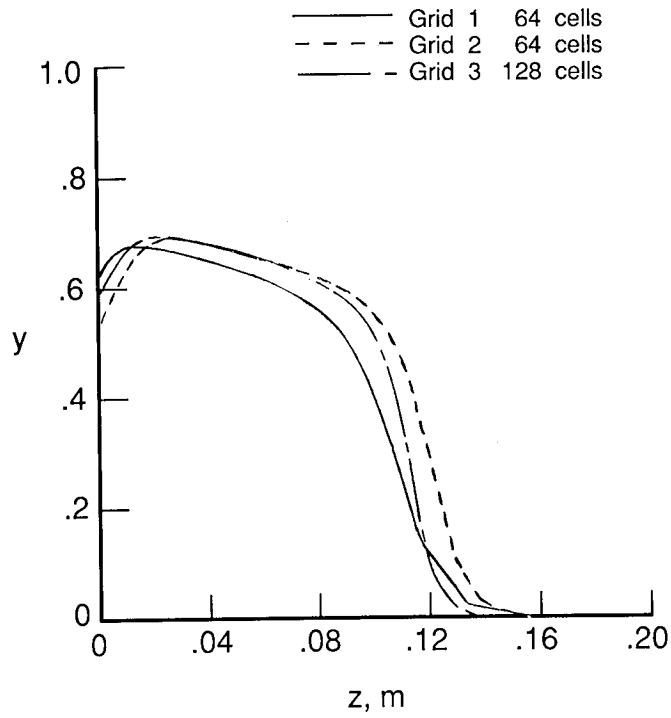

(g) N mole fraction.

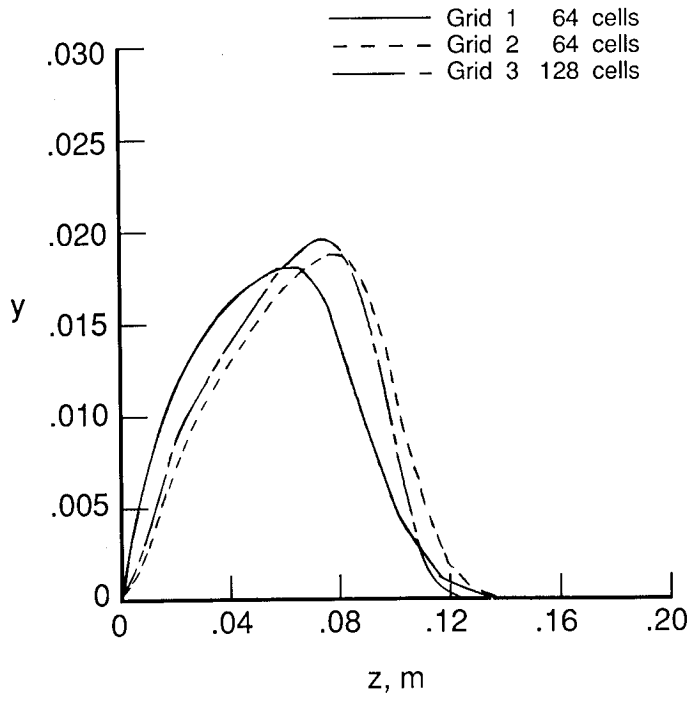

(h) O^+ mole fraction.

Figure 5. Continued.

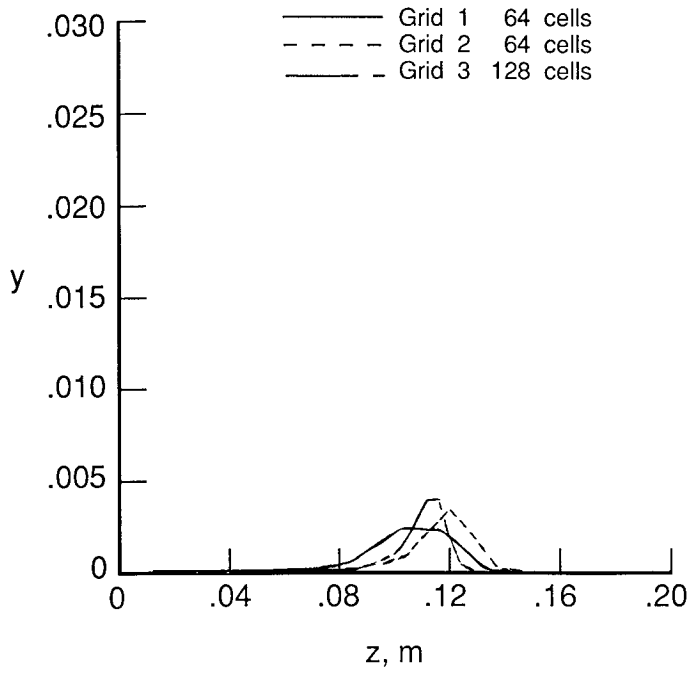

(i) NO^+ mole fraction.

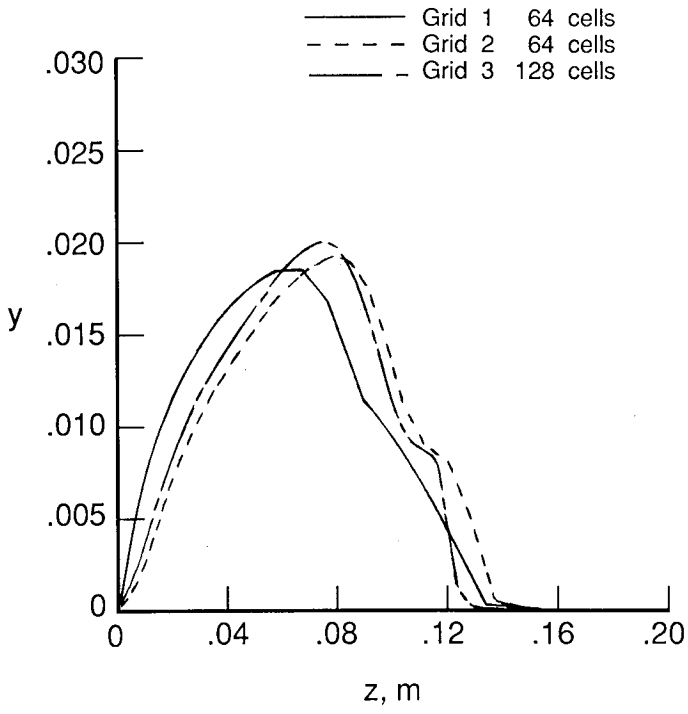

(j) e^- mole fraction.

Figure 5. Concluded.

Report Documentation Page

1. Report No.	2. Government Accession No.	3. Recipient's Catalog No.
NASA TP-2867		

4. Title and Subtitle	5. Report Date
Conservation Equations and Physical Models for Hypersonic Air Flows in Thermal and Chemical Nonequilibrium	February 1989
	6. Performing Organization Code
7. Author(s)	8. Performing Organization Report No.
Peter A. Gnoffo, Roop N. Gupta, and Judy L. Shinn	L-16477
9. Performing Organization Name and Address	10. Work Unit No.
NASA Langley Research Center Hampton, VA 23665-5225	506-40-91-02
	11. Contract or Grant No.
12. Sponsoring Agency Name and Address	13. Type of Report and Period Covered
National Aeronautics and Space Administration Washington, DC 20546-0001	Technical Paper
	14. Sponsoring Agency Code

15. Supplementary Notes

Peter A. Gnoffo and Judy L. Shinn: Langley Research Center, Hampton, Virginia.
Roop N. Gupta: Scientific Research & Technology, Inc., Hampton, Virginia.

16. Abstract

The conservation equations for simulating hypersonic flows in thermal and chemical nonequilibrium and details of the associated physical models are presented. These details include the curve fits used for defining thermodynamic properties of the 11-species air model (N, O, N_2, O_2, NO, N^+, O^+, N_2^+, O_2^+, NO^+, and e^-), curve fits for collision cross sections, expressions for transport properties, chemical kinetic models, and vibrational and electronic energy relaxation models. The expressions are formulated in the context of either a two- or three-temperature model. Greater emphasis is placed on the two-temperature model, in which it is assumed that the translational and rotational energy modes are in equilibrium at the translational temperature, and the vibrational, electronic, and electron translational energy modes are in equilibrium at the vibrational temperature. The eigenvalues and eigenvectors associated with the Jacobian of the flux vector are also presented in order to accommodate the "upwind" based numerical solutions of the complete equation set.

17. Key Words (Suggested by Authors(s))	18. Distribution Statement
Hypersonic flow Thermal nonequilibrium Chemical nonequilibrium Upwind schemes Aeroassist Flight Experiment	Unclassified—Unlimited Subject Category 34

19. Security Classif.(of this report)	20. Security Classif.(of this page)	21. No. of Pages	22. Price
Unclassified	Unclassified	61	A04

NASA FORM 1626 OCT 86 NASA-Langley, 1989

For sale by the National Technical Information Service, Springfield, Virginia 22161-2171